

**Molecular mechanisms of inhibitory signaling in the heart and brain**

A DISSERTATION  
SUBMITTED TO THE FACULTY OF  
UNIVERSITY OF MINNESOTA  
BY

**Nicole M. Wydeven**

IN PARTIAL FULFILLMENT OF THE REQUIREMENTS  
FOR THE DEGREE OF  
DOCTOR OF PHILOSOPHY

**Kevin D. Wickman, Advisor**

June, 2014



## Acknowledgements

My most sincere thanks go to my advisor and mentor, Dr. Kevin Wickman. This work would not have been possible without his guidance and support over the last five years. He has set an example of excellence as a researcher, mentor, instructor, and role model.

I would like to thank my committee members for their encouragement, insightful comments, and challenging questions. To Dr. Jonathan Marchant (chair) for teaching me the importance of seeing how my work fits into the bigger picture. To Dr. Stan Thayer for introducing me to neuropharmacology as an undergraduate and teaching me the value of hypothesis driven research. To Dr. Paulo Kofuji for his expertise and technical insight into potassium channel electrophysiology.

I would like to thank Dr. Kelsey Mirkovic, Dr. Matt Hearing, Lydia Kotecki, Dr. Nicole Victoria, and Dr. Ezequiel Marron Fernandez de Velasco for assistance with manuscript preparation, experimental design, and helpful advice on analysis, which was provided throughout my tenure at the University of Minnesota.

Further, I would like to thank my collaborators Dr. Kirill Martemyanov, Dr. Ekaterina Posokhova, Dr. David Weaver, Dr. Mark Thomas, Dr. Michael Bennyworth, Dr. Matt Hearing, Dr. Alena Talkachova, and Dr. Thomas Xie.

I would like to acknowledge Yang Yang and Dr. Fang Li for their structural insights, Dr. Jose Colón-Sáez, Joseph Patton, and Zhilian Xia for technical assistance, Ian Romaine, the Vanderbilt Institute of Chemical Biology Chemical Synthesis Core, and the Vanderbilt MLPCN Specialized Chemistry Center for ML297 synthesis, and Daniele Young, Jaime Palmersheim, Natalia Martemyanova, and Jennifer Kutzke for maintenance of the mouse colonies and technical support. I would further like to thank Dr. Simonds (NIH/NIDDK) for the gift of the anti-G $\beta$ 5 and anti-R7BP antibodies, Dr. Okamura for the permission to use *Dr-VSP*, and Texas Institute for Genomic Medicine (TIGM) for providing *Rgs6*<sup>-/-</sup> mouse line

I would like to give a special thanks to my family and friends for providing overwhelming support, especially my husband Nicholas Blau.

This work is supported by NIH grants T32 DA07234 (NW), RO1 MH061933 (KW), R01 DA011806 (KW), DA034696 (KW), RO1 HL105550 (KW/KAM), T32 DA07234 (KM and KA), P30 NS062158 (MJT), T32 DA007097 (MCH), P30 CA068485 (CDW), and a McKnight Land-Grant Award (KAM).

## Abstract

G protein-gated inwardly-rectifying K<sup>+</sup> (GIRK/Kir3) channels mediate the inhibitory effect of many neurotransmitters on excitable cells of the heart and brain. Dysregulation of GIRK signaling is known to underlie a number of disorders, including arrhythmia, epilepsy, depression, anxiety, schizophrenia, and drug addiction. GIRK channels are gated by inhibitory G<sub>i/o</sub> proteins and temporally modulated by Regulators of G protein Signaling (RGS) proteins. GIRK channels are tetramers consisting of various combinations of four mammalian Kir subunits (GIRK1-4). This dissertation focuses on neuronal and cardiac GIRK signaling cascades as targets for new pharmacotherapies in the treatment of anxiety-related disorders and cardiac arrhythmias.

Both robust GIRK channel activity and modulation by a new class of GIRK-specific drugs depend on the GIRK1 subunit. The presence of GIRK1 in channel complexes is necessary for robust channel activity. We first sought to better understand the potentiating influence of GIRK1, using the GABA<sub>B</sub> receptor and GIRK1/GIRK2 heteromer as a model system. We found residues in both the distal carboxyl-terminal domain and channel core that underlie the GIRK1-dependent potentiation of receptor-dependent and receptor-independent heteromeric channel activity. Further, ML297, the prototypical member of a new family of small molecule GIRK channel modulators, selectively activates GIRK1-containing channels. We found that ML297 activates GIRK channels via a unique mechanism that requires two amino acids specific to the GIRK1 subunit. In addition, ML297 reduces anxiety-related behavior in mice, in a GIRK1-dependent manner, without triggering addiction-related behavior. Thus, ML297 is a new

tool for probing the therapeutic potential of GIRK channel modulation, which may benefit individuals with anxiety-related disorders.

Cardiac GIRK signaling plays a role in the parasympathetic regulation of heart rate (HR). Parasympathetic activity decreases HR by inhibiting pacemaker cells in the sino-atrial node (SAN). RGS proteins are negative modulators of the parasympathetic regulation of HR and the prototypical M<sub>2</sub> muscarinic receptor (M<sub>2</sub>R)-dependent signaling pathway in the SAN that involves the muscarinic-gated atrial K<sup>+</sup> channel I<sub>KACH</sub> (a GIRK1/GIRK4 tetramer). We first identified RGS6 as a temporal regulator of cardiac M<sub>2</sub>R-I<sub>KACH</sub> signaling in atrial myocytes and SAN cells. Both RGS4 and RGS6 have been implicated in the negative modulation of the parasympathetic regulation of HR and the M<sub>2</sub>R-I<sub>KACH</sub> signaling pathway. We next looked at the contribution of RGS4 and RGS6 to the modulation of M<sub>2</sub>R-I<sub>KACH</sub> signaling. Ablation of *Rgs6*, but not *Rgs4*, correlated with decreased resting HR and a significant delay of M<sub>2</sub>R-I<sub>KACH</sub> deactivation rate. Thus, RGS6, and not RGS4, is the primary RGS modulator of cardiac M<sub>2</sub>R-I<sub>KACH</sub>. Taken together, these findings suggest that RGS6 is a potential pharmacotherapeutic target as the dysregulation of parasympathetic influence has been linked to sinus node dysfunction and arrhythmia.

## Table of Contents

Acknowledgements	i
Abstract	ii
Table of Contents	iv
List of Tables	vii
List of Figures	viii
List of Abbreviations	x
<b>CHAPTER 1. INTRODUCTION</b>	<b>1</b>
<b>I. CONTROL OF CELLULAR EXCITABILITY</b>	<b>2</b>
Heterotrimeric GTP-binding proteins	3
G protein-coupled receptors	4
GPCR activation of G proteins	4
G <sub>i/o</sub> G proteins regulate cell excitability	5
<b>II. GIRK CHANNELS</b>	<b>8</b>
Electrophysiological properties of GIRK channels	8
Channel formation and trafficking	9
GIRK splice variants	10
GIRK subunit distribution	11
Cofactors of GIRK activation	13
GIRK channel gating: structural insights	14
Structural and functional differences among GIRK subunits	18
Temporal regulation of G protein signaling	20

	Pharmacology of GIRK channels	22
	GIRK channels and disease	25
	Neuronal and Cardiac GIRK signaling	26
	III. SUMMARY	28
<b>CHAPTER 2.</b>	<b>Structural elements in the GIRK1 subunit that potentiate G protein-gated potassium channel activity</b>	30
	Introduction	31
	Materials and Methods	32
	Results	34
	Discussion	56
<b>CHAPTER 3.</b>	<b>Mechanisms underlying the activation of G protein-gated inwardly-rectifying K<sup>+</sup> (GIRK) channels by the novel anxiolytic drug, ML297</b>	60
	Introduction	61
	Materials and Methods	62
	Results	69
	Discussion	86
<b>CHAPTER 4.</b>	<b>RGS6/Gβ5 complex accelerates I<sub>K<sub>ACh</sub></sub> gating kinetics in atrial myocytes and modulates parasympathetic regulation of heart rate</b>	92
	Introduction	93
	Materials and Methods	94
	Results	101

	Discussion	113
<b>CHAPTER 5.</b>	<b>RGS6, not RGS4, is the dominant regulator of G protein signaling (RGS) modulator of the parasympathetic regulation of mouse heart rate</b>	
	Introduction	115
	Materials and Methods	116
	Results	117
	Discussion	123
<b>CHAPTER 6.</b>	<b>DISCUSSION</b>	134
	General summary and significance	141
	Key functional domains in GIRK1	142
	Mechanisms of ML297 activation and selectivity	144
	Therapeutic potential of ML297	150
	RGS influence on parasympathetic heart rate regulation	154
	Future directions	156
<b>REFERENCES</b>		160



## List of Tables

Table 2.1	Summary of single-channel data.	55
Table 5.1	HRV analysis of wild-type and $Rgs^{-/-}$ hearts.	128

## List of Figures

Figure 1.1	Inhibitory $G_{i/o}$ G protein signaling pathway.	7
Figure 1.2	GIRK subunit alignment and secondary structure.	17
Figure 2.1	The potentiating influence of GIRK1.	36
Figure 2.2	GIRK1-dependent potentiation of GABA <sub>B</sub> R-GIRK currents in hippocampal neurons.	37
Figure 2.3	Impact of the GIRK1 distal C-terminus.	40
Figure 2.4	Characterization of GIRK1 C-terminal deletion constructs.	41
Figure 2.5	Impact of Q404.	42
Figure 2.6	Characterization of GIRK1(Q404A) mutant.	43
Figure 2.7	Impact of the GIRK1 core.	49
Figure 2.8	Characterization of GIRK1/GIRK2 NT, TM, and CT chimeras.	50
Figure 2.9	Impact of the GIRK1 P-loop and M2 domain.	51
Figure 2.10	Characterization of GIRK1 core chimeras.	52
Figure 2.11	Impact of GIRK1 P-loop residues.	53
Figure 2.12	Characterization of GIRK2 P-loop point mutants.	54
Figure 3.1	ML297- and baclofen-induced GIRK currents: whole-cell.	73
Figure 3.2	ML297- and baclofen-induced GIRK currents: single-channel.	74
Figure 3.3	ML297- and baclofen-induced GIRK currents: PIP <sub>2</sub> dependence.	75
Figure 3.4	ML297- and baclofen-induced GIRK currents in hippocampal neurons.	76
Figure 3.5	ML297- and baclofen-induced GIRK currents in hippocampal neurons.	77

Figure 3.6	Structural elements of GIRK1 required for ML297 activation.	80
Figure 3.7	Structural elements in GIRK1 required for ML297 activation.	81
Figure 3.8	Structural elements in GIRK1 required for ML297 activation.	82
Figure 3.9	Behavioral impact of ML297.	85
Figure 3.10	Structural elements involved in GIRK channel activation by Gβγ, PIP <sub>2</sub> , Na <sup>+</sup> , and ML297.	89
Figure 4.1	Depiction of measured parameters for the whole-cell CCh-induced current studies.	99
Figure 4.2	RGS6 protein level and complex formation in the mouse heart.	103
Figure 4.3	Quantitative analysis of RGS6 distribution across tissues.	104
Figure 4.4	RGS6 is present in isolated atrial cardiomyocytes.	105
Figure 4.5	Impact of <i>Rgs6</i> ablation on M <sub>2</sub> R-I <sub>KACH</sub> signaling in atrial myocytes.	107
Figure 4.6	Impact of <i>Rgs6</i> ablation on M <sub>2</sub> R-I <sub>KACH</sub> signaling in atrial myocytes and SAN cells.	108
Figure 4.7	RGS6/Gβ5 forms a complex with GIRK4.	110
Figure 4.8	Effect of <i>Rgs6</i> ablation on resting HR and muscarinic regulation.	111
Figure 4.9	Quantitative analysis of ECG intervals in <i>Rgs6</i> <sup>-/-</sup> mice.	112
Figure 5.1	Characterization of <i>Rgs4</i> <sup>-/-</sup> mice.	125
Figure 5.2	Impact of RGS ablation on HR and CCh-induced bradycardia.	127
Figure 5.3	Impact of RGS ablation on M <sub>2</sub> R-I <sub>KACH</sub> signaling in SAN cells.	130
Figure 5.4	Influence of another R7 RGS protein revealed by <i>Rgs4</i> ablation.	133
Figure 5.5	<i>Rgs4</i> ablation in isoproterenol-stimulated hearts.	136
Figure 5.6	M <sub>2</sub> R-I <sub>KACH</sub> signaling evaluated by slow perfusion of CCh.	138

## List of Abbreviations

AC	adenylyl cyclase
ACh	acetylcholine
AGS	activators of G protein signaling
ANOVA	analysis of variance
cAMP	3'-5'-cyclic adenosine monophosphate
CCh	carbachol
CHO cells	Chinese hamster ovary cells
CNS	central nervous system
DAG	diacyl glycerol
DEP	disheveled, egl-10, pleckstrin domain
DHEX	DEP helical extension domain
E <sub>K</sub>	equilibrium potential of potassium
ER	endoplasmic reticulum
GABA	γ-aminobutyric acid
GAP	GTPase-accelerating protein
GGL	G protein gamma-like domain
GIRK	G protein-gated inwardly-rectifying K <sup>+</sup> channel
GPCR	G protein-coupled receptor
HEK or HEK293 cells	human embryonic kidney cells
HR	heart rate
HRV	heart rate variability
I <sub>KACH</sub>	cardiac K <sup>+</sup> channel, GIRK1/GIRK4 tetramer
IP3	inositol 1,4,5-triphosphate
IRK1	Kir2.1 channel
Kir	inwardly-rectifying K <sup>+</sup> channel
M <sub>2</sub> R	type 2 muscarinic receptor
NMR	nuclear magnetic resonance
PIP <sub>2</sub>	phosphatidylinositol-4,5-bisphosphate
PKA	protein kinase A
PKC	protein kinase C
PLC	phospholipase C
PSD95	postsynaptic density 95
PTX	pertussis toxin
R7BP	R7 family binding protein
RGS	regulator of G protein signaling
SAN	sinoatrial node
SAP97	synapse associated protein 97
SNX27	sorting nexin 27
VTA	ventral tegmental area

# **CHAPTER 1**

## **INTRODUCTION**

## **I. CONTROL OF CELLULAR EXCITABILITY**

Nerve cells and muscle cells have a lipid-based plasma membrane that is responsive to electrical and chemical stimulation. These excitable cells use electrical signals generated by separating electrical charges across the plasma membrane to communicate with other cells or trigger muscle cell contraction. Control and maintenance of cellular excitability is a fundamental physiological process. Dysregulation of cell excitability is a major underlying factor of prevalent and debilitating diseases, including cardiac arrhythmias and neurological disorders, such as epilepsy, schizophrenia and depression. Cell excitability is regulated by many hormones and neurotransmitters that act through cell surface receptors coupled to heterotrimeric GTP-binding proteins (G proteins), leading to the modulation of enzymes and ion channels. G proteins are active in nearly every organ system and, thus, their surface receptors are considered to be one of the most important drug targets by the pharmaceutical industry. Currently, more than 30% of all available therapies target G protein signaling [1]. These treatments target high blood pressure, arrhythmias, pain, anxiety, depression, attention-deficit disorder, epilepsy and other seizure-inducing conditions. Unfortunately, medications targeting G protein signaling often have adverse side effects, due in part to the widespread activity of these signaling cascades. The mechanisms underlying the functional and spatial organization of G protein signaling cascades are still poorly understood. However, by understanding the many facets of G protein signaling, it may be possible to improve current pharmacotherapies by making them more selective and efficacious, while reducing unwanted side effects.

## **Heterotrimeric GTP-binding proteins**

Heterotrimeric G proteins consist of an  $\alpha$ ,  $\beta$ , and  $\gamma$  subunit [2, 3]. There are 21 human  $G\alpha$  subunits, 5  $G\beta$  subunits, and 12  $G\gamma$  subunits [4-6]. There are different  $G\alpha$  subtypes, including  $G\alpha_s$ ,  $G\alpha_q$ ,  $G\alpha_{i/o}$ , and  $G\alpha_{12}$ , all of which contain a conserved GTPase domain and helical domain [7-9]. The GTPase domain is responsible for the hydrolysis of GTP and creating the binding surfaces for interactions with surface receptors, the  $G\beta\gamma$  dimer, and downstream effector proteins [2]. This domain also has three small loops that undergo significant conformational changes between the inactive GDP-bound and active GTP-bound states [10-12]. The helical domain of the  $G\alpha$  acts to enclose the GDP/GTP binding site. Most  $G\alpha$  subunits are anchored to the plasma membrane through the post-translational addition of a palmitoyl, and for  $G\alpha_{i/o}$ , myristoyl moiety to the N-terminus [13, 14].  $G\alpha$  subtypes differ in the identity of their downstream effectors.  $G\alpha_s$  and  $G\alpha_q$  promote excitatory effects within the cell, whereas  $G\alpha_{i/o}$  promotes inhibitory changes [2].

$G\beta$  and  $G\gamma$  subunits form a protein dimer and act together as a single functional unit. The  $G\beta$  subunit has an N-terminal  $\alpha$ -helix while the remainder of the subunit forms a large seven-bladed  $\beta$ -propeller structure. The  $G\gamma$  subunit is smaller and has an N-terminal  $\alpha$ -helix that forms a coiled-coil domain with the  $G\beta$  N-terminus [15]. Additionally, the small C-terminus of the  $G\gamma$  subunit interacts with  $G\beta$  blades 5 and 6 [15]. Together, these interactions are responsible for the  $G\beta\gamma$  dimer formation, which only separates under denaturing conditions [3, 15, 16]. The  $G\beta\gamma$  dimer, like  $G\alpha$ , is also anchored to the membrane via a farnesyl or geranylgeranyl moiety that is added to the  $G\gamma$  C-terminus through a post-translational isoprenylation [17]. The  $G\beta$  subunit of the  $G\beta\gamma$

dimer interacts with the  $G\alpha$  subunit. The  $G\beta$  binding site on the  $G\alpha$  subunit is a hydrophobic pocket formed by two of the flexible loops and the N-terminus [10, 16]. Both  $G\alpha$  and  $G\beta\gamma$  go on to act on downstream effectors, making the heterotrimeric G protein a ubiquitous signaling protein.

### **G protein-coupled receptors**

Surface receptors that couple to heterotrimeric G proteins are known as G protein-coupled receptors, or GPCRs. The GPCR superfamily is made up of vast and diverse group of receptors that are encoded by nearly 800 human genes and interact with numerous hormones and neurotransmitters [18]. Common to all GPCRs is a seven transmembrane-spanning  $\alpha$ -helix domain, an extracellular N-terminus, an intracellular C-terminus, three extracellular inter-helical loops, and three intracellular inter-helical loops [2]. The GPCR superfamily can be phylogenically divided into 5 separate families: rhodopsin, secretin, glutamate, adhesion, and frizzled-taste-2 [19]. There is evidence that GPCR members of the rhodopsin and glutamate families can form homo- and heterodimers, yielding further diversity and complexity to this superfamily [20-25]. Yet, despite the vastness of this superfamily of receptors, GPCRs signal through a relatively small but important group of G protein subtypes.

### **GPCR activation of G proteins**

Ligand binding often occurs at the extracellular N-terminal domain of GPCRs, resulting in a conformational change of the receptor's membrane-spanning domains, which activates heterotrimeric G proteins [20]. There are two leading proposals regarding



how inactive G proteins encounter GPCRs in their active state. The “collision-coupling” theory postulates that many inactive G proteins are free floating in the membrane where they collide with and become activated by ligand-bound GPCRs [26]. Alternatively, the “pre-coupling” or “preassembly” theory suggests that inactive G proteins are already associated with inactive GPCRs and become activated when GPCRs are activated [27]. While evidence is mounting for the latter, experiments to date have primarily been performed *in vitro* and thus mechanisms underlying G protein-GPCR encounters remain somewhat unclear [28-32].

However they couple, heterotrimeric G proteins are activated by ligand-bound GPCRs. Upon ligand binding, the transmembrane regions and the intracellular loops of GPCRs shift causing the  $G\alpha$  subunit to release its bound GDP (reviewed in [2]). After it dissociates from GDP,  $G\alpha$  readily binds GTP due to its high intracellular concentration, causing a significant conformational change which results in the dissociation of  $G\alpha$ -GTP from both the receptor and the  $G\beta\gamma$  dimer [2]. Active GTP-bound  $G\alpha$  and the released  $G\beta\gamma$  are both free to act on many downstream effectors, including cyclases, lipases, and ion channels [9, 33, 34]. These signaling cascades are ultimately terminated by the hydrolysis of bound GTP back to GDP, prompting  $G\alpha$  to reassociate with the  $G\beta\gamma$  dimer and a return to the initial heterotrimeric conformation for subsequent activation.

### **$G_{i/o}$ G proteins regulate cell excitability**

Activation of GPCRs coupled to the  $G\alpha_{i/o}$  family of G proteins promotes activation of signaling cascades that exert a hyperpolarizing influence that is critical for regulation of cell excitability. The  $G_{i/o}$  protein family is made up of  $G\alpha_i$  and  $G\alpha_o$

isoforms:  $G\alpha_{i1}$ ,  $G\alpha_{i2}$ ,  $G\alpha_{i3}$ ,  $G\alpha_{oA}$ , and  $G\alpha_{oB}$  [4]. This family of  $G_{i/o}$  proteins is unique in their sensitivity to pertussis toxin (PTX), which is produced by the bacterium *Bordetella pertussis*. Specifically, PTX promotes ADP-ribosylation of the  $G\alpha$  subunit, which locks the  $G\alpha$  subunit into an inactive GDP-bound state and disrupts interactions with activated GPCRs [35-39].

Upon  $G_{i/o}$  activation, GTP-bound  $G\alpha_{i/o}$  and free  $G\beta\gamma$  act on downstream effectors that reduce cell excitability or inhibit excitatory processes. There are three main pathways in which this occurs: inhibition of adenylyl cyclase, inhibition of  $Ca^{2+}$  channels, and activation of  $K^+$  channels (**Fig. 1.1**). Active  $G\alpha_{i/o}$  inhibits the activity of adenylyl cyclase (AC), which normally catalyzes the conversion of ATP to cAMP (3'-5'-cyclic adenosine monophosphate), a cofactor for the prominent Protein Kinase A (PKA) [40-42]. Alternatively,  $G\beta\gamma$  can directly inhibit  $Ca^{2+}$  influx through certain types of voltage-gated  $Ca^{2+}$  channels and activate a specialized subset of inwardly-rectifying  $K^+$  channels that normally allow an efflux of  $K^+$  and hyperpolarize the cellular membrane [43-49]. These specialized  $K^+$  channels are G protein-gated inwardly-rectifying K<sup>+</sup> ion (GIRK) channels.

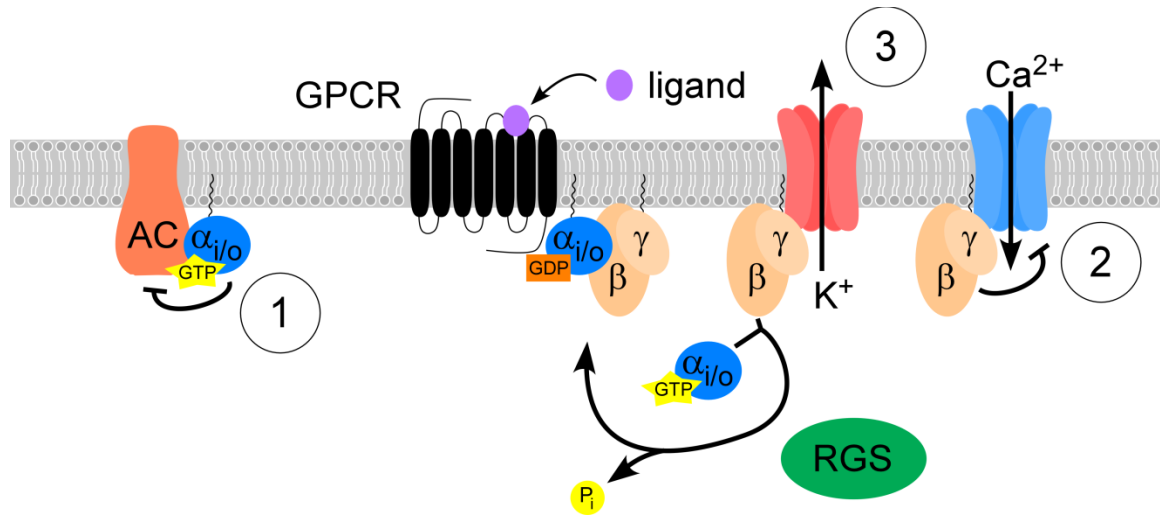


**Figure 1.1. Inhibitory G<sub>i/o</sub> G protein signaling pathway.** This diagram demonstrates the downstream effects of heteromeric G<sub>i/o</sub> protein activation via GPCR activation. **1.** GTP-bound G<sub>α<sub>i/o</sub></sub> inhibits adenylyl cyclase activity, preventing the conversion of ATP into second messenger cAMP. **2.** Released Gβγ can inhibit certain types of voltage-gated calcium channels, inhibiting calcium influx. **3.** Released Gβγ activates G protein-gated inwardly-rectifying potassium channels, or GIRK channels, causing an efflux of potassium ions and hyperpolarization of the cell membrane. An RGS protein is included, as these proteins catalyze the hydrolysis of GTP to GDP, returning the G protein to its inactive heterotrimeric state.

## II. GIRK CHANNELS

GIRK channels play a key role in the maintenance of cellular excitability throughout the brain and heart, where they regulate synaptic transmission and heart rate, respectively [50, 51]. Under physiological conditions, the basal level of GIRK activity contributes in the maintenance of neuronal resting membrane potential [52]. Upon receptor activation of GIRK channels, the membrane becomes hyperpolarized, reducing cell excitability. GIRK channel activation can result in the direct suppression of neuron firing or can contribute to the inhibitory tone of a neuronal network [53-56]. Dysregulation of GIRK signaling is known to be an underlying factor in a number of disorders, including arrhythmia, epilepsy, depression, anxiety, schizophrenia, and drug addiction [57]. Thus, GIRK channels have been, and remain, an important topic of study for more than two decades. The work that lies herein has given novel insight into the function and regulation of these channels that will impact the field.

### **Electrophysiological properties of GIRK channels**

GIRK channels are members of the inward-rectifier potassium channel family (KirX) [58]. This channel family is characterized by their strong inwardly-rectifying current-voltage relationships. The inward-rectification of GIRK channels has been linked to intracellular  $Mg^{2+}$  and polyamines [58, 59]. These positively charged molecules block outward current by occluding the pore at depolarized potentials, or potentials above the equilibrium potential for potassium ( $E_K$ ). [58-61]. Equilibrium potentials for ions can be calculated using the Nernst equation. The Nernst equation adapted for the calculation of the equilibrium potential of potassium ( $E_K$ ) is defined below:

$$E_K = \frac{RT}{F} \ln \frac{[K]_{out}}{[K]_{in}}$$

At physiological conditions, where  $[K^+]_{out} = 4$  mM and  $[K^+]_{in} = 155$  mM,  $E_K$  is -90 mV. However, many electrophysiology experiments, including those described in this work, are done in high extracellular  $K^+$  (e.g.  $[K^+]_{out} = 25$  mM). This shifts the experimental  $E_K$  to -40 mV. In the current-voltage relationship of GIRK channels, the current changes from negative to positive near -90 mV (or near -40 mV when  $[K^+]_{out} = 25$  mM), making this the reversal potential. This relationship is true of all inward-rectifying potassium channels, including GIRK channels.

### **Channel formation and trafficking**

GIRK channels are tetrameric complexes that form one channel pore at the plasma membrane with eight transmembrane domains [57, 62-66]. There are four mammalian GIRK subunits: GIRK1 (Kir3.1), GIRK2 (Kir3.2), GIRK3 (Kir3.3), and GIRK4 (Kir3.4), all of which are highly conserved in sequence and structure [67]. Each subunit is composed of a cytosolic N-terminus, two membrane-spanning domains, two extracellular loops, one pore domain, and a cytosolic C-terminus. Four GIRK subunits come together to form a tetrameric channel. The pore domain contains the selectivity filter that permits only the passage of  $K^+$  ions through the channel opening.

The identity and location of their trafficking motifs differ across the GIRK subunits. GIRK2 and GIRK4 contain endoplasmic reticulum (ER) export motifs as well as post-Golgi surface-promoting signals that allow both subunits to form functional homotetrameric channels at the plasma membrane [68]. The ER export motifs are located

on the N-terminus: GIRK2 residues 18-25 (DQDVESPV) and GIRK4 residues 10-17 (NQDMEIGV) [68]. The post-Golgi surface-promoting signals are highly-acidic regions in the distal C-terminus of both subunits: GIRK2 residues 394-401 (ELETEEEEE) and GIRK4 residues 391-408 (EAEKEAEAEHDEEEEPNG) [68]. Furthermore, the phosphorylation of GIRK2 residue T397 can potentially increase the surface expression of GIRK2 [68]. These motifs are not conserved in GIRK1 and GIRK3, thus GIRK1 and GIRK3 cannot be independently exported from the ER to form functional homomeric channels, but instead require interaction with GIRK2 or GIRK4 subunits for transport to the membrane [64, 68-70].

Interestingly, GIRK3 has been shown to decrease the surface expression of heteromeric channels containing GIRK2/GIRK3 or GIRK1/GIRK2/GIRK3 [68]. It has also been shown that the presence of GIRK3 can reduce currents produced by GIRK2 homomeric or GIRK1/GIRK2 heteromeric channels [66, 71]. The negative effect of GIRK3 can be attributed to both the absence of any forward trafficking signals and the presence of a lysosomal targeting signal in the distal C-terminus: GIRK3 residues 351-354 (YWSI) [68]. As another form of regulation, GIRK2 contains an endocytosis signal (also known as internalization motif) in the N-terminus that controls the surface expression of GIRK2 homomeric and GIRK1/GIRK2 heteromeric channels: GIRK2 residues 11-12 (VL) [68].

### **GIRK splice variants**

Alternative splicing can yield many protein variations from the same gene. Structural and functional differences between splice variants could be exploited as a

therapeutic strategy. The murine *Kcnj6* gene that encodes GIRK2 undergoes alternative splicing to yield four different GIRK2 isoforms: GIRK2A, GIRK2B, GIRK2C, and GIRK2D. GIRK2A-C are expressed in the brain, while GIRK2D is primarily expressed in the testes [57, 72-74]. GIRK2A contains all of the forward trafficking domains and internalization motif previously described [68, 72]. GIRK2C is identical to GIRK2A, with the exception of 11 additional amino acid residues at the end of the C-terminus, which contain a PDZ binding domain: GIRK2C residues 421-425 (ESKV) [73, 75]. Alternatively, GIRK2B is a lesser expressed truncated variant that lacks the last 96 residues of the GIRK2A C-terminus (residues 318-414), and the C-terminal forward trafficking motif, ELETEEE [68, 74]. GIRK2D was the final isoform identified and is identical to GIRK2A minus the presence of the first 18 amino acid residues [76]. This lack of the N-terminal internalization motif promotes stronger surface expression and reduced intracellular protein levels compared to GIRK2A [68, 76].

GIRK1 C-terminal splice variants have also been isolated from brain and heart tissue, in addition to certain cancer cell lines, and are referred to as hGIRK1a,b,c,d,e [77-79]. Unlike wild-type GIRK1, these isoforms are limited in their ability to form functional heteromeric channels. No isoforms of GIRK3 or GIRK4 have yet been reported [57].

## **GIRK subunit distribution**

### *Central Nervous System*

GIRK1, GIRK2 and GIRK3 are broadly distributed in the central nervous system (CNS) [50]. GIRK4 does not demonstrate expression in the CNS, apart from expression

in the hypothalamus [50, 80, 81]. Within the CNS, GIRK1, GIRK2, and GIRK3 exhibit overlapping but distinct distribution patterns [50]. While most neuron populations express GIRK1, GIRK2, and GIRK3, biochemical and genetic approaches have demonstrated that the predominant CNS GIRK channel contains GIRK1 and GIRK2 [63]. Ablation of GIRK2 results in a near to complete loss of GIRK current in many brain regions including the hippocampus [52, 82], cerebellum [83], substantia nigra [82], locus coeruleus [84, 85], and ventral tegmental area (VTA) [86]. GIRK subunits also display cell-type specific distribution within brain regions. For example, the VTA of the midbrain is known for its two prominent cell types: dopaminergic and GABAergic neurons [87]. VTA GABA neurons express GIRK1, GIRK2, and GIRK3 whereas VTA dopamine neurons only express GIRK2 and GIRK3 [87]. Furthermore, dopamine neurons in the substantia nigra, also part of the midbrain, only express GIRK2A and GIRK2C-containing channels [88].

#### *Distribution in cardiac tissue and other regions*

GIRK1 and GIRK4 are expressed in cardiac atrial tissue, where together they form the  $I_{K_{ACh}}$  channel [69].  $I_{K_{ACh}}$ -dependent currents have been observed in the sinoatrial node, the AV node and atrial cardiomyocytes [51, 89]. GIRK channels play a role in other regions of the body as well, including the testes and the islet cells of the pancreas. All four GIRK subunits are expressed in mouse pancreas islet cells, where they are involved in epinephrine-mediated signaling and mediate in part the inhibition of insulin secretion [90]. GIRK2, specifically GIRK2D, is expressed in the testes, where it plays a role in sperm function during fertilization in both mice and boars [76, 91].



## **Cofactors of GIRK channel activation**

In addition to the binding of the  $G\beta\gamma$  subunit, GIRK channels require the presence of phosphatidylinositol-4,5-bisphosphate ( $PIP_2$ ) to open and hyperpolarize the cell membrane [92, 93].  $PIP_2$  is a specialized phospholipid located on the inner leaflet of the plasma membrane where it is involved in both excitatory and inhibitory signaling cascades [94].  $PIP_2$  is mostly thought of as an intermediate in the  $G\alpha_q$  activation of Protein Kinase C (PKC) and  $Ca^{2+}$  influx. In this pathway, phospholipase C (PLC), activated by  $G\alpha_q$ , breaks down  $PIP_2$  into two excitatory second messengers: diacylglycerol (DAG) and inositol 1,4,5-triphosphate ( $IP_3$ ). DAG goes on to activate PKC, while  $IP_3$  is released to the cytosol where it releases  $Ca^{2+}$  from the ER into the cytosol. Increased cytosolic  $Ca^{2+}$  concentration can result in a number of excitatory actions, including muscle cell contraction [95].  $PIP_2$ , when not broken down into its excitatory counterparts, plays an inhibitory role at the plasma membrane, where it interacts with several types of potassium channels and is required for their subsequent activation and efflux of  $K^+$  ions. Inwardly-rectifying potassium channels (Kir1-7) require  $PIP_2$  for their activation [96]. GIRK channels are unique from their other inward-rectifying counterparts in that, in addition to  $PIP_2$ , they also require  $G\beta\gamma$  for activation [92]. GIRK channels have a reduced binding affinity for  $PIP_2$  compared to other inward-rectifying  $K^+$  channels that are constitutively activated by  $PIP_2$  alone, but  $G\beta\gamma$  increases the strength of the  $PIP_2$ -GIRK interaction [94, 97].

Along with  $PIP_2$ , it has also been found that intracellular  $Na^+$  is able to activate GIRK channels ( $EC_{50}$  30-40 mM) [73, 97-101].  $Na^+$  is not thought to be necessary for GIRK activation, but rather can activate GIRK channels as part of an excitatory feedback

mechanism. In this context, excitatory mechanisms that increase the intracellular  $\text{Na}^+$  concentration above the normal range of 5-15 mM would cause an increased level of GIRK activity, which would return the cell to a hyperpolarized state [93]. In summary, GIRK channels require both  $\text{G}\beta\gamma$  and  $\text{PIP}_2$  for channel activation whereas  $\text{Na}^+$  can further enhance basal and receptor-induced GIRK channel activity.

### **GIRK channel gating: structural insights**

Functional studies have shown that  $\text{G}\beta\gamma$  and  $\text{PIP}_2$  are required for channel activation. Yet, until recently, it was unclear how these cofactors were physically influencing GIRK channel gating. X-ray crystallography and functional NMR studies revealed partial cytosolic structures and chimeric structures of inwardly-rectifying  $\text{K}^+$  channels [102-105]. More recently, a complete crystal structure of the GIRK2 homomeric channel was resolved [93]. This study identified the exact binding sites of  $\text{Na}^+$  and  $\text{PIP}_2$ . The crystal structure of the GIRK2- $\text{G}\beta\gamma$  interaction was resolved shortly after [106]. The GIRK2 structure, in the absence of cofactors, gives a detailed view of what is considered to be the closed state of the channel. The ‘closed’ structure suggests that there are two gates within the GIRK channel. The first gate—the inner helix gate—is formed by the four M2 helical domains, one from each subunit, as they are the inner helices that line the pore opening. The side chain of phenylalanine residue 190 on each M2 helix makes up the narrowest part of the pore. The second gate—the G loop gate—is formed by the G-loop (the loop connecting the  $\beta\text{H}$ - $\beta\text{I}$  sheets) located in the cytosolic domains just below the plasma membrane (**Fig. 1.2**).

The resolved crystal structure of GIRK2 revealed the Na<sup>+</sup> binding site. Na<sup>+</sup> binds in the cytosolic region of GIRK2, right underneath the βC-βD loop (**Fig. 1.2, see also Fig. 3.10**). GIRK2 residue D226 has been shown to be a critical determinant of Na<sup>+</sup> activation [93]. The loss of the negative charge provided by the aspartic acid residue (by mutating it to the uncharged asparagine residue) disrupts the binding, and subsequent activation, of Na<sup>+</sup> to the GIRK2 channel [97-99]. Along with D226, there are other residues thought to coordinate Na<sup>+</sup> binding, including R228, N229, S230, along with some residues from the βE-βG loop, L273 and V274 (**Fig. 1.2**).

The PIP<sub>2</sub> binding site is at the interface of the transmembrane domains and the cytosolic domains (**see Fig. 3.10**). Many positively-charged GIRK2 residues in this area coordinate the interaction with the negatively-charged PIP<sub>2</sub> molecule, including K62, K192, K197, and K198. PIP<sub>2</sub> binding to GIRK2, in the absence of Gβγ or a constitutively active mutation, produced only a slight rotation of the inner M2 helices, a modest displacement of the interfacial helix, and a weakened electrostatic state of F190, the most constricted part of the pore. PIP<sub>2</sub> alone does not open either channel gate, which is consistent with previous studies that show PIP<sub>2</sub> alone cannot open GIRK channels in electrophysiology experiments [92, 97].

The Gβγ binding surface is a very large portion (700Å<sup>2</sup>) of the outward-facing plane of the cytosolic domains [106]. The Gβγ binding surface is made up of the βK, βL, βM, βN sheets from one subunit, and of the βD, βE sheets from the adjacent subunit (**Fig. 1.2, see also Fig. 3.10**). All of these structures are conserved across the inward-rectifying family, but only GIRK channels are able to interact with Gβγ. There are residues unique to GIRK channels within these structures that are essential to this protein-protein

interaction. These include: Q246 and F252 on the  $\beta$ D- $\beta$ E loop, L340, S341/T341, L342 on the  $\beta$ L- $\beta$ M loop (**Fig. 1.2**). Further, there are electrostatic interactions between several acidic residues (unique to GIRK channels) on the  $\beta$ L- $\beta$ M loop and the electropositive surface of the G $\beta$  subunit.

Taken together with years of functional data on these channels, the new resolved structures of open and closed channels give a clear model of GIRK channel gating. Alone, Na<sup>+</sup>, PIP<sub>2</sub>, and G $\beta\gamma$  are able to evoke small amounts of GIRK current, but together they activate GIRK channels to a greater, and perhaps full, extent [106]. Upon G $\beta\gamma$  binding to GIRK2, which already is interacting with PIP<sub>2</sub>, the cytoplasmic domains rotate (4° counter-clockwise) with respect the transmembrane domains, causing a splaying of the inner M2 helices. This conformation is only partially open when compared to the PIP<sub>2</sub>-bound constitutively active GIRK2 mutant, in which the inner helices further splay open due to a greater rotation of the cytoplasmic domains (8° counter-clockwise) [106]. These differences in open conformation are likely attributable to the bursts of channel activity characterized in single-channel electrophysiology. This detailed structure-function mechanism of GIRK channel gating is important to the investigation of inherent GIRK channel properties across subunits (Chapter 2) and to understanding how new GIRK agonists modulate GIRK channel gating mechanisms (Chapter 3).

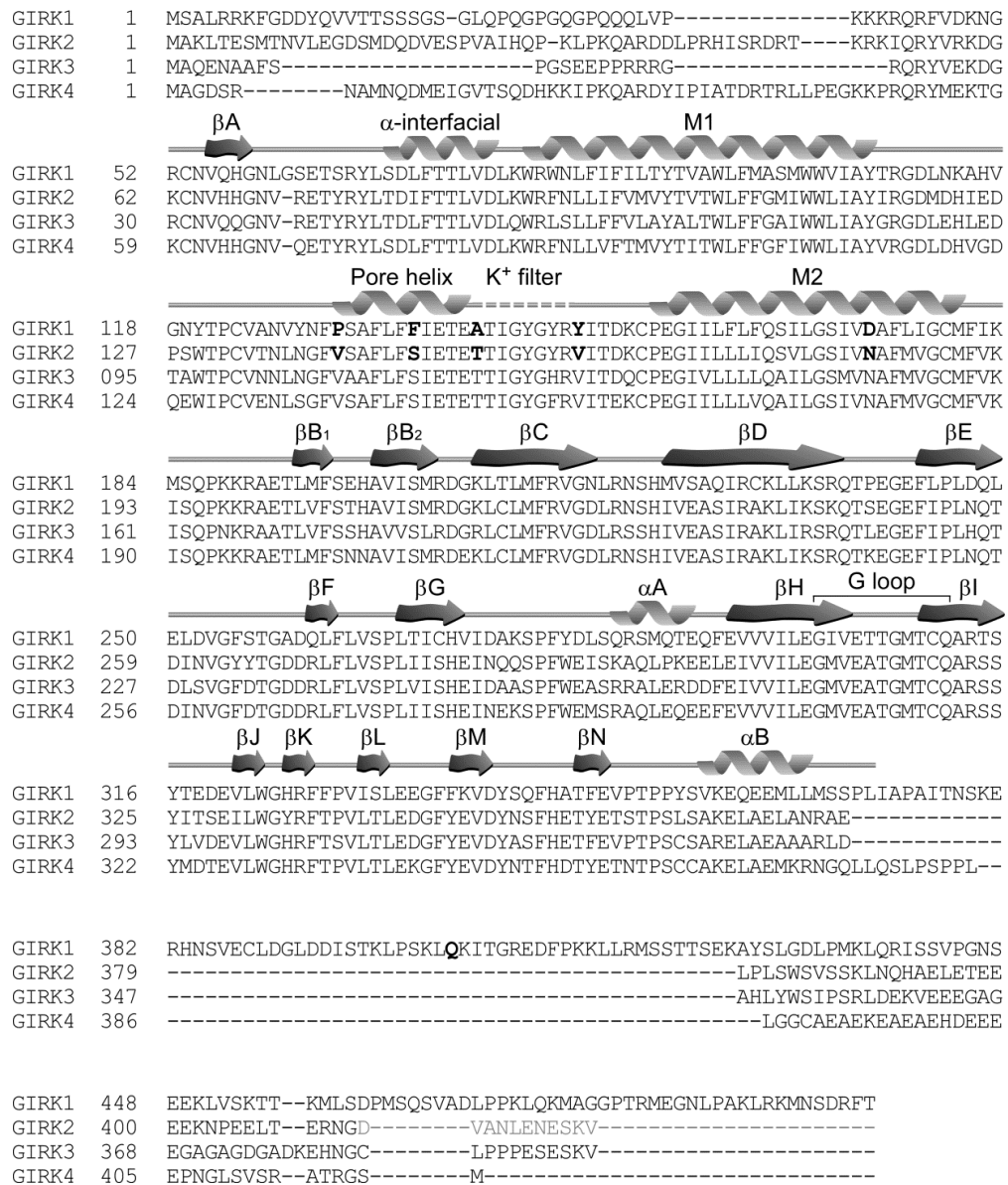


**Figure 1.2. GIRK subunit alignment and secondary structure.** The four mammalian GIRK channel amino acid sequences are aligned to convey the conserved sequence homology shared by these subunits. Accession numbers: NM008426 (GIRK1), NM010606 (GIRK2), NM008429 (GIRK3), and NM017297 (GIRK4). The bolded residues in the pore helix,  $K^+$  filter, and distal C-terminus are residues studied in Chapters 2 and 3. The light gray sequence at the end of GIRK2 represents the sequence unique to GIRK2C, while the rest of the GIRK2 sequence is shared by GIRK2A and GIRK2C. Secondary structure, adapted from [103], is overlaid onto sequences to map specific regions as they relate to cofactor interactions and gating. Spiral shapes represent  $\alpha$ -helices and arrows represent  $\beta$ -sheets. The lines that connect these structures are loops.

## **Structural and functional differences among GIRK subunits**

### *PDZ binding motifs*

A PDZ binding motif is located at the end of the C-terminus of both GIRK2C and GIRK3 that is absent from GIRK1, GIRK4, and other GIRK2 isoforms. The presence of this PDZ binding motif seems to confer differences in expression and/or function. In terms of expression, GIRK2C forms more surface channels relative to GIRK2A [68]. On GIRK3, this PDZ binding motif is thought to negatively regulate the level of GIRK channels at the cell surface. The PDZ binding motif on GIRK3 has been shown to interact with Sorting Nexin 27 (SNX27), a protein that associates with the early endosome, causing GIRK3-containing channels to be internalized at a higher rate relative to non-GIRK3-containing channels [107]. While GIRK2C has been shown to interact with SNX27, it is believed that internalization is specific to GIRK3, as the surface expression of GIRK2C is unaffected by SNX27 [107]. GIRK3 is thought to play more of a regulatory role, as the genetic ablation of *Girk3* does not affect hippocampal GIRK currents [82]. The difference between the behavior of the PDZ binding motifs of GIRK2C and GIRK3 could be attributed to the strength of the forward trafficking motif of GIRK2C, and the presence of the lysosomal targeting signal in GIRK3. There is yet to be a function associated with the PDZ binding motif of GIRK2C, but a few binding partners have been suggested in the literature: PSD95, SNX27, and SAP97 [88, 107, 108]. Some data suggest that there is a potential difference in trafficking or intracellular compartmentalization between GIRK2A and GIRK2C, but more studies are needed [109].

### *GIRK1-containing channels*

There are inherent differences in channels containing GIRK1, as compared to channels lacking GIRK1. First, single channel properties are altered. For example, heteromeric channels that contain GIRK1 exhibit relatively long mean open times of 1-2 ms, whereas GIRK2 homomeric channels demonstrate short mean open times of <0.5 ms [66, 70, 73, 110]. Next, binding affinities for cofactors PIP<sub>2</sub> and Na<sup>+</sup> differ across subunits. GIRK1-containing channels have a higher binding affinity for PIP<sub>2</sub> relative to GIRK2 homomers [111]. In addition, GIRK2 and GIRK4 subunits contain the residue needed for Na<sup>+</sup> binding (GIRK2 D226; GIRK4 D223), where GIRK1 does not (GIRK1 N217) [97-99]. Finally, GIRK1-containing channels demonstrate robust receptor-induced currents compared to their homomeric counterparts as observed in whole-cell patch-clamp electrophysiology experiments [82]. The mechanisms underlying single-channel and whole-cell electrophysiological properties unique to GIRK1-containing channels are explored in the work described in Chapter 2.

### *Chimeric and mutagenesis studies*

Early structure-function studies of GIRK channels were successful in identifying regions essential for important channel interactions and inherent channel properties. For example, a chimeric study comparing different regions of GIRK1 to those of IRK1 (Kir2.1) was used to identify the regions of GIRK channels required for their hallmark interaction with Gβγ long before crystallography was used to study channel gating [110]. This chimeric method was further used in exploring inherent structures of GIRK channels that lead to enhanced channel activity [112-115]. The success of these studies is what led

to the selection of this chimeric method for the work in Chapter 2, as the structural determinants for robust GIRK1-containing channel activity remained unclear. As such, this work used a chimeric strategy to exchange GIRK2 domains for homologous GIRK1 domains to elucidate the important structures and mechanisms that underlie the robust activity of GIRK1-containing channels.

### **Temporal regulation of G Protein signaling**

The strength of G protein-dependent signaling can be regulated at the G protein level by multiple mechanisms. The activation and deactivation kinetics associated with the opening of GIRK channels are dependent upon the binding efficiency of  $G\beta\gamma$  to the channel and the inherent GTPase activity of  $G\alpha_{i/o}$  which can release or sequester  $G\beta\gamma$  depending on its state [116-118]. The  $G\alpha$  subunit can be modulated by proteins that accelerate GTPase activity, influence the nucleotide exchange of GDP to GTP, or interrupt protein-protein interactions between G protein subunits[119]. For example, Activators of G protein Signaling (AGS) proteins can promote guanine nucleotide exchange in a similar manner to GPCRs or compete with  $G\beta\gamma$  to bind GDP- $G\alpha$  causing free  $G\beta\gamma$  without GPCR activation [120-122]. Regulators of G protein Signaling (RGS) proteins on the other hand, promote hydrolysis of the GTP bound to active  $G\alpha$  subunits [123, 124] (**Fig. 1.1**). These proteins have a highly-conserved RGS domain of about 120 amino acid residues that has GTPase-Accelerating Protein (GAP) activity [125]. RGS proteins are divided into subfamilies based on the identity of their other functional domains, many of which may determine affinity or selectivity for different  $G\alpha$  isoforms [126, 127].



### *Subfamilies of RGS proteins*

There are over 30 RGS proteins that are divided into four subfamilies (R4, R7, R12, RZ), some of which have other functional domains that mediate protein-protein interactions, subcellular localization, target specificity, and protein stability [128, 129]. Only the R4 and R7 subfamilies will be discussed here, as their members are key players in Chapters 4 and 5. Members of the large R4 RGS subfamily contain only the RGS domain and small N- and C-terminal regions. These proteins are often anchored to the membrane by their N-terminal domains, which contain an amphipathic helix that can directly interact with phospholipids [130]. Nearly all R4 RGS proteins can bind and have GAP activity for all  $G\alpha_q$  and  $G\alpha_{i/o}$  isoforms [124, 131]. Notably, RGS4 belongs to this family.

The R7 RGS family has four members: RGS6, RGS7, RGS9, and RGS11. In addition to an RGS domain, these proteins contain a G protein Gamma-like (GGL) domain, a Disheveled, Egl-10, Pleckstrin (DEP) domain, and a DEP helical extension (DHEX) domain [132]. The GGL domain very specifically binds one  $G\beta$  isoform:  $G\beta 5$  [133, 134]. The coiled-coil interaction between an R7 RGS protein and  $G\beta 5$  is integral to the protein stability of R7 RGS proteins [135]. Without  $G\beta 5$ , these proteins undergo proteolytic degradation [136]. The DEP domain and DHEX domain form a single functional domain that allows R7 RGS proteins to interact R7BP (R7 family Binding Protein) [137]. R7BP is anchored to the plasma membrane and functions to stabilize and localize R7 RGS proteins to the plasma membrane through their interaction with the DEP/DHEX domain [138].

### *RGS proteins and GIRK channels*

Kinetics of GIRK activation and deactivation are much slower in reconstituted systems compared to that of physiological systems [139]. By expressing RGS proteins in reconstituted systems, activation and deactivation kinetics of GIRK channels are restored to rates comparable to those observed in physiological conditions. This has been demonstrated with several members of the R4 RGS family, including RGS4 [140-144]. There is some evidence of protein-protein interactions between RGS proteins and GIRK channels. GIRK1 and GIRK4 have been co-immunoprecipitated with RGS4 [145]. RGS7/G $\beta$ 5 can be co-immunoprecipitated by GIRK1, GIRK2 and GIRK3 [146].

### **Pharmacology of GIRK channels**

GIRK channels can be manipulated indirectly by compounds that target GPCRs and G<sub>i/o</sub> proteins, but often other cellular components are also affected. In order to study GIRK channels in a more direct and meaningful way, direct channel manipulation by pharmacological compounds is highly desirable. While several compounds can directly act on GIRK channels, they unfortunately can act on several other types of potassium channels as well. At the beginning of this work (in 2009), the pharmacological landscape of GIRK channels was not nearly as developed as it is today in 2014. The work described in Chapter 3 focuses on the characterization of a new class of selective GIRK activators and inhibitors, specifically the prototype of this drug class: ML297.

### *Girk channel blockers*

Barium and cesium block inwardly-rectifying potassium channels, including GIRK channels, by physically occluding the pore [62]. At higher concentrations, barium is able to block other types of potassium channels; however at 0.1-0.3 mM it is relatively selective for inward-rectifying K<sup>+</sup> channels [62, 147]. Early studies also revealed that quinidine and quinine can fully block GIRK channels [148-150]. Quinine, an anti-malarial compound, also has anti-pyretic, analgesic, and anti-inflammatory effects [151]. Quinidine, a stereoisomer of quinine, is an anti-arrhythmic agent and its main mechanism of action is to block fast inward sodium current in the heart, prolonging QT intervals [152]. While these compounds block GIRK channels, their promiscuity for other ion channels makes them a poor tool for the study of GIRK channels. More recently, Tertiapin, a peptide toxin found in bee venom, was demonstrated to block certain Kir channels, including those that contain GIRK1/GIRK4, as well as certain types of Ca<sup>2+</sup>-gated K<sup>+</sup> channels [153-155]. The synthetic form, rTertiapin-q, blocks the channel pore through an interaction with the amino acid sequence connecting M1 and M2 [156]. rTertiapin-q has been used in many electrophysiology studies of GIRK channels [155, 157, 158].

Small molecule GIRK channel antagonists with a level of specificity for GIRK channels have also been identified. Blood-brain barrier impenetrable drugs that selectively activate or inhibit GIRK1/GIRK4 heterotetramers (the cardiac I<sub>KACH</sub> channel) could represent efficacious therapies for certain types of cardiac arrhythmias. NIP-142 blocks GIRK1/GIRK4 channels expressed in HEK cells, and blocks HERG channels at higher concentrations [159]. Two drugs that can inhibit GIRK1/GIRK4 heteromers

(NTC-801 and NIP-151) showed promise in preclinical studies in the treatment of atrial fibrillation [160, 161]. NIP-151 potently blocks GIRK1/GIRK4 current in reconstituted systems [160]. NTC-801 is a novel, potent, and selective GIRK1/GIRK4 blocker and less-potent GIRK1/GIRK2 blocker [161]. However, there is still a lack of GIRK1/GIRK4 channel activators for the treatment of cardiac disorders.

### *GIRK channel activators*

Compounds that can directly activate GIRK channels include alcohols, naringin, and certain volatile anesthetics [162-165]. Alcohols with up to a 4-carbon length chain activate GIRK1/GIRK2 heteromeric channels; however, those with longer carbon chains act to inhibit GIRK channels [166]. The residues that form the cytosolic alcohol binding pocket observed in IRK1 and GIRK2 are also conserved in GIRK1 [162, 163, 167]. Halothane, a prototypical anesthetic, activates basal GIRK activity, but was shown to block GPCR-agonist-induced currents [165]. Naringin selectively activates GIRK1-containing channels and the structural determinants of this selectivity are GIRK1 residues Y148 and Y150. These residues are located within the extracellular naringin binding site, which overlaps with the rTertiapin-q binding site [164]. The downside of naringin is that, while selective, it lacks in potency [164].

Recently, a new drug class that can selectively activate GIRK channels was identified in a high-throughput screen [168]. These compounds showed selectivity for GIRK1-containing channels [169]. The prototype for this new drug class, named ML297, is not only selective for GIRK1-containing channels, but discerns between GIRK1/GIRK2 and GIRK1/GIRK4 channels [169]. In collaboration with another group,

much of the work identifying structures of GIRK1 shown in Chapter 2 served as a platform for investigating the mechanism of ML297 GIRK1 selectivity discussed in Chapter 3.

### **GIRK channels and disease**

There are subunit-specific constitutive knockout mice that have been studied extensively and have subsequently demonstrated a wide array of phenotypes that suggest roles for GIRK channels in many physiological processes [57, 170]. Because of these knockout studies, GIRK channels are thought to play a role in several disorders, including anxiety, neuropathic pain, epilepsy, addiction, obesity, and arrhythmias [170]. Furthermore, *GIRK* polymorphisms identified in the human population have been linked to disease states. There is a human polymorphism in *GIRK2* that is associated with increased dosing requirements for opioid anti-nociception and another that is associated with ethanol intake and stress [171-173]. The human *GIRK2* gene is located on chromosome 21 and is up-regulated by the trisomy of chromosome 21 that causes Down's syndrome [174, 175]. Surprisingly, there was a significant decrease in contextual recall found in rodent models of a triploid *GIRK2* mutation [176]. Recently, a human polymorphism in *GIRK1* was shown to be genetically linked with schizophrenia [177]. In this study, lower GIRK1 expression levels were observed in post-mortem brains from schizophrenic and bipolar individuals, suggesting that altered GIRK1 expression is linked to schizophrenia and bipolar disorders. There are multiple mutations in the human *GIRK1* and *GIRK4* genes that are associated with long QT syndrome and atrial fibrillation [178-180]. Furthermore, identified mutations of *GIRK4* were found to be associated with

hyperaldosteronism and hypertension [181, 182]. Taken together, GIRK channels are an important target for therapeutic intervention in a number of disorders associated with the brain and the heart.

### **Neuronal and Cardiac GIRK signaling**

Inhibitory G protein signaling cascades through GIRK channels offer a great deal of diversity and complexity. GIRK channels interact with the 5 isoforms of  $G_{i/o}$  proteins which in turn interact with many different GPCRs. GIRK channels have been demonstrated to be downstream effectors for many GPCRs, including adenosine, serotonin, dopamine, opioid, glutamate, adrenergic, GABAergic, and muscarinic receptors [57]. Two well-studied signaling cascades are used in this work to study intrinsic and extrinsic factors that impact GIRK signaling: the neuronal  $GABA_B$ R-GIRK cascade and the cardiac  $M_2$ R- $I_{K_{ACh}}$  cascade.

#### *Neuronal $GABA_B$ R-GIRK*

GABA, or  $\gamma$ -aminobutyric acid, is the main inhibitory neurotransmitter in the nervous system, and it acts on two different receptors:  $GABA_A$  and  $GABA_B$ . The  $GABA_A$  receptor is a chloride ion channel and the  $GABA_B$  receptor is a GPCR coupled to inhibitory  $G_{i/o}$  proteins [183, 184]. The  $GABA_B$  receptor is a functional heterodimer of  $GABA_B$ R1 and  $GABA_B$ R2 subunits [185-188]. Both subunits have the seven transmembrane domain structure characteristic to GPCRs.  $GABA_B$ R1 contains the N-terminal ligand-binding domain and a C-terminal  $\alpha$ -helix that contains an ER retention motif [189, 190].  $GABA_B$ R2 contains the  $G_{i/o}$  protein interaction site in its intracellular

loops, and also a C-terminal  $\alpha$ -helix that forms a coiled-coil interaction with the GABA<sub>B</sub>R1 C-terminal helix [188, 191, 192]. GABA<sub>B</sub>R2 is responsible for membrane trafficking and G protein interaction, while GABA<sub>B</sub>R1 is responsible for ligand binding, together making a functional receptor [190, 193].

GIRK channels are known to act as downstream effectors of GABA<sub>B</sub>Rs in numerous brain regions, including the hippocampus, cerebellum, VTA and substantia nigra, thalamus, locus coeruleus and prefrontal cortex [83, 87, 194-198]. The first evidence of GIRK channels being downstream effectors of the GABA<sub>B</sub>R was identified by electrophysiology in hippocampal slices in 1997 [52]. GIRK and GABA<sub>B</sub>R are known to co-localize sub-cellularly within neurons, and evidence suggests that GABA<sub>B</sub> receptors and GIRK channels are localized in close proximity at the membrane, and in fact may be physically coupled either directly or indirectly through scaffolding proteins [195, 199-201].

#### *Cardiac M<sub>2</sub>R-I<sub>KACH</sub>*

Acetylcholine (ACh) functions within the peripheral and central nervous systems, through several cholinergic receptor subtypes. Nicotinic receptors are ion channels permeable to Na<sup>+</sup>, K<sup>+</sup> and to a lesser extent Ca<sup>2+</sup>. On the other hand, muscarinic receptors are GPCRs that couple to both excitatory G<sub>q</sub> proteins (M<sub>1</sub>, M<sub>3</sub>, and M<sub>5</sub>), and inhibitory G<sub>i/o</sub> proteins (M<sub>2</sub> and M<sub>4</sub>) [202, 203]. The M<sub>2</sub> receptor is often referred to as the atrial muscarinic receptor as it plays a key role in the parasympathetic regulation of heart rate [51, 204]. Ligand binding at this receptor promotes activation of a tetrameric K<sup>+</sup> channel

formed by GIRK1 and GIRK4 subunits, also known as  $I_{KACH}$  [69], which hyperpolarizes the cell, decreases excitability and ultimately reduces heart rate [205, 206].

Temporal regulation of  $M_2R$ - $I_{KACH}$  signaling is thought to be important to cardiac pacing, as vagal control of heart rate occurs rapidly [207]. The kinetics of the endogenous atrial  $M_2R$ - $I_{KACH}$  signaling pathway are fast compared to those measured when the signaling pathway was reconstituted in CHO cells [140]. Interestingly, by co-expressing an RGS protein (RGS4) with  $M_2R$  and  $I_{KACH}$  in CHO cells, the kinetic profile was restored to that observed in atrial myocytes [140].

### **III. SUMMARY**

The last five years have yielded novel structural and pharmacological insights into GIRK channels and their regulation, some of which have been enriched by the work described in this dissertation. The work discussed in Chapters 2 and 3 studies the structural elements in GIRK1 within the context of the  $GABA_B$ R-GIRK cascade in either transfected cells or in cultured hippocampal neurons. Chapter 2 is focused on the mechanism behind the robust channel activity of GIRK1 containing channels and identifying key structural determinants within GIRK1 responsible for it. Chapter 3 is focused on identifying the structural determinants of GIRK1 responsible for the selectivity of ML297 for GIRK1 containing channels. Furthermore, Chapter 3 focuses on the mechanism of ML297 activation of GIRK channels, the efficacy of the drug in cultured hippocampal neurons, and the anxiolytic properties of ML297 when administered in a rodent model.



The work in Chapters 4 and 5 is dedicated to characterizing the RGS proteins involved in the modulation of  $I_{KACH}$ , and their subsequent effect on the parasympathetic regulation of heart rate. The work in Chapter 4 was done right as another study on the same topic was published. In 2008, it was demonstrated that RGS4 was expressed in the mouse sinoatrial node, that genetic disruption of RGS4 slowed down the deactivation kinetics associated with  $I_{KACH}$ , and that it enhanced  $M_2R$ -agonist induced bradycardia [89]. Chapter 4 offers up another RGS protein that regulates the kinetics of  $I_{KACH}$ : RGS6. Subsequent work described in Chapter 5 addresses how both RGS4 and RGS6 work to alter the kinetics of  $M_2R$ - $I_{KACH}$  signaling in the mouse sinoatrial node and the resultant effects on the parasympathetic regulation of heart rate.

## **CHAPTER 2**

### **Structural elements in the GIRK1 subunit that potentiate G protein-gated potassium channel activity**

**Wydeven N, Young D, Mirkovic K, Wickman K. Structural elements in the GirK1 subunit that potentiate G protein-gated potassium channel activity. Proc. Natl. Acad. Sci. USA 2012; 109(52):21492-7**

## Introduction

Many neurotransmitters inhibit neurons by activating receptors linked to heterotrimeric GTP binding proteins (G proteins). A prototypical effector in such signaling pathways is the G protein-gated inwardly-rectifying K<sup>+</sup> (GIRK/K<sub>IR</sub>3) channel (reviewed in [57]). GIRK channels are tetramers, with each subunit possessing intracellular amino (N)- and carboxyl (C)-termini and a core domain containing two transmembrane segments, two short extracellular loops, and a hydrophobic domain (P-loop) that contributes to the pore and K<sup>+</sup> selectivity filter. Four mammalian *Girk* genes have been identified (*Girk1-4*). The classical mode of GIRK channel activation involves the direct binding of Gβγ subunits, which stabilizes a low-affinity interaction between the channel and phosphatidylinositol 4,5-bisphosphate (PIP<sub>2</sub>).

GIRK2 plays a key role in neuronal GIRK channel formation (*e.g.*, [52]). Overlapping expression patterns and the impact of *Girk2* ablation on *Girk1* expression, however, argue that most neuronal GIRK channels contain both GIRK1 and GIRK2 [50, 208]. In support of this contention, *Girk1* ablation yields a near-complete loss of GIRK-dependent signaling in neurons that express GIRK1 (*e.g.*, [82]). These findings are surprising because GIRK2 forms functional homomers in expression systems that exhibit G protein-dependent gating, K<sup>+</sup> selectivity, and inward rectification [73]. Moreover, GIRK2 homomers have been identified in midbrain dopamine neurons [88]. Nevertheless, work in expression systems has shown clearly that GIRK1 potentiates receptor-dependent and receptor-independent currents when co-expressed with GIRK2 or GIRK4 [66, 69, 73, 209].

Many studies have provided insight into the structural basis of channel regulation by G proteins, PIP<sub>2</sub>, and Na<sup>+</sup>, as well as channel gating mechanisms [57]. Most of the relevant structural elements, however, are well-conserved across GIRK subunits and thus cannot explain how GIRK1 potentiates GIRK signaling. Here, we sought new insights into the structural elements unique to GIRK1 that potentiate GIRK channel activity, using mutagenesis approaches exploiting insights from previous biochemical and crystallography studies.

## **Materials and Methods**

*Animals*—Studies adhered to the National Institutes of Health Guide for the Care and Use of Laboratory Animals, and were granted approval by the Institutional Animal Care and Use Committee. The generation of *Girk1*<sup>-/-</sup> mice was described previously [210].

*Molecular biology*—pcDNA3-based expression constructs containing rat GIRK1 (GIRK1-AU5) and mouse GIRK2a (GIRK2-myc) coding sequences served as parent constructs. GIRK1 C-terminal deletion constructs were generated by polymerase chain reaction (PCR). GIRK1/GIRK2 chimeras were generated by overlap extension PCR. Point mutations were introduced using the Quickchange II XL kit (Agilent Technologies). All constructs were validated by DNA sequencing. Expression constructs for human Gβ1 (FLAG-Gβ1) and Gγ2 (HA-Gγ2) were purchased from the Missouri S&T cDNA Resource Center.

*Cell culture and biochemistry*—For biochemical assays, HEK293FT cells (Invitrogen™ /Life Technologies) were transfected using the calcium phosphate

technique and collected for analysis 36-54 h later. For electrophysiological studies, HEK293 cells (ATCC) were transfected with Lipofectamine<sup>TM</sup> LTX reagent (Invitrogen<sup>TM</sup>/Life Technologies); experiments were conducted 18-36 h later. Some cells were treated with pertussis toxin (Tocris Bioscience) for 12-18 h prior to electrophysiological characterization. Primary cultures of hippocampal neurons were prepared as described [146]. For quantitative reverse transcriptase PCR (qRT-PCR) and biotinylation studies, neurons were plated onto 3-cm petri dishes and kept in culture for 10-12 days prior to experimentation. qRT-PCR conditions for *GABA<sub>B</sub>RI* and *Girk2* were described previously [211].

Immunoblotting and HEK cell biotinylation experiments were performed as described [212]. Blots were probed with primary antibodies targeting c-myc (11667149001, 1:500; Hoffmann-La Roche),  $\beta$ -actin (ab6276, 1:10,000; Abcam), AU5 (A190-227A, 1:1,000; Bethyl Laboratories), or GIRK2 (APC-006, 1:200; Alomone Labs), and either donkey anti-mouse (926-32212, 1:7,000; LI-COR Biosciences) or anti-rabbit (926-68072, 1:7,000; LI-COR) secondary antibodies. Blots were developed and band intensities quantified using the Odyssey<sup>®</sup> Infrared imaging system (LI-COR).

*Electrophysiology*—Conditions for measuring baclofen-induced whole-cell GIRK currents were described previously [146]. Receptor-independent (basal) GIRK current was determined by measuring the decrease in holding current in the high-K<sup>+</sup> bath solution evoked by 0.3 mM Ba<sup>2+</sup>. Measured and command potentials were not corrected for liquid junction potential. An Axopatch 200B patch clamp amplifier (Molecular Devices) was used for measurement of cell-attached, single-channel activity. Borosilicate patch pipettes (4-6 M $\Omega$ ) were filled with (in mM): 150 KCl, 1 MgCl<sub>2</sub>, 5 EGTA/KOH, 5

HEPES/KOH, and 0.1 baclofen (pH 7.4). To zero the cell membrane potential, baclofen-induced single channel activity was measured in a high-K<sup>+</sup> (150 mM) bath solution (in mM): 150 KCl, 1.8 CaCl<sub>2</sub>, 0.5 MgCl<sub>2</sub>, 5.5 D-glucose, 5 HEPES/KOH (pH 7.4). Effective zeroing of the membrane potential using this approach was validated by measuring the reversal potential of the high-conductance, weakly-rectifying Trek1 K<sup>+</sup> channel. Immediately after gigaseal formation, membrane potential was clamped at -75 mV, recordings were low-pass filtered at 2 kHz, sampled at 10 kHz, and stored on hard disk for analysis using pCLAMP v. 9.0 software. Analysis of single-channel conductance and mean open time was performed on 5-15 s recordings taken within the 30-s timeframe immediately following seal formation.

*Data analysis*—Data are presented throughout as the mean±SEM. Statistical analyses were performed with Prism 5 (GraphPad Software). Group comparisons were typically made using Student's *t*-test or one-way ANOVA followed by Tukey's HSD *post hoc* test when appropriate. Open-state dwell-time data were analyzed using the Kolmogorov-Smirnoff test, while single channel amplitude data were analyzed with the Kruskal Wallis test, with pairwise comparisons made using Dunn's Multiple Comparison test. In all analyses, the level of significance was set at  $P < 0.05$ .

## **Results**

### *GIRK1-dependent potentiation of GABA<sub>B</sub>R-GIRK signaling*

HEK cells expressing the GABA<sub>B</sub> receptor (GABA<sub>B</sub>R) subunits GABA<sub>B</sub>R1 and GABA<sub>B</sub>R2, along with epitope-tagged GIRK1 and GIRK2, exhibited large currents in response to a saturating concentration of the GABA<sub>B</sub>R agonist baclofen, as well as

receptor-independent or basal ( $\text{Ba}^{2+}$ -sensitive) whole-cell currents (**Fig. 2.1A,B**). In contrast, currents in cells expressing  $\text{GABA}_B\text{R}$  and GIRK2 were small. Consistent with previous observations [199, 213], pre-treatment of cells expressing the GIRK1/GIRK2 heteromer with pertussis toxin, which uncouples  $\text{G}_{i/o}$  G proteins from activated receptors, eliminated the baclofen-induced but not basal current (**Fig. 2.1B**). Thus, GIRK1 potentiates GIRK currents in both receptor-dependent and receptor-independent manners. GIRK2 levels at the cell surface measured using a biotinylation approach were not significantly different with or without GIRK1 present (**Fig. 2.1C,D**). Moreover, the ratio of surface-to-total GIRK2 protein was unaltered, indicating that GIRK1 does not impact the surface trafficking of GIRK2-containing channels.

We also examined the impact of *Girk1* ablation on  $\text{GABA}_B\text{R}$ -GIRK signaling in mouse hippocampal cultures. *Girk1* ablation yielded a dramatic reduction (~80%) in baclofen-induced currents in large pyramidal-shaped neurons (**Fig. 2.2A**). Interestingly, the small residual currents in neurons from *Girk1*<sup>-/-</sup> mice correlated with a significant increase in *GABA<sub>B</sub>R1* and *Girk2* expression (**Fig. 2.2B**). There was no difference, however, in total or surface GIRK2 protein levels in cultures from wild-type and *Girk1*<sup>-/-</sup> mice (**Fig. 2.2C**). Collectively, these data indicate that the potentiating effect of GIRK1 on GIRK currents in heterologous and native systems is not due to increased protein levels or surface targeting of GIRK2.

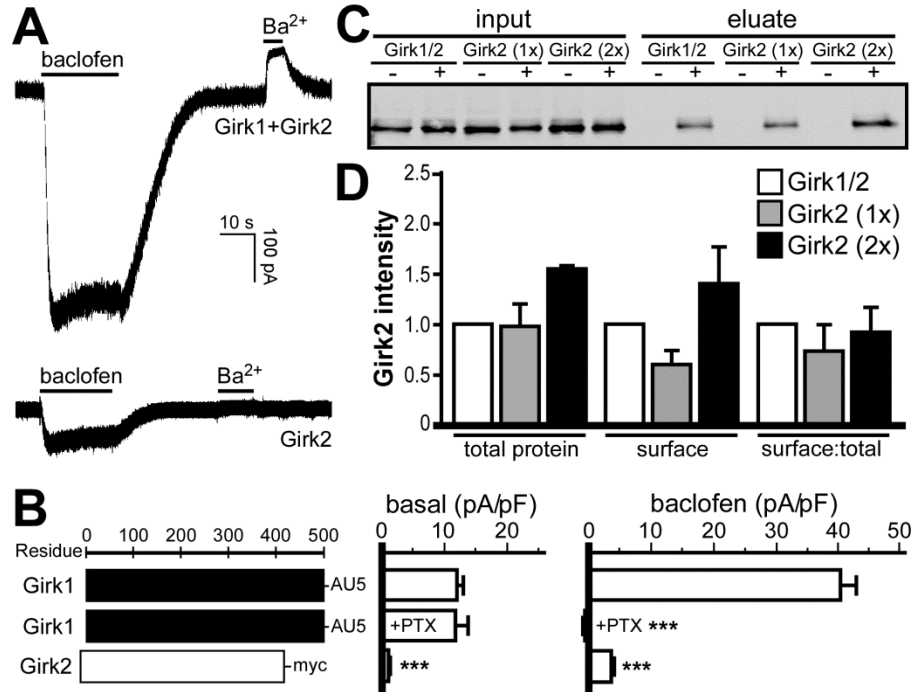


**Figure 2.1. The potentiating influence of GIRK1.** **A)** Baclofen-induced and basal ( $Ba^{2+}$ -sensitive) currents, measured in a high- $K^+$  bath solution (25 mM) at a holding potential of -70 mV, in cells expressing  $GABA_B$ R and either GIRK1/GIRK2 or GIRK2 alone. Bars denote the duration of baclofen (100  $\mu$ M) and  $Ba^{2+}$  (0.3 mM) applications. **B)** Summary of currents measured in cells expressing GIRK2 and  $GABA_B$ R, along with the subunit depicted on the left ( $n=15-61$ /group). GIRK2 homomeric currents were measured in cells transfected with double (2x) the amount of GIRK2 used in cells transfected with GIRK1 and GIRK2. A subset of cells expressing GIRK1/GIRK2 was pre-treated (24 h) with pertussis toxin (PTX, 0.1 ng/ml). A significant impact of group was observed for basal ( $F_{2,94}=9.5$ ,  $P<0.001$ ) and baclofen-induced ( $F_{2,98}=61.1$ ,  $P<0.001$ ) currents. Symbols: \*\*\*  $P<0.001$ , respectively, vs. GIRK1/GIRK2. **C)** Blot from a biotinylation experiment probing total and surface GIRK2 protein levels in cells transfected with GIRK1 and GIRK2 (GIRK1/2), GIRK2 alone (1x), and GIRK2 alone at twice the concentration (2x). **D)** Quantification of biotinylation data ( $n=3$  separate experiments). No significant differences were detected between groups.



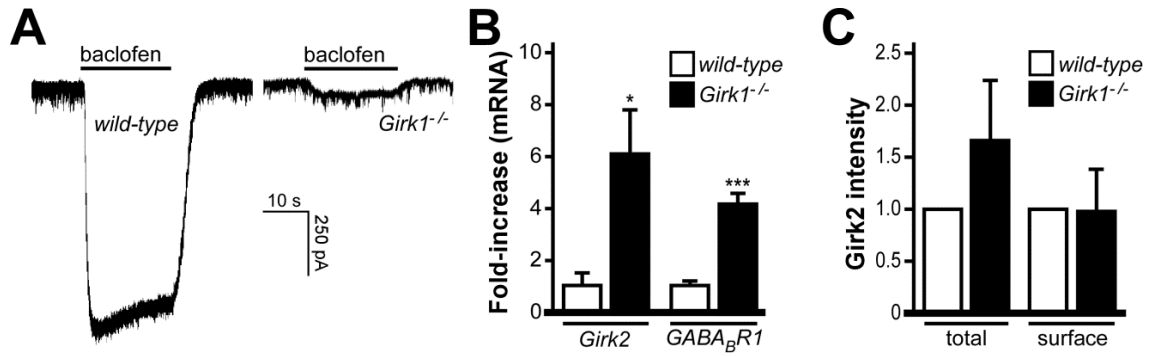


**Figure 2.2. GIRK1-dependent potentiation of GABA<sub>B</sub>R-GIRK currents in hippocampal neurons.** **A)** Representative currents induced by baclofen (100  $\mu$ M) in hippocampal neurons from wild-type ( $7.3 \pm 1.0$  pA/pF, n=8) and *Girk1*<sup>-/-</sup> ( $1.6 \pm 0.3$  pA/pF, n=10;  $P < 0.001$ ) mice. **B)** qRT-PCR analysis of *GABA<sub>B</sub>R1* and *Girk2* expression in hippocampal cultures from wild-type and *Girk1*<sup>-/-</sup> mice (n=3 separate cultures). Symbols: \*,\*\*\*  $P < 0.05$  and  $0.001$  vs. wild-type. **C)** Total and surface GIRK2 protein in hippocampal cultures from wild-type and *Girk1*<sup>-/-</sup> mice (n=3 separate cultures).

### *Influence of the distal C-terminus*

Multiple intracellular domains have been implicated in the binding of G $\beta$  $\gamma$  to GIRK subunits [57]. These elements are highly-conserved across GIRK subunits, however, and thus cannot explain the potentiating influence of GIRK1. While the unique distal C-terminal GIRK1 domain between residues 390-462 does not bind G $\beta$  $\gamma$  directly, it has been shown to enhance the binding of the GIRK1 C-terminus to G $\beta$  $\gamma$  [214]. As such, we used a targeted deletion strategy to probe the functional relevance of this and surrounding domains (**Fig. 2.3**). The deletion mutants were expressed at levels comparable to GIRK1 (**Fig. 2.4A,B**), and the protein levels and surface trafficking of GIRK2 was comparable in cells expressing GIRK1 or deletions (**Fig. 2.4C-E**).

Basal and baclofen-induced currents were measured in cells transfected with GIRK1 deletion constructs, GIRK2, and GABA<sub>B</sub>R (**Fig. 2.3A**). The first construct tested (GIRK1 $\Delta$ 462) revealed that the last 39 amino acids of GIRK1 are not required for normal basal or GABA<sub>B</sub>R-dependent GIRK currents. Basal current for GIRK1 $\Delta$ 409/GIRK2 and GIRK1 $\Delta$ 406/GIRK2 heteromers was, however, significantly lower than those measured for GIRK1/GIRK2, while GABA<sub>B</sub>R-dependent GIRK currents were preserved. Further deletion (GIRK1 $\Delta$ 399) correlated with a significant decrease in baclofen-induced GIRK currents. Thus, structures between residues 409 and 462 uniquely support robust basal activity, while residues 399-406 are important for robust GABA<sub>B</sub>R-dependent GIRK currents.

A sharp distinction in baclofen-induced currents was observed for GIRK1 $\Delta$ 406/GIRK2 and GIRK1 $\Delta$ 403/GIRK2 heteromers. Mutation of the pertinent

residues individually to alanine (Q404A, K405A, I406A), in the context of the GIRK1 $\Delta$ 406 backbone, identified Q404 as a possible determinant of robust receptor-induced current (**Fig. 2.3B,C**). Basal current observed with the GIRK1(Q404A) mutation was smaller than GIRK1 $\Delta$ 406, though this difference was not statistically significant.

We next engineered the Q404A mutation into full-length GIRK1. While basal activity was not different in cells expressing GABA<sub>B</sub>R, GIRK2, and either GIRK1 or GIRK1(Q404A), baclofen-induced currents were ~30% lower in cells expressing GIRK1(Q404A) (**Fig. 2.5A**). This difference was not related to reduced expression of GIRK1(Q404A) (**Fig. 2.6A,B**), or to a negative influence of GIRK1(Q404A) on the protein level or surface trafficking of GIRK2 (**Fig. 2.6C,D**). The EC<sub>50</sub> for baclofen activation of GIRK1(Q404A)/GIRK2 heteromers (0.76  $\mu$ M; 0.52-1.11  $\mu$ M, 95% CI), measured by sequential application of increasing baclofen concentrations (0.01-300  $\mu$ M), was slightly but significantly greater ( $F_{1,42}=4.3$ ;  $P<0.05$ ) than that measured for GIRK1/GIRK2 (0.47  $\mu$ M; 0.36-0.61  $\mu$ M, 95% CI). When co-expressed with GIRK2 and G $\beta\gamma$  (G $\beta_1$  and G $\gamma_2$ ), GIRK1 and GIRK1(Q404A) supported robust and indistinguishable Ba<sup>2+</sup>-sensitive currents (**Fig. 2.5B,C**). Collectively, these data are consistent with a role for Q404 in enhancing the channel-G $\beta\gamma$  interaction.

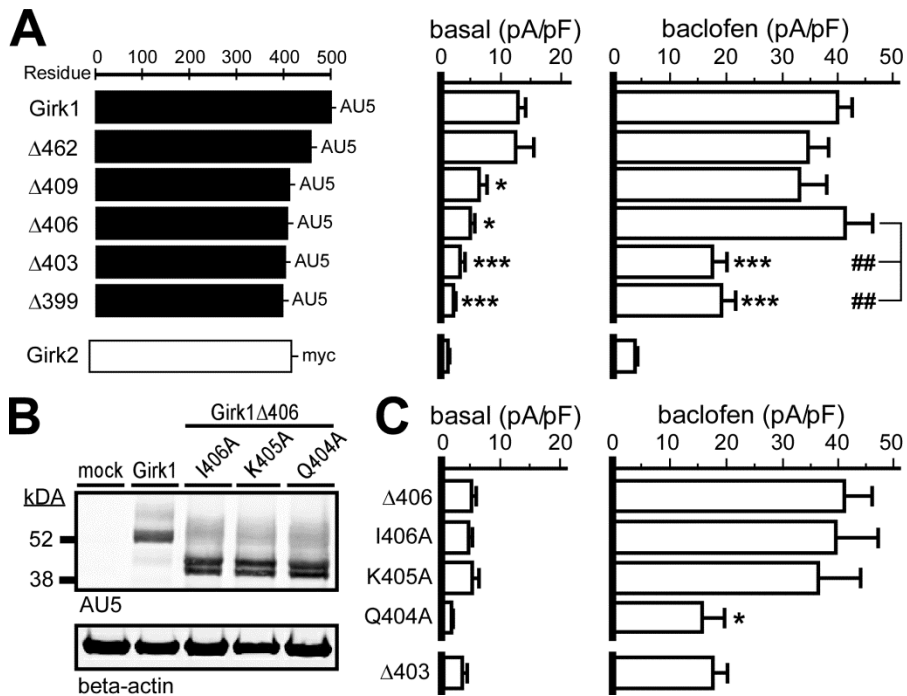


**Figure 2.3. Impact of the GIRK1 distal C-terminus.** **A)** Basal and baclofen-induced currents in cells expressing GABA<sub>B</sub>R, GIRK2, and the subunit depicted on the left (n=12-61/group). A significant impact of group was observed for basal ( $F_{5,137}=8.4$ ,  $P<0.001$ ) and baclofen-induced ( $F_{5,141}=6.7$ ,  $P<0.001$ ) currents. Symbols: \*,\*\*\*  $P<0.05$  and 0.001, respectively, vs. GIRK1/GIRK2; ##  $P<0.01$  vs. GIRK1 $\Delta$ 406/GIRK2. GIRK2 homomeric basal and baclofen-induced currents are shown for comparison, but were not included in the analysis. **B)** Immunoblot of I406A, K405A, and Q404A point mutants, generated on the GIRK1 $\Delta$ 406 backbone. **C)** Basal and baclofen-induced currents in cells expressing GABA<sub>B</sub>R, GIRK2, and the construct depicted on the left (n=8-18/group). A significant impact of group was observed for baclofen-induced ( $F_{3,42}=3.0$ ,  $P<0.05$ ) but not basal ( $F_{3,41}=2.6$ ,  $P=0.06$ ) current. Symbols: \*  $P<0.05$  vs. GIRK1 $\Delta$ 406/GIRK2.

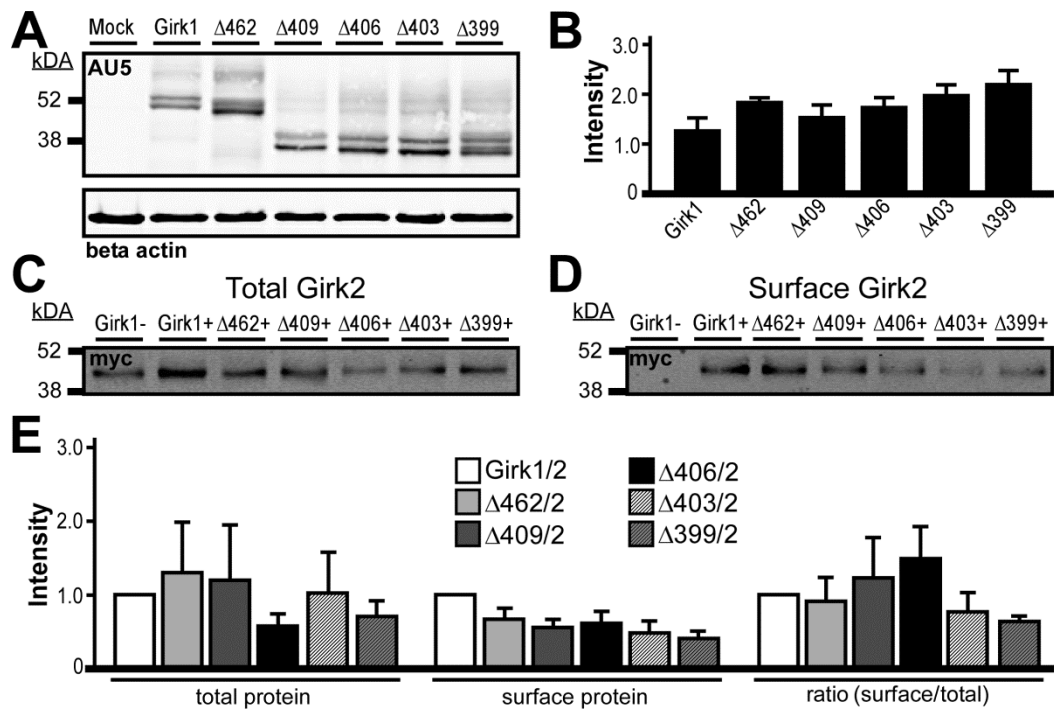


**Figure 2.4. Characterization of GIRK1 C-terminal deletion constructs.** **A)** Expression levels of AU5-tagged GIRK1 and GIRK1 deletion mutants were assessed by immunoblotting. **B)** The summed intensity of core and core-glycosylated forms of GIRK1 (doublet) was normalized to  $\beta$ -actin (lower blot). All mutants expressed at or slightly above the level of GIRK1 ( $F_{6,20}=1.4$ ,  $P=0.3$ ;  $n=3$  separate transfections). **C,D)** Representative blots from a biotinylation experiment measuring total and surface myc-tagged GIRK2 protein level in cells transfected with GIRK2 and either GIRK1 or GIRK1 deletion mutant. **E)** Quantification of biotinylation data. No significant impact of group was found for total ( $F_{6,27}=0.3$ ,  $P=0.95$ ) or surface ( $F_{6,27}=2.3$ ,  $P=0.1$ ) GIRK2 protein ( $n=4$  separate experiments).

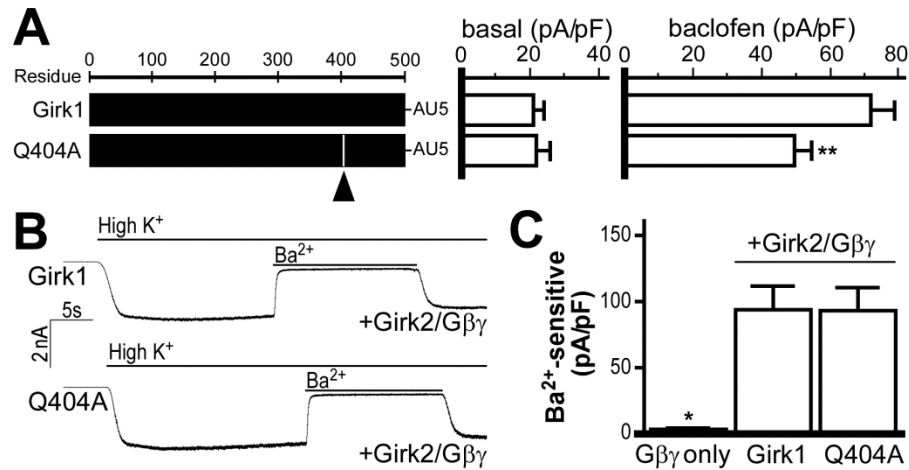


**Figure 2.5. Impact of Q404.** **A**) Basal and baclofen-induced currents in cells expressing  $GABA_B$ R, GIRK2, and the depicted construct ( $n=19-20$ /group). A significant difference between groups was observed for baclofen-induced ( $t_{37}=2.8$ ,  $P<0.01$ ) but not basal ( $t_{35}=0.2$ ,  $P=0.9$ ) current. Symbols: \*\* $P<0.01$  vs. GIRK1. **B**)  $Ba^{2+}$ -sensitive currents measured in high- $K^+$  bath solution in cells expressing  $G\beta 1\gamma 2$  and either GIRK1/GIRK2 or GIRK1(Q404A)/GIRK2 ( $V_{hold} = -70$  mV). Bars denote the duration of  $Ba^{2+}$  (0.3 mM) application. **C**) Summary of  $Ba^{2+}$ -sensitive currents in cells transfected with  $G\beta 1\gamma 2$  and empty vector ( $G\beta\gamma$  only), GIRK1/GIRK2, or GIRK1(Q404A)/GIRK2. A significant impact of group was observed ( $F_{2,29}=4.6$ ,  $P<0.05$ ). Symbols: \*  $P<0.05$ , respectively, vs. GIRK1.

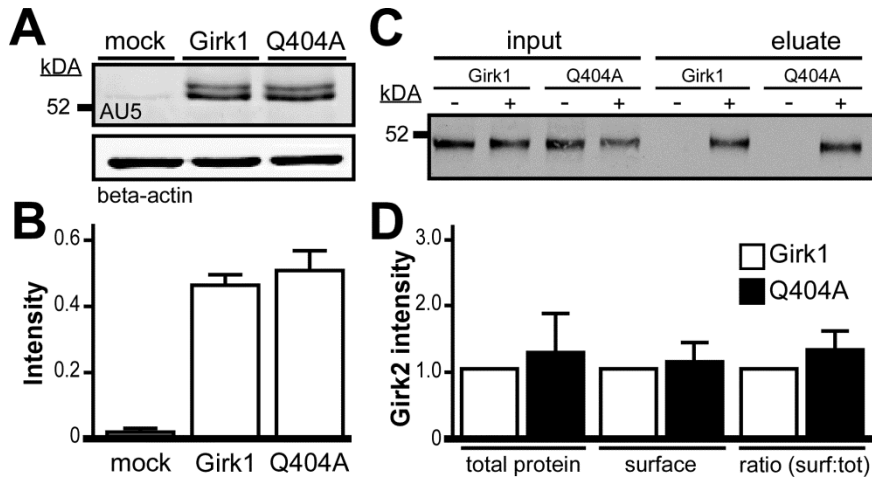


**Figure 2.6. Characterization of GIRK1(Q404A) mutant.** **A,B)** Expression of AU5-tagged GIRK1 and GIRK1(Q404A) was assessed by quantitative immunoblotting, with the summed intensity of core and core-glycosylated forms of GIRK1 normalized to  $\beta$ -actin. Levels of GIRK1(Q404A) were not different from GIRK1 ( $t_6=0.6$ ,  $P=0.6$ ;  $n=3$ ). **C)** Blot from a biotinylation experiment measuring total and surface GIRK2 protein levels in cells transfected with GIRK1/GIRK2 or GIRK1(Q404A)/GIRK2. **D)** Quantification of biotinylation data. No differences were observed for total ( $t_4=0.5$ ,  $P=0.7$ ) or surface ( $t_4=0.4$ ,  $P=0.7$ ) GIRK2 protein levels ( $n=5$ ).

### *Impact of the GIRK1 core*

Baclofen-induced currents observed for GIRK1 $\Delta$ 399/GIRK2 were significantly larger than those carried by GIRK2 homomers ( $t_{34}=5.6$ ,  $P<0.001$ ), arguing that structures between residues 1-399 also contribute to the GIRK1-dependent potentiation of GIRK channel activity. Unfortunately, GIRK1 expression levels declined with more aggressive deletions (not shown). As such, we generated 3 chimeras incorporating N-terminal (GIRK1 residues 1-85), core (GIRK1 residues 86-180), or C-terminal (GIRK1 residues 181-501) domains from GIRK1 within a GIRK2 backbone, and expressed them with GIRK2 and GABA<sub>B</sub>R (**Fig. 2.7**). All three chimeras (NT, TM, CT) were expressed at higher levels than GIRK1 (**Fig. 2.8A**), but none significantly altered the surface trafficking of GIRK2 (**Fig. 2.8B**). Only the GIRK1 core domain (TM) conferred a partial but significant potentiation of basal and baclofen-induced currents (**Fig. 2.7A**).

Single channel conductance and mean open time values are larger for GIRK1-containing channels than GIRK1-lacking counterparts [69, 112]. Enhancement of these unitary properties should increase basal and receptor-induced whole-cell GIRK currents. Thus, we next measured single channel conductance and mean open times of baclofen-activated GIRK channels in cells expressing GIRK1/GIRK2, GIRK2 alone, or TM/GIRK2. In cells expressing GIRK1 and GIRK2, most channel openings were reasonably well-resolved (**Fig. 2.7B**), exhibiting a prominent single-channel conductance of 35 pS (**Table 2.1, Fig. 2.8C**). The open-state dwell time data for GIRK1/GIRK2 heteromers was modeled best with two terms (0.4 and 2.2 ms; **Table 2.1, Fig. 2.8D**). In cells expressing GIRK2 homomers, events were less well-resolved; analysis revealed a single channel conductance of 11 pS and a mean open time of 0.3 ms. Channels observed



in cells expressing TM and GIRK2 exhibited an intermediate conductance (21 pS) and mean open times (0.4 and 1.7 ms), values significantly different from those of both GIRK1/GIRK2 heteromers and GIRK2 homomers (**Table 2.1**). These data suggest that larger whole-cell currents seen in cells expressing TM/GIRK2 as compared to GIRK2 homomers can be attributed, at least in part, to an enhancement of single-channel conductance and mean open time.

A second set of chimeras with overlapping GIRK1 content was generated to better resolve potentiating elements within the 95-residue domain (**Fig. 2.9**). The 3 chimeras (M1-P, P, P-M2) were expressed at levels comparable to the TM chimera (**Fig. 2.10A,B**). Single channel conductance and open times were significantly lower for all 3 chimeras relative to TM, but significantly greater than those for GIRK2 homomers (**Table 2.1**). All 3 chimeras supported basal currents comparable to those measured for the TM chimera (**Fig. 2.9B**), implicating the GIRK1 P-loop as a key potentiating influence on basal channel activity. Interestingly, baclofen-induced currents supported by the M1-P and P (but not P-M2) chimeras were significantly larger than those measured for the TM chimera, indicating that the GIRK1 P-loop also enhances GABA<sub>B</sub>R-GIRK current, and that this influence is tempered by structural content between GIRK1 residues 150 and 180.

Six residues differ between GIRK1 and GIRK2 within this region, and all are found within the M2 domain (**Fig. 2.9A**). To identify the structural basis for the inhibitory influence of the M2 domain, we introduced GIRK1-specific residues into the M2 domain of the P chimera, focusing on three substitutions predicted to exert the most significant structural impact (L173F, I175F, N184D). While cells expressing GABA<sub>B</sub>R,

GIRK2, and either P(I175F) or P(N184D) exhibited basal and baclofen-induced currents comparable to or greater than cells expressing the TM chimera, currents supported by the P(L173F) mutant were indistinguishable from those seen in cells expressing TM. Moreover, baclofen-induced currents in cells expressing P(L173F) were significantly lower than currents measured in cells expressing the P chimera (**Fig. 2.9C**). The single channel conductance (but not mean open time) measured in cells co-expressing GIRK2 and P(L173F) was also significantly lower than that measured for the P chimera (**Table 2.1**). Collectively, these data suggest that residue F162 in the GIRK1 M2 domain is a selective inhibitory influence on the receptor-dependent gating of heteromeric GIRK channels.

Only four residues differ between GIRK1 and GIRK2 within the P-loop (**Fig. 2.11A**). To determine which residue(s) confer potentiation of basal and baclofen-induced currents, we generated GIRK2 point mutants containing one or more GIRK1 residues at the analogous positions. No enhancement of basal activity was observed when the single mutants were co-expressed with GIRK2 (**Fig. 2.11C**). GIRK2(S148F) did tend to support larger baclofen-induced currents, despite the fact that total protein levels for this mutant were significantly lower than GIRK2 (**Fig. 2.12**). Mean open-time for channels in cells expressing GIRK2(S148F) and GIRK2, however, was significantly longer than that of a GIRK2 homomer, suggesting that the mutant was expressed and available to influence the unitary properties of the expressed channel.

We next evaluated the GIRK2(S148F/T153A) double mutant, or FA mutant, reasoning that this dual substitution would promote a redistribution of intra-subunit interactions. T153 in GIRK2 is located at the junction between the K<sup>+</sup> selectivity filter

and pore helix (**Fig. 2.11B**), and it participates in an intra-subunit interaction with W106. Introduction of the GIRK1-specific alanine at this position should preclude this interaction and foster an intra-subunit interaction between W106 and the GIRK1-specific phenylalanine incorporated at position 148. Total expression levels of the FA mutant were, like GIRK2(S148F), significantly lower than GIRK2 (**Fig. 2.12**). Basal activity and unitary channel properties measured in cells expressing FA and GIRK2 was comparable to those seen in cells expressing GIRK2(S148F), and while baclofen-induced currents were larger than those measured in cells expressing GIRK2(S148F), the difference was not significant (**Fig. 2.11C**).

V142P and V161Y substitutions were next introduced independently to the FA mutant to generate PFA and FAY triple mutants. Introduction of the proline at position 142 should cause a premature termination of the pore helix, while the V161Y substitution should strengthen inter-subunit interactions by promoting aromatic stacking with Y159 (conserved in all GIRK subunits) in the adjacent GIRK subunit (**Fig. 2.11B**). PFA protein levels were low in whole-cell extracts from transfected cells (**Fig. 2.12**), and PFA/GIRK2 co-expression yielded basal and baclofen-induced responses comparable to those of GIRK2 homomers. In contrast, total protein levels for FAY were notably higher than those of the PFA, FA, and S148F mutants (**Fig. 2.12**), and FAY/GIRK2 co-expression recapitulated the enhanced basal and baclofen-induced currents seen with the P chimera (referred to as PFAY in **Fig. 2.11C**).

Importantly, reversal potentials for the baclofen-induced currents measured in the high-K<sup>+</sup> recording solution were similar ( $F_{2,16}=2.6$ ,  $P=0.1$ ) for cells expressing GIRK1/GIRK2 ( $-42\pm 1$  mV,  $n=5$ ), P/GIRK2 ( $-33\pm 5$  mV,  $n=5$ ), and FAY/GIRK2 ( $-36\pm 1$

mV, n=7), and were close to the K<sup>+</sup> equilibrium potential (-43 mV). Thus, the potentiation of basal and baclofen-induced currents observed with P chimera and FAY mutant was not attributable to marked alterations in channel selectivity. Moreover, channels measured in cells expressing GIRK2 and FAY or P chimera exhibited significantly longer mean open times and slightly larger single-channel conductances than GIRK2 homomers, arguing that the potentiating influence of these P-loop residues on basal and baclofen-induced currents is mediated, at least in part, by an enhancement of unitary channel properties.

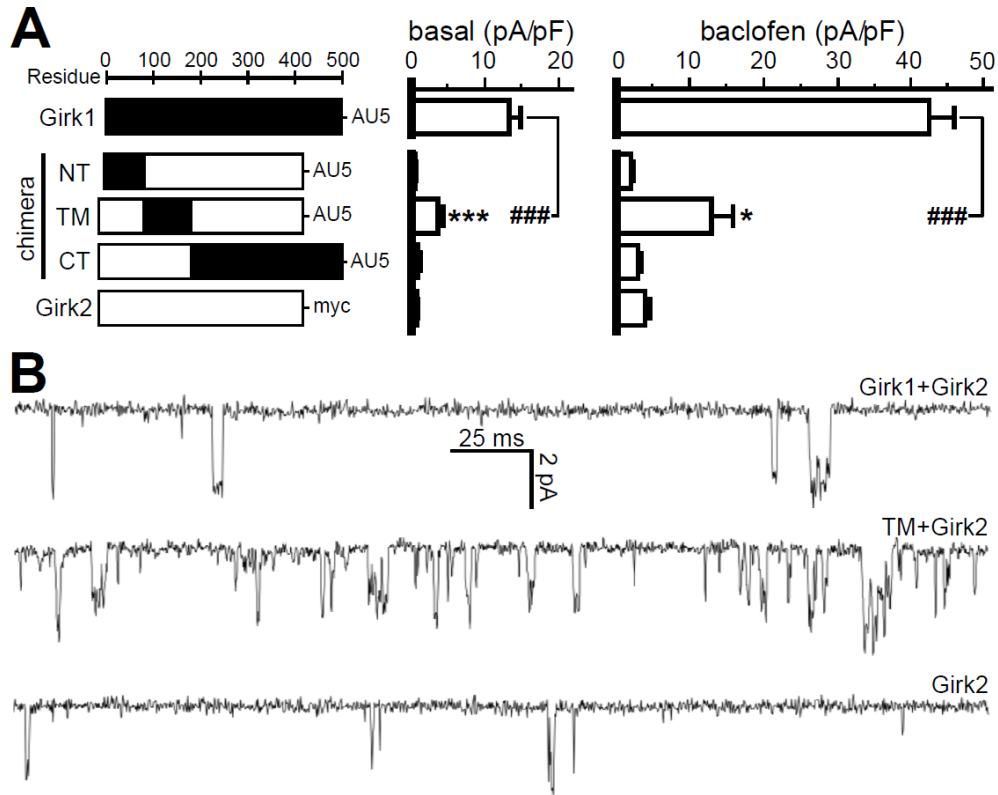


**Figure 2.7. Impact of the GIRK1 core.** **A**) Basal and baclofen-induced currents in cells expressing GABA<sub>B</sub>R, GIRK2, and the depicted construct (n=10-34/group). A significant impact of group was observed for basal ( $F_{5,105}=10.3$ ,  $P<0.001$ ) and baclofen-induced ( $F_{5,110}=10.9$ ,  $P<0.001$ ) currents. Symbols: \*,\*\*\*  $P<0.05$  and  $0.001$ , respectively, vs. GIRK2 homomer; ###  $P<0.001$  vs. GIRK1/GIRK2. **B**) Representative segments (300 ms) of cell-attached recordings ( $V_{\text{hold}} = -75$  mV), measured with 100  $\mu\text{M}$  baclofen in the high- $\text{K}^+$  (150 mM) pipette solution, from cells expressing GABA<sub>B</sub>R, GIRK2, and either GIRK1 (top), TM chimera (middle), or GIRK2 (bottom). A patch with higher activity (and at least 2 channels) is shown for TM to emphasize the profile overlap with GIRK1/GIRK2 heteromers and GIRK2 homomers.

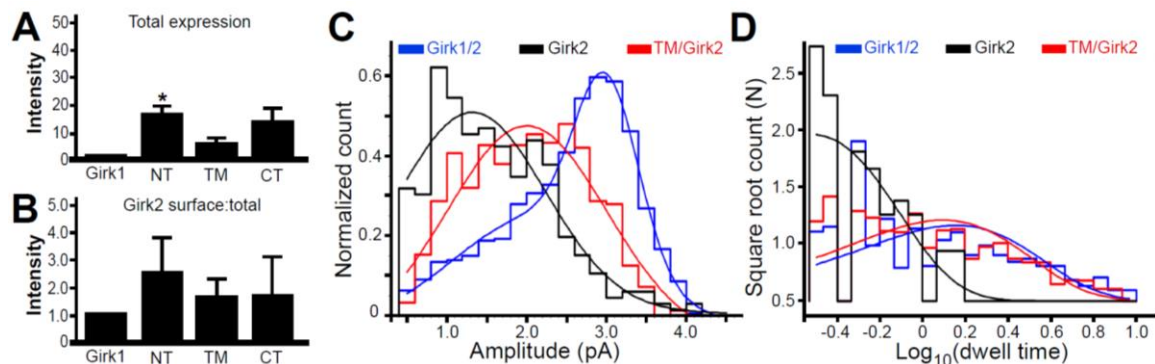


**Figure 2.8. Characterization of GIRK1/GIRK2 NT, TM, and CT chimeras.** **A)** Summary of expression of AU5-tagged GIRK1 and GIRK1 chimeras, as assessed by quantitative immunoblotting (n=3 separate transfections). A significant impact of group was observed ( $F_{3,15}=4.5$ ,  $P<0.05$ ). Symbols: \*  $P<0.05$  vs. GIRK1. **B)** Ratio of surface-to-total GIRK2 protein measured in cells transfected with GIRK2 and either GIRK1 or chimera (n=3 separate transfections); no significant impact of group was observed ( $F_{3,11}=0.3$ ,  $P=0.8$ ). **C,D)** Amplitude and open-state dwell time histograms for channels observed in cells expressing GABA<sub>B</sub>R, GIRK2, and either GIRK1, GIRK2, or TM chimera. Single channel conductance and mean open times were extracted from Gaussian or log exponential fits, respectively, of these data, and are summarized in **Table 2.1**.

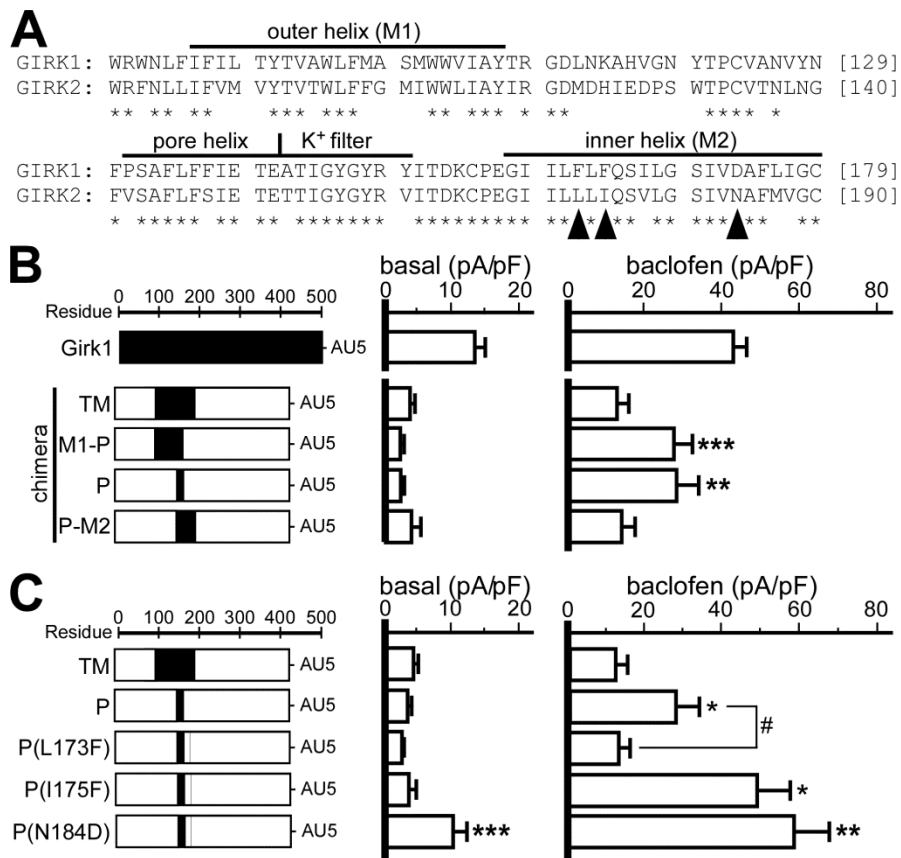


**Figure 2.9. Impact of the GIRK1 P-loop and M2 domain.** **A)** Sequence alignment of GIRK1 and GIRK2 core domains, with key structural elements highlighted. The arrowheads denote 3 residues tested for their influence on the M2-dependent inhibition of baclofen-induced currents. **B)** Basal and baclofen-induced currents in cells expressing GABA<sub>B</sub>R, GIRK2, and the depicted chimera (n=12-22 per group). A significant impact of group was observed for baclofen-induced ( $F_{3,54}=7.6$ ,  $P<0.001$ ) but not basal ( $F_{3,55}=1.0$ ,  $P=0.4$ ) current. Symbols: \*\*,\*\*\*  $P<0.01$  and  $0.001$ , respectively, vs. TM. Basal and baclofen-induced currents for GIRK1/GIRK2 are presented for comparison, but were not included in the statistical analysis. **C)** Basal and baclofen-induced currents in cells expressing GABA<sub>B</sub>R, GIRK2, and the depicted construct (n=7-22/group). A significant impact of group was observed for baclofen-induced ( $F_{4,55}=15.6$ ,  $P<0.001$ ) and basal ( $F_{4,54}=9.8$ ,  $P<0.001$ ) currents. Symbols: \*,\*\*  $P<0.05$  and  $P<0.01$ , respectively, vs. TM; #  $P<0.05$  vs. P.

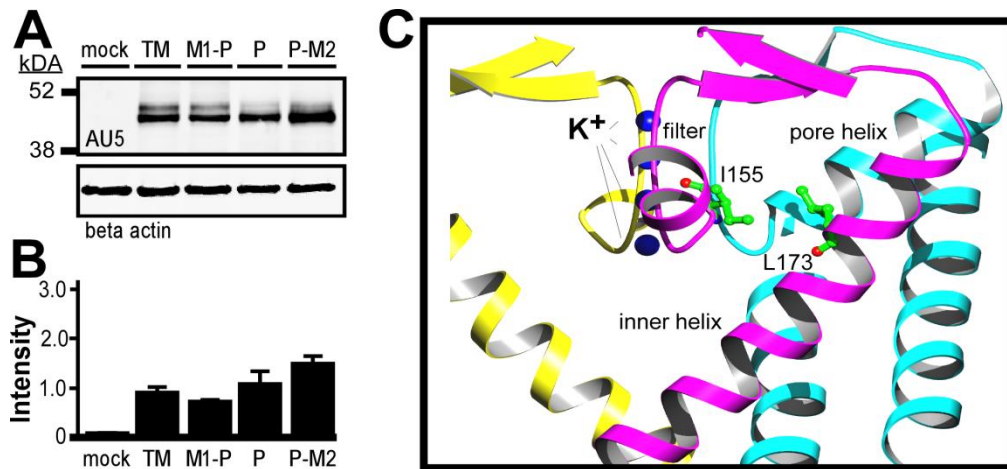


**Figure 2.10. Characterization of GIRK1 core chimeras.** A,B) Quantitative immunoblotting of the AU5-tagged GIRK1 core chimeras TM, M1-P, P, and P-M2. The intensity of TM and mutant bands was normalized to  $\beta$ -actin (lower blot). No significant impact of group was observed ( $F_{3,11}=3.4$ ,  $P=0.07$ ;  $n=3$  separate transfections). C) Modeling of the GIRK2 homomer (PBD 3SYQ) in the open conformation, with one subunit (facing the viewer) removed for clarity. The three remaining subunits are displayed in different colors: light, medium, and dark gray. The model highlights residues L173 in the M2 (inner helix) domain of the dark gray subunit and I155 in the selectivity filter of the adjacent (medium gray) subunit.



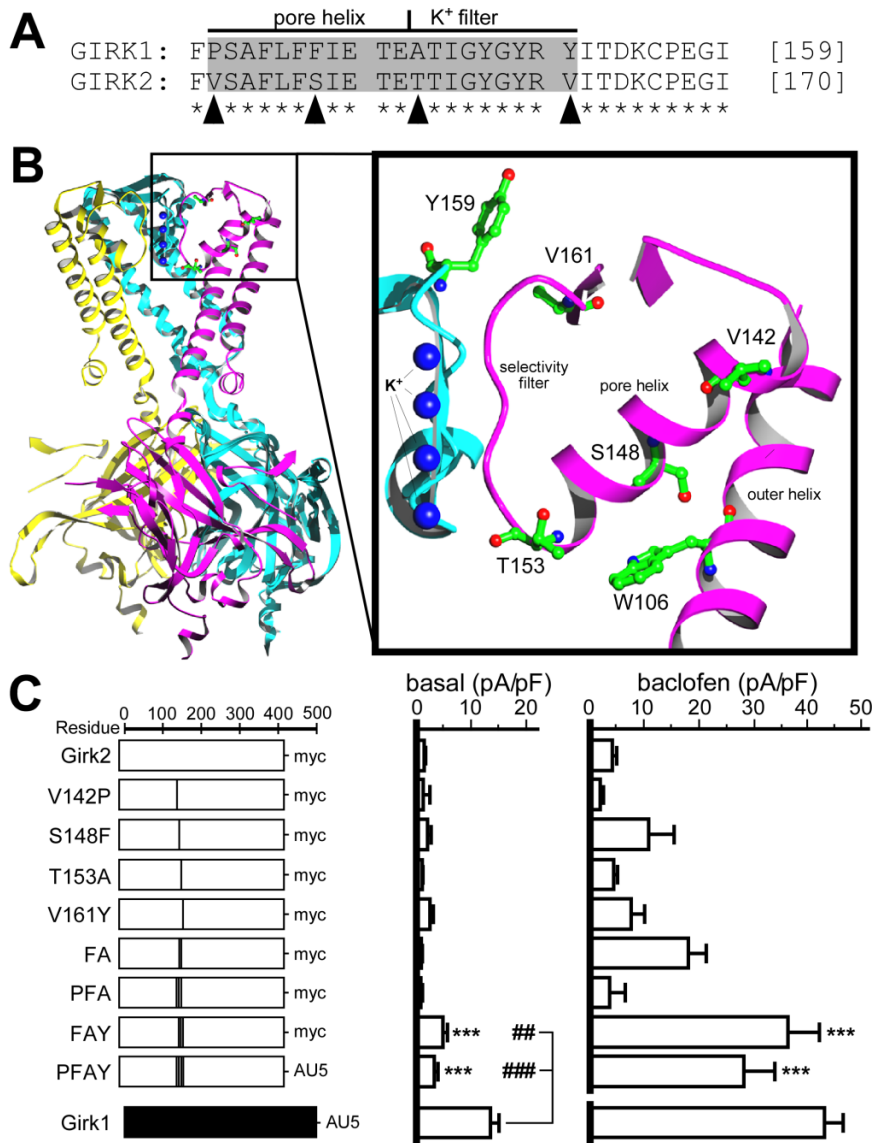


**Figure 2.11. Impact of GIRK1 P-loop residues.** **A)** Alignment of GIRK1 and GIRK2 P-loop domains. The arrowheads denote the four amino acid differences between GIRK1 and GIRK2 in this domain. **B)** Modeling of the GIRK2 homomer (PBD 3SYQ) in the open conformation, with one subunit (facing the viewer) removed for clarity. The three remaining subunits are displayed in different colors: light, medium, and dark gray. The right inset shows detailed structures within the pore, with the M2 domain (inner helix) of the dark gray subunit removed for clarity. **C)** Basal and baclofen-induced currents in cells expressing GABA<sub>B</sub>R, GIRK2, and the depicted construct (n=6-17/group). A significant impact of group was observed for basal ( $F_{8,83}=9.8$ ,  $P<0.001$ ) and baclofen-induced ( $F_{8,81}=14.1$ ;  $P<0.001$ ) currents. Symbols: \*\*\*  $P<0.001$  vs. GIRK2 homomer; ##,###  $P<0.01$  and  $P<0.001$ , respectively, vs. GIRK1/GIRK2 heteromer (only select comparisons shown).

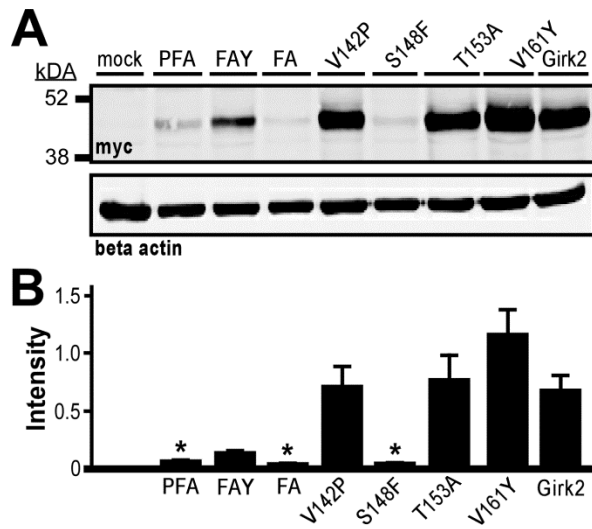


**Figure 2.12. Characterization of GIRK2 P-loop point mutants.** **A)** Expression of myc-tagged GIRK2 and P-loop mutants (upper blot), as assessed by quantitative immunoblotting (n=3 separate transfections). **B)** The intensity of GIRK2 and mutants was normalized to  $\beta$ -actin (lower blot in A). A significant impact of group was observed ( $F_{7,23}=11.9$ ,  $P<0.001$ ). Symbols: \*  $P<0.05$  vs. GIRK2.

Subunit	Conductance (pS)	Open time (ms)
GIRK1	35 ± 1	0.4 ± 0.5 (54%)
	22 ± 2	2.2 ± 0.4 (46%)
TM	21 ± 1 <sup>*,†</sup>	0.4 ± 0.5 (49%) <sup>*,†</sup>
		1.7 ± 0.3 (51%)
M1-P	18 ± 1 <sup>*,†,‡</sup>	0.2 ± 0.5 (56%) <sup>*,†,‡</sup>
		1.2 ± 0.3 (44%)
P	17 ± 1 <sup>*,†,‡</sup>	0.5 ± 0.3 (64%) <sup>*,†,‡</sup>
		2.4 ± 0.5 (36%)
P-M2	17 ± 1 <sup>*,†,‡</sup>	1.1 ± 0.1 <sup>*,†,‡,§</sup>
P(L173F)	13 ± 1 <sup>*,‡,§</sup>	0.9 ± 0.1 <sup>*,†,‡</sup>
FAY	16 ± 1 <sup>*,†,‡</sup>	0.2 ± 0.4 (60%) <sup>*,†,‡</sup>
		1.5 ± 0.3 (40%)
FA	13 ± 1 <sup>*,‡,§</sup>	0.7 ± 0.2 <sup>*,†,‡,§</sup>
S148F	14 ± 1 <sup>*,‡,§</sup>	0.8 ± 0.1 <sup>*,†,‡,§</sup>
T153A	14 ± 1 <sup>*,‡,§</sup>	0.8 ± 0.2 <sup>*,†,‡,§</sup>
V161Y	18 ± 1 <sup>*,†</sup>	0.6 ± 0.1 <sup>*,†,‡,§</sup>
GIRK2	11 ± 1 <sup>*</sup>	0.3 ± 0.2 <sup>*,‡</sup>

**Table 2.1. Summary of single-channel data.** Single-channel conductance and open times derived from channel events (n = 250–892) measured in three to five cells expressing GIRK2 and the subunit listed on the left. Amplitude data were binned in a conventional histogram (0.2-pA bin width; 0.4- to 4.4-pA constraints), normalized, and fit using a Gaussian function. Models with different term number were compared automatically, and results from the optimal fit are listed here. Open-state dwell-time data were binned in a logarithmic histogram (15 bins per decade; 0.3- to 10-ms constraints). Square roots of bin counts were determined, and resultant histograms were fit using an exponential (log-probability) function. Optimal fits were determined for each channel. For two-term fits, the influence of each term is listed as a percentage. The GIRK2(V142P) mutant was not evaluated because of low-level whole-cell activity. \*P < 0.001 vs. GIRK1/GIRK2; †P < 0.05 vs. GIRK2; ‡P < 0.05 vs. TM; §P < 0.05 vs. P.

## Discussion

Previous chimeric studies explored the influence of intracellular and core domains of GIRK1 on channel function [110, 112, 113, 115], leading to the identification of N- and multiple C-terminal domains critical for promoting direct interactions with G $\beta\gamma$ , including the “ $\beta$ L- $\beta$ M sheet” (residues 331-340) and L333 [57]. These structures form a binding pocket that maps onto the external face of an extended cytosolic ion permeation pathway [102]. Given the conservation of these and other critical domains across GIRK subunits, they cannot explain the potentiating influence of GIRK1 on GIRK currents. Moreover, while the distal C-terminal domain of GIRK1 (residues 325-501) can confer enhanced G $\beta\gamma$ -dependent activation to a heteromeric channel consisting of GIRK4 and an IRK1/GIRK1 chimera, robust receptor-induced currents required the GIRK1 core domain [110]. Thus, structural features of GIRK1 might enhance receptor-dependent GIRK signaling via mechanisms that do not involve G $\beta\gamma$  binding.

Structural insights into the unique distal C-terminal domain of GIRK1 are limited as published crystal structures were derived from recombinant proteins lacking the distal regions of the N- and C-terminal domains. While this domain alone does not bind G $\beta\gamma$ , its presence significantly strengthened binding of G $\beta\gamma$  to the GIRK1 C-terminus [214]. Thus, the potentiating effect of GIRK1 on GIRK-dependent signaling might reflect in part the presence of distal C-terminal domain that confers a stronger association between the channel and G $\beta\gamma$ . Here, we identified a single residue within this domain (Q404) that selectively influences receptor-induced GIRK channel activity. Available evidence is consistent with the possibility that this residue strengthens the channel-G $\beta\gamma$  interaction. It

is also possible, however, that Q404 strengthens the allosteric coupling that translates G $\beta$  $\gamma$  binding to an increase in channel gating.

Three amino acids (F137, A142, Y150) in the P-loop were found to collaborate to enhance heteromeric channel activity, probably via the redistribution of intra-subunit interactions and strengthening of inter-subunit interactions that leads to enhanced single channel conductance and mean open time, and perhaps enhanced gating. F137 was identified previously as an enhancer of basal and receptor-dependent currents carried by the GIRK1/GIRK4 heteromer [114]. While the precise structural impact of the phenylalanine substitution is unknown, manipulations at this site influence diverse channel properties. Indeed, an S148T substitution in GIRK2 yields highly-active homomeric channels [215]. Perhaps more surprisingly, GIRK1(F137S) homomers reach the cell surface and are functional, despite the lack of an ER export signal that precludes surface trafficking of GIRK1 [68].

Our data show that the positive collective influence of F137, A142, Y150 on basal and receptor-induced GIRK currents is tempered by F162 in the GIRK1 M2 domain. Using the structure of the GIRK2 homomer as a template, one would predict that replacing L173 (the analogous position in GIRK2) with the relatively bulky phenylalanine would result in a Van der Waals interaction with I155 of the adjacent GIRK subunit, pushing I155 toward the K<sup>+</sup> permeation pathway (**Fig. 2.10C**). In support of this contention, the unitary conductance of channels formed with P(L173F) was lower than that of the P chimera, and the longer mean open times (2.4 ms) observed with the P chimera were not seen for P(L173F). The relatively selective influence of this residue on

receptor-dependent current argues that it is involved in conformational changes in the channel triggered by  $G\beta\gamma$  binding.

While pore-related structures that enhance unitary properties should increase basal (and receptor-dependent) whole-cell current, we found that the domain between 409-462 in the distal C-terminus is a significant and selective determinant of receptor-independent channel activity. The impact of the distal C-terminus of GIRK1 on basal activity might relate to channel interactions with  $G\alpha$  subunits.  $G\alpha_{i3}$  was found to interact with the distal GIRK1 C-terminus, leading to a reduction in basal activity and increased  $G\beta\gamma$ -dependent activation of GIRK1(F137S) homomers [216]. In contrast, basal activity of GIRK2 homomers was insensitive to  $G\alpha_{i3}$ -dependent modulation. In light of the substantial basal activity of GIRK channels seen in neurons (*e.g.*, [158]), refinement of the impact of the distal GIRK1 C-terminal domain on basal activity is warranted.

The single-channel conductance and mean open time of GIRK1-containing channels are both larger than those of GIRK1-lacking channels. Our data reveal that GIRK1 core domain accounts for much of the influence of GIRK1 on mean open time, and some of its influence on unitary conductance. Presumably, structures in the proximal N- and/or C-terminal domains of GIRK1 that contribute to the cytoplasmic pore participate in modulating these unitary channel properties. Given the robust influence of GIRK1 on GIRK channel activity, it seems likely that GIRK1 also enhances other aspects of channel function, including gating. In addition to an inner helix gate formed by the 2<sup>nd</sup> transmembrane segments, GIRK channels possess a G-loop gate found near the interface of the cytoplasmic domain and membrane [93]. Binding of  $G\beta\gamma$  to GIRK2 homomers

opens the G-loop gate in the absence of PIP<sub>2</sub>, and both G-loop and inner helix gates in the presence of PIP<sub>2</sub> [93]. While these gates are conserved across GIRK subunits, GIRK1 and GIRK2 do differ with regard to PIP<sub>2</sub> affinity [111]. Subunit-dependent differences in channel modulation by Na<sup>+</sup> also support the contention that subtle differences associated with GIRK channel gates may translate into significant differences in channel activity [98].

The existence of four GIRK subunit genes, and their overlapping but distinct expression patterns, suggests that subunit composition influences GIRK channel function in tangible ways. Given the critical contributions made by GIRK channels to complex behavior and organ physiology [57], a detailed understanding of intrinsic and extrinsic factors that influence channel function is warranted. Here, we explored the structural underpinnings of the clearest GIRK subunit-dependent functional difference described to date. These efforts have refined the map of features influencing receptor-dependent and independent activity of GIRK1-containing channels, the dominant GIRK channel type in the brain and heart.

## CHAPTER 3

**Mechanisms underlying the activation of G protein-gated inwardly-rectifying K<sup>+</sup> (GIRK) channels by the novel anxiolytic drug, ML297**

**Wydeven N, Marron E, Du Y, Bennyworth M, Hearing M, Fischer R, Thomas M, Herring C, Weaver CD, Wickman K. Structural elements conferring selectivity of a novel anxiolytic compound (ML297) for G protein-gated inwardly-rectifying K<sup>+</sup> (GIRK) channels containing GIRK1. *Proc. Natl. Acad. Sci. USA 2014: Under Review.***



## Introduction

Signal transduction involving inhibitory ( $G_{i/o}$ ) G proteins titrates the excitability of neurons, cardiac myocytes, and endocrine cells, influencing behavior, cardiac output, and energy homeostasis [170]. G protein-gated inwardly-rectifying potassium ( $K^+$ ) (GIRK/Kir3) channels are a common effector for  $G_{i/o}$ -dependent signaling pathways in the heart and nervous system [57, 217]. Polymorphisms and mutations in human GIRK channels have been linked to arrhythmias, hyperaldosteronism (and associated hypertension), schizophrenia, sensitivity to analgesics, and alcohol dependence [170].

GIRK channels are activated by binding of the G protein  $G\beta\gamma$  subunit [57, 170, 217].  $G\beta\gamma$  binding strengthens channel affinity for phosphatidylinositol-4,5-bisphosphate ( $PIP_2$ ), a co-factor for channel gating [92, 101]. GIRK channels are also activated in a G protein-independent manner by ethanol [162, 163], volatile anesthetics [165, 218], and the flavonoid naringin [164]. Many psychoactive and clinically-relevant compounds with other primary molecular targets inhibit GIRK channels, albeit at relatively high doses [170, 219]. The lack of selective GIRK channel modulators, and in particular, drugs that discriminate among GIRK channel subtypes, has hampered investigation into their physiological relevance and therapeutic potential.

GIRK channels are homo- and heterotetramers formed by GIRK1, GIRK2, GIRK3, and GIRK4 subunits [57, 217]. GIRK subunits exhibit overlapping but distinct cellular expression patterns, yielding multiple channel subtypes [170]. Though it cannot form functional homomers [68], GIRK1 is an integral subunit of the cardiac GIRK channel and most neuronal GIRK channels [63, 69]. GIRK1 confers robust basal and receptor-dependent activity to GIRK heteromers, attributable in part to unique residues in

the pore and second transmembrane domain [110, 114, 220]. The intracellular C-terminal domain also contributes to the potentiating influence of GIRK1 on channel activity, likely due to the presence of unique structures that modify the interaction between the channel and G $\beta\gamma$ , G $\alpha$ , and PIP<sub>2</sub>, and render the channel susceptible to phosphoregulation [57, 170, 217].

Recently, we identified a new class of small molecule GIRK channel modulators [169]. The prototype (ML297) is a potent agonist selective for GIRK1-containing channels. At present, however, the selectivity of ML297 *in vivo* is untested and mechanisms underlying its selective activation of GIRK1-containing channels are unclear. The goals of this study were to identify the structural basis of ML297 efficacy and selectivity for GIRK1-containing channels, explore the mechanisms underlying channel activation, and probe further its therapeutic potential. We report that ML297 activates GIRK1-containing channels in unique fashion, requiring only two amino acids unique to GIRK1, and suggest that ML297 or derivatives might represent a new class of anxiolytic compounds with limited sedative and addictive liabilities.

## **Materials and Methods**

*Animals*—Animal experiments were approved by the Institutional Animal Care and Use Committee at the University of Minnesota. Male C57BL/6J mice were purchased from The Jackson Laboratory (Bar Harbor, ME) for some behavioral studies. Wild-type and *Girk1*<sup>-/-</sup> mice generated on-site from crosses of *Girk1*<sup>+/-</sup> mice were used for other behavioral studies and for establishing hippocampal cultures. Generation of

*Girk1*<sup>-/-</sup> mice was described previously [210]. The *Girk1* null mutation was backcrossed against the C57BL/6J strain for >20 rounds prior to establishing the crosses in this study.

*Plasmids/DNA*—Expression constructs for GABA<sub>B</sub>R1, GABA<sub>B</sub>R2, and Dr-VSP were kindly provided by Dr. Paul Slesinger; Dr-VSP was provided with the permission of Dr. Yasushi Okamura. Plasmids containing rat GIRK1 (GIRK1-AU5) and mouse GIRK2A (GIRK2-myc) coding sequences served as parent constructs for mutagenesis. GIRK1/GIRK2 chimeras were generated by overlap extension PCR [220], and point mutations were introduced using the QuikChange II XL site-directed mutagenesis kit (Agilent Technologies, Inc.; Santa Clara, CA).

*Whole-cell experiments*—ML297 was synthesized in the Vanderbilt Institute of Chemical Biology Chemical Synthesis Core and Vanderbilt MLPCN Specialized Chemistry Center. Hippocampal cultures were prepared as described [146], and kept in culture for 10-14 d prior to electrophysiological analysis. HEK293 cells were maintained according to ATCC recommendations and were transfected using the calcium phosphate technique; electrophysiological studies were carried out 16-24 h later. Conditions for measuring and analyzing whole-cell drug-induced GIRK currents were described previously [220].

*Data analysis*—Data are presented as mean±SEM. Statistical analyses were done with Prism 5 (GraphPad Software, Inc.; La Jolla, CA) and SigmaPlot 11 (Systat Software, Inc.; San Jose, CA). The least squares fitting method was used for non-linear fitting of dose-response data, Hill co-efficient analysis, and EC<sub>50</sub> analysis. Behavioral data were analyzed by one-way ANOVA or two-way ANOVA; Dunnett's *post hoc* testing was used for pairwise comparisons, as appropriate.

*Outside-out recordings*—HEK293 cells stably expressing GIRK1/GIRK2 or GIRK2 alone were used for single-channel recordings [169]. For some experiments, cells were transfected with GABA<sub>B</sub>R1 and GABA<sub>B</sub>R2 using the calcium phosphate technique, and electrophysiological experiments were carried out 16-24 h later [220]. Borosilicate patch pipettes (3.5-4.5 MΩ) coated with HIPEC<sup>®</sup> R6101 elastomer (Dow Corning Corp.; Midland, MI) were filled with (in mM): 150 KCl, 1 MgCl<sub>2</sub>, 5 EGTA/KOH, 5 HEPES/KOH (pH=7.4). The bath solution contained (in mM): 150 KCl, 1.8 CaCl<sub>2</sub>, 0.5 MgCl<sub>2</sub>, 15 D-glucose, 5 HEPES/KOH (pH 7.4). To measure the impact of baclofen on unitary GIRK currents, Na<sub>2</sub>-ATP (2 mM) and Na-GTP (0.3 mM) were added to the pipette solution. After adopting the outside-out configuration, the holding potential was set to -70 mV. Bath solution containing ML297 (0.1, 0.25, and 1 μM) or baclofen (100 μM) was applied to the chamber by gravity flow. Currents were recorded using an Axopatch 200B patch clamp amplifier (Molecular Devices), low-pass filtered at 2-5 kHz, sampled at 10 kHz, and stored on hard disk for analysis using pCLAMP v. 9.2 software.

Analysis of single-channel parameters was performed on 10 s recordings taken before and after vehicle or drug application. To calculate channel mean open time, dwell-time data were binned in a logarithmic histogram (15 bins/decade) using min/max constraints for amplitude (0.4-4.4 pA) and dwell-time (0.3-10 ms). Square roots of bin counts were determined and resultant histograms were fit using a standard exponential (log probability) function, with variable metric search method and maximum likelihood minimization method. Single-channel amplitude data were binned in a conventional histogram (0.2 pA bin width) using min/max constraints for amplitude (0.4-4.4 pA). Histograms were normalized and fit using a Gaussian function, with Levenberg-

Marquardt search method and sum of squared errors minimization method. Models with different numbers of terms were compared automatically. Optimal model parameters for each channel type were determined. Open-state dwell-time data were analyzed using the Kolmogorov-Smirnoff test. Conductance of the channel was calculated plotting the amplitude values against different potential ranging from -50 to -100 mV and fitting the results to a linear regression.

*Thallium flux assays*—Expression constructs used in the thallium flux assay were prepared from human GIRK expression plasmids described previously [169], using the GENEART site-directed mutagenesis system (Life Technologies; Carlsbad, CA); PCR reactions were conducted using AccuPrime Pfx DNA polymerase (Life Technologies). Amplified constructs were transformed into DH5 $\alpha$ -T1R cells (Life Technologies). DNA from selected colonies was obtained from liquid cultures and purified using the QIAprep Spin kit (Qiagen; Germantown, MD).

HEK-293 cells (ATCC; Manassas, VA) were maintained in T75 flasks at 37°C and 5% CO<sub>2</sub> in Minimal Essential Medium (Mediatech; Manassas, VA) containing 10% (v/v) fetal bovine serum (Sigma-Aldrich; Saint Louis, MO) and 1x Glutagro (Mediatech), referred to henceforth as cell culture medium. Cells were dislodged from 90% confluent T75 flasks (Corning) using TrypLE Express (Life Technologies). HEK cells in suspension (2 mL) in cell culture medium were added to 6-well plates to achieve ~60% confluence after one night of incubation at 37°C and 5% CO<sub>2</sub>. Transfections were performed using FuGENE® 6 (Promega; Madison, WI), according to manufacturer specifications. In brief, FuGENE® 6 was mixed with Opti-MEM (Life Technologies) and incubated for 5 min at room temperature. Subsequently, the mixture was combined by

gentle pipetting with expression plasmids. Following the 15 min incubation, the FuGENE/DNA mixture was added drop-wise to a well of a 6-well plate and mixed with a gentle side-to-side motion. Once the desired number of wells had been treated, the 6-well plates were returned to the cell culture incubator (37°C and 5% CO<sub>2</sub>) overnight. The next day, cells were lifted using TrypLE-Express, resuspended in cell culture medium (~500 cells/ $\mu$ L), and transferred to a total of 48 wells of an amine-coated, black-walled, clear-bottom, 384-well plate (Beckton-Dickinson; Franklin Lakes, NJ). Additional transfections from the 6-well plate were added to the other wells of the 384-well plate with each plate always containing 48 wells of mock-transfected HEK-293 cells. Thus, each 384-well plate contained one set of mock-transfected controls and up to 7 transfection conditions.

Transiently-transfected cells in 384-well plates were incubated overnight at 37° C and 5% CO<sub>2</sub>. The next day, cell culture medium was removed and replaced with 20  $\mu$ L/well of a dye loading solution containing 0.4  $\mu$ M Thallos (TEFlabs, Austin, TX) in assay buffer (Hanks Balanced Salt Solution plus 20 mM HEPES, pH 7.3) and 0.04% (w/v) Pluronic F-127 (Sigma-Aldrich, St. Louis, MO). Following a 1-h incubation, the dye loading solution was replaced with assay buffer (20  $\mu$ L/well) and the plates were loaded into a Hamamatsu FDSS 6000 (Bridgewater, NJ). Data were acquired at 1 Hz (excitation 470 $\pm$ 20 nm, emission 540 $\pm$ 30 nm) for 10 s prior to the addition of assay buffer (20  $\mu$ L/well), a concentration series of ML297, or a single concentration of the non-selective GIRK inhibitor SCH23390 (Sigma-Aldrich). After 4 min, “5x” thallium stimulus buffer (10  $\mu$ L/well) was added and data collection continued for an additional 2 min. The thallium stimulus buffer contained (in mM): 125 NaHCO<sub>3</sub>, 1.8 CaSO<sub>4</sub>, 1

MgSO<sub>4</sub>, 5 glucose, 2.4 Tl<sub>2</sub>SO<sub>4</sub>, 10 HEPES (pH 7.4). As a positive control, 4 wells/transfection were tested with thallium stimulus buffer containing a 5% (v/v) solution (final concentration of 78 mM) of the non-selective GIRK channel activator methyl pentanediol (MPD; Sigma).

ML297 was dissolved in DMSO to concentrations of 10 mM, diluted by hand in 7 x 3-fold steps in DMSO, and then further diluted in assay buffer (1:500) to achieve “2x” solutions. Diluted samples were used within 1 h of dilution. Final DMSO concentrations in all studies were 0.1%. Changes in thallium flux induced by either ML297 or MPD were analyzed as described<sup>1</sup>; in brief, each point in each wave was divided by the first point in that wave (F/F<sub>0</sub>). Then, the average wave arising from vehicle-control wells for each transfected construct was subtracted from waves measured in ML297- or MPD-treated wells. The slopes of these vehicle control-subtracted waves were calculated from 10 data points beginning 2 s after thallium stimulus addition. The choice to use slope values instead of amplitudes helped prevent shifts in potency that can result from indicator dye or detector saturation due to large increases in channel activity. For each wild-type and mutant construct tested, the slope values obtained from a maximally-effective concentration of ML297 (10 μM) were divided by the slope values obtained in 78 mM MPD, and thus the efficacy of ML297 for each wild-type and mutant construct is expressed as a percentage of MPD efficacy for that same construct.

*Behavioral assays*—For the motor activity study, mice were injected with ML297 (3, 10, 30, or 60 mg/kg i.p.) or vehicle (saline + 10% Tween-80), placed into a novel open-field environment (22x42 cm), and activity was monitored by video camera for 60 min. Distance traveled was determined by video analysis software (ANY-maze<sup>TM</sup> v4.96;

Stoelting Co., Wood Dale, IL). Anxiety-related behavior was measured using an elevated plus maze (EPM, Med-Associates, Inc.; St. Albans, VT). Thirty minutes prior to testing, mice were injected with ML297 (3, 10, or 30 mg/kg i.p.) or vehicle (0.5% hydroxypropyl cellulose/4% DMSO); these dosing conditions were used for subsequent tests as well. Mice were placed in the center of the EPM, and the time spent within the open and closed arms, along with total distance traveled, was recorded for 5 min. Anxiety-like behavior was determined by the proportion of arm exploration in the open arm (open arm time/(open arm + closed arm time)). For the stress-induced hyperthermia (SIH) test, mice were injected with ML297 or vehicle 30 min prior to testing. Subsequently, an initial rectal temperature was determined using a RET-3 rectal probe (Physitemp Instruments, Inc.; Clifton, NJ); the probe was dipped into silicon oil, inserted ~1.5 cm into the rectum, and held there until a stable rectal temperature was observed (~20 s). Mice were then returned to their home cage for 10 min, followed by second rectal temperature measurement. The difference between the second and first temperature measurements was determined and evaluated across treatment groups. The forced swim test (FST) was conducted with clear cylinders (18-cm diameter x 25 cm tall) filled up to 13 cm with 25°C water. Animals were placed in the water and movement was tracked from the side by a video camera. Immobility in the last 4 min of a 6-min session was determined using ANY-maze<sup>TM</sup> software.

The conditioned place preference (CPP) test spanned 12 d and was conducted in an apparatus (22x45x20 cm) divided into two compartments by an opaque wall with guillotine-style door. The floor of one compartment consisted of an array of 2.3 mm stainless steel rods, centered every 6.4 mm (grid). The floor of the other compartment



consisted thin chicken wire with openings of 2.5x2.5 mm (mesh). All data were acquired by video camera and movements analyzed with ANY-maze<sup>TM</sup> software. Prior to beginning the study, mice were habituated to experimenter by 5 d of handling. During the pre-conditioning test, mice were placed in the apparatus and allowed free exploration for 20 min; time spent in the “grid” and “mesh” chambers was recorded. Any mice displaying a severe preference (>800 s) for any one side were excluded from further testing. Mice were then assigned to drug treatment (3, 10, or 30 mg/kg ML297) or vehicle (0.5% hydroxypropyl cellulose and 4% DMSO in water) treatment groups, and paired with either the “grid” or “mesh” compartment (CS+). The other chamber (CS-) was paired with a saline treatment. Assignments were counterbalanced based upon pre-conditioning test performance. During the conditioning trials, subjects were injected with either drug or vehicle, and after a 15-min delay were confined for 30 min in the corresponding CS+ chamber. A total of 4 drug/vehicle and 4 saline trials were performed in alternating fashion, with only one trial performed per day. Side preferences were evaluated twice, first on the day following the 4<sup>th</sup> conditioning session, and again on the day after the final conditioning session. Place preference was determined by calculating the difference in time spent in the CS+ and CS- chambers during the test sessions; “Preference” is defined as CS+ - CS- within a given test session.

## **Results**

We began by comparing whole-cell currents evoked by ML297 and the GABA<sub>B</sub> receptor (GABA<sub>B</sub>R) agonist baclofen in transfected HEK293 cells. ML297 evoked concentration-dependent inward currents in cells expressing GABA<sub>B</sub>R and the

prototypical neuronal GIRK channel (GIRK1/GIRK2; **Fig. 3.1A**). The  $EC_{50}$  for ML297-induced activation of GIRK1/GIRK2 channels was  $233 \pm 38$  nM; 10  $\mu$ M ML297 evoked a maximal response (**Fig. 3.1B**). Activation and deactivation kinetics of the ML297-induced current were concentration-dependent, increasing and decreasing, respectively, with higher ML297 concentrations (**Fig. 3.1C**). Maximal ML297-induced currents were larger than those evoked by a saturating concentration of baclofen (100  $\mu$ M; **Fig. 3.1D**). Reversal potentials measured for basal, baclofen-induced, and ML297-induced GIRK currents were comparable and close to the predicted value for a  $K^+$ -selective channel ( $E_K = -43$  mV; **Fig. 3.1E**). Inward rectification, however, was markedly stronger for basal and baclofen-induced currents than for ML297-induced current (**Fig. 3.1E,F**).

We next measured the effect of ML297 on GIRK1/GIRK2 channels in outside-out patches from transfected cells (**Fig. 3.2**). ML297 evoked a concentration-dependent increase in activity (NPo) of GIRK1/GIRK2 channels (**Fig. 3.2A,B**), but had no effect on GIRK2 homomers (**Fig. 3.2B**). At the highest ML297 concentration tested (1  $\mu$ M), GIRK1/GIRK2 channel activity was enhanced 8-fold over basal levels, complicating extraction of unitary channel properties. At lower concentrations (100 nM), ML297 promoted the occurrence of longer opening events without altering single channel conductance ( $29.3 \pm 0.5$  pS before vs.  $31.3 \pm 1.5$  pS after;  $P=0.3$ ) (**Fig. 3.2A,C**). Baclofen (100  $\mu$ M) also increased channel activity without altering single-channel conductance ( $29.3 \pm 0.5$  pS before vs.  $29.1 \pm 1.6$  pS after;  $P=0.9$ ). In contrast to ML297, however, baclofen primarily increased the frequency of shorter-lived events (**Fig. 3.2D**). Collectively, data from whole-cell and single-channel experiments suggested that baclofen and ML297 activate GIRK channels in distinct manners.

We next examined the impact of the *Danio rerio* voltage-sensitive phosphatase (*Dr-VSP*) on baclofen- and ML297-induced GIRK currents (**Fig. 3.3**). *Dr-VSP* is activated by strong depolarization, leading to depletion of membrane-bound PIP<sub>2</sub> [221]. GIRK currents induced by baclofen and ML297 were recorded twice in each cell, once prior to and once after *Dr-VSP* activation (**Fig. 3.3A**). GIRK currents induced by baclofen and ML297 were strongly attenuated following *Dr-VSP* activation (**Fig. 3.3A,B**). In contrast, no attenuation of GIRK currents was seen in cells lacking *Dr-VSP* (**Fig. 3.3C**). Thus, ML297-induced activation of GIRK1-containing channels, like other modes of GIRK channel activation, requires PIP<sub>2</sub>.

To test whether the potency, efficacy, and selectivity of ML297 for GIRK1-containing channels are retained in cells that normally express GIRK channels, we next measured ML297-induced currents in cultured hippocampal neurons, which express GIRK1, GIRK2, and GIRK3 [109]. ML297 evoked a concentration-dependent inward current ( $V_{\text{hold}} = -70$  mV) in pyramidal-shaped hippocampal neurons from wild-type mice (**Fig. 3.4A,B**). The EC<sub>50</sub> ( $377 \pm 70$  nM) was comparable to that measured with recombinant GIRK1/GIRK2 channels ( $233 \pm 38$  nM; **Fig. 3.1B**), and ML297-induced current kinetics in hippocampal neurons showed a concentration dependence comparable to that seen in transfected cells (**Fig. 2.4C**). Currents evoked by application of 10  $\mu$ M ML297 were comparable in magnitude to those evoked by a saturating concentration of baclofen (100  $\mu$ M; **Fig. 3.5A,B**). Unlike baclofen-induced responses, however, ML297-induced currents showed little acute desensitization (**Fig. 3.5C**), and the kinetics were slower than those measured for baclofen (**Fig. 3.5D**). Importantly, while ML297 and vehicle had negligible effects on holding current in neurons from *Girk1*<sup>-/-</sup> mice, baclofen

evoked reliable (albeit small) currents in these neurons (**Fig. 3.5A,B**), likely attributable to activation of residual GIRK1-lacking channels [220].

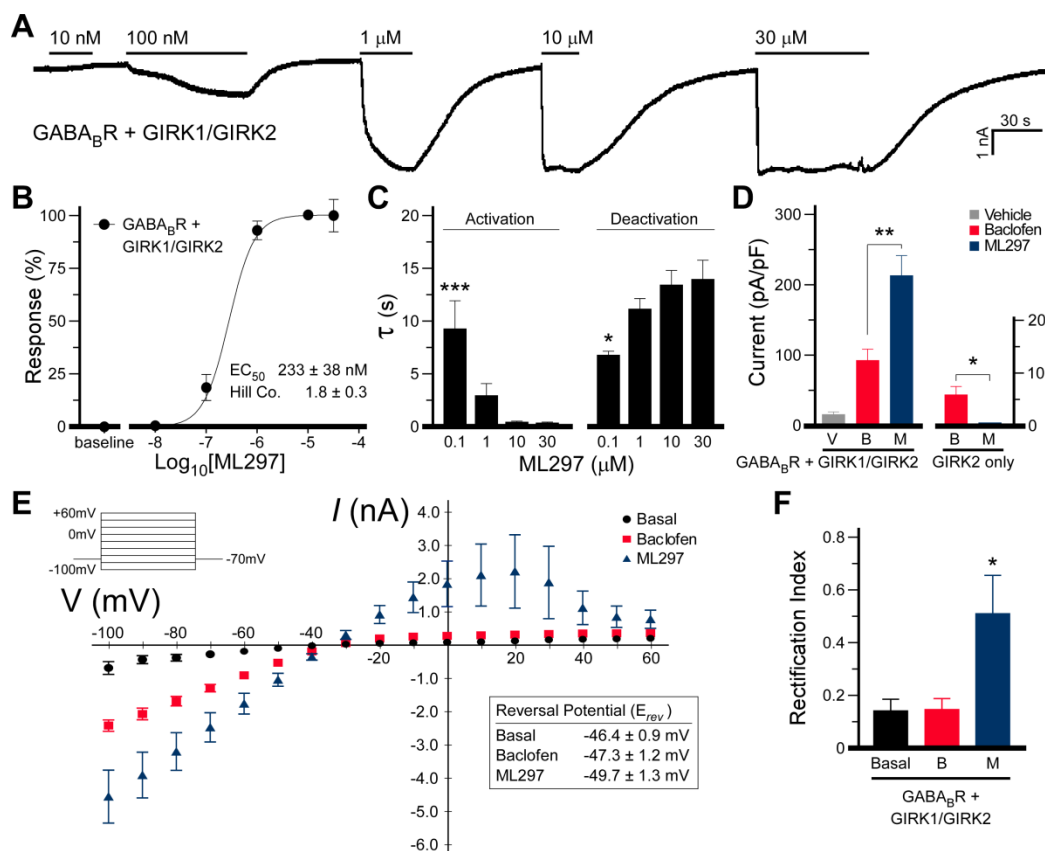


**Figure 3.1. ML297- and baclofen-induced GIRK currents: whole-cell.** (A) Trace showing the effect of increasing concentrations of ML297 on holding current ( $V_{hold} = -70$  mV) in a cell expressing  $GABA_BR$ , GIRK1, and GIRK2. Horizontal bars above the trace denote the duration of ML297 application. (B) Concentration-response of ML297-evoked currents in transfected cells. Steady-state currents at each concentration were normalized to the response measured with  $10 \mu M$  ML297 ( $n=6$  recordings/concentration). (C) Activation and deactivation kinetics ( $\tau$ , time constant) for the ML297-induced current in transfected cells. A significant effect of concentration was observed for both activation ( $F_{3,21}=10.2$ ;  $P<0.001$ ) and deactivation ( $F_{3,21}=4.8$ ;  $P<0.05$ ) rate. \*,\*\*\* $P<0.05$  and  $0.001$ , respectively, vs.  $30 \mu M$  ML297. (D) Peak currents evoked by vehicle (V, 0.1% DMSO), baclofen (B,  $100 \mu M$ ), or ML297 (M,  $10 \mu M$ ) in cells expressing  $GABA_BR$ , GIRK1, and GIRK2 ( $F_{2,26}=12.2$ ;  $P<0.001$ ,  $n=4-15$ /condition) or  $GABA_BR$  and GIRK2 alone ( $t_{10}=3.1$ ;  $P<0.05$ ,  $n=6$  recordings/group). \*,\*\* $P<0.05$  and  $0.01$ , respectively. (E) I-V plot for basal GIRK current (measured in  $25$  mM  $K^+$ , circles), together with plots for GIRK currents evoked by baclofen ( $100 \mu M$ ; squares) or ML297 ( $10 \mu M$ ; triangles) ( $n=3$  recordings/group). (F) Rectification index (ratio of current measured at  $0$  mV and  $-80$  mV) for basal GIRK current ('Basal'), or GIRK currents evoked by baclofen (B,  $100 \mu M$ ) or ML297 (M,  $10 \mu M$ ). A significant impact of group on rectification index was observed ( $F_{2,11}=5.5$ ;  $P<0.05$ ). \* $P<0.05$  vs. basal and baclofen groups.

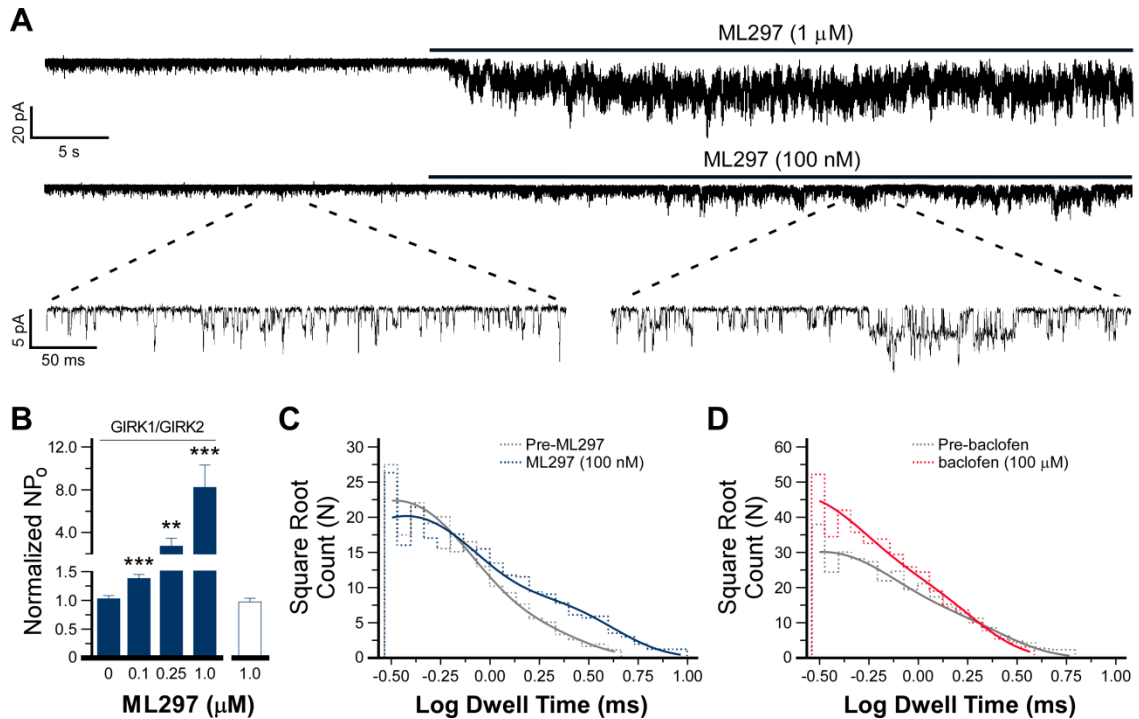


**Figure 3.2. ML297- and baclofen-induced GIRK currents: single-channel.** (a) Representative traces showing the effect of 100 nM and 1 μM ML297 on the activity of recombinant GIRK1/GIRK2 channels measured in the outside-out configuration. Segments of the recording made prior to and after application of 100 nM ML297 are shown below on an expanded time scale. (b) Summary of the impact of ML297 (0, 0.1, 0.25, 1 μM) on the activity (NPo) of recombinant GIRK1/GIRK2 heteromeric (filled bars) and GIRK2 homomeric (open bar) channels. NPo data were normalized to channel activity (basal) measured prior to drug application. A significant effect of concentration was seen for experiments involving GIRK1/GIRK2 channels ( $F_{3,13}=29.7$ ;  $P<0.001$ ). \*\*, \*\*\* $P<0.01$  and  $0.001$ , respectively, vs. basal activity (0 μM). (c) Open time histograms and curve fits for GIRK1/GIRK2 channel activity measured before (gray) and after (black) application of ML297 (100 nM). Histograms were fit best with a double exponential; pre-application values were  $0.3\pm 0.2$  ms and  $1.0\pm 0.4$  ms. After ML297 application, corresponding values were  $0.4\pm 0.1$  ms and  $1.8\pm 0.2$  ms (pre vs. post comparison; K-S statistic = 0.047, 19759 events;  $P<0.001$ ). (d) Open time histograms and curve fits for GIRK1/GIRK2 channel activity measured before (gray) and after (black) the application of baclofen (100 μM, left). Histograms were fit best with a double exponential function; pre-baclofen open time values were  $0.3\pm 0.2$  ms and  $1.0\pm 0.2$  ms. After baclofen, the corresponding values were  $0.2\pm 0.3$  ms and  $0.7\pm 0.2$  ms (pre vs. post comparison; K-S statistic = 0.105, 58196 events;  $P<0.001$ ).

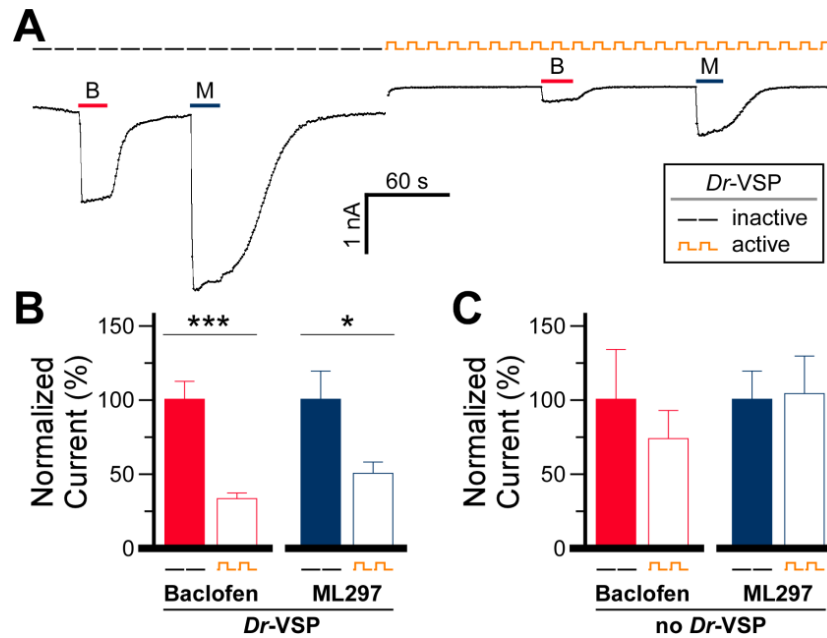


**Figure 3.3. ML297- and baclofen-induced GIRK currents: PIP<sub>2</sub> dependence.** (A) Traces showing the effect of PIP<sub>2</sub> depletion on currents evoked by baclofen- (B, 100 μM) and ML297- (M, 10 μM). Black dashes denote the cell being held at -70 mV, keeping *Dr-VSP* in an inactive state. Step symbols (□ □) denote the *Dr-VSP* activation protocol, which involved alternating 500 ms voltage steps between -70 and +100 mV; at least 120 steps to +100 mV were made prior to the 2<sup>nd</sup> application of baclofen and ML297. (B) Summary of responses evoked by baclofen (B, 100 μM) and ML297 (M, 10 μM) in cells expressing GABA<sub>B</sub>R, GIRK1, GIRK2, and *Dr-VSP*. Peak amplitudes of the 2<sup>nd</sup> responses were normalized to the amplitude of the first response. *Dr-VSP* activation significantly decreased baclofen- ( $t_{16}=4.6$ ;  $P<0.001$ ) and ML297- ( $t_{16}=2.3$ ;  $P<0.05$ ) induced currents (n=9 recordings/condition). \*,\*\*\* $P<0.05$  and 0.001, respectively. (C) Summary of responses evoked by baclofen (B, 100 μM) and ML297 (M, 10 μM) in cells expressing GABA<sub>B</sub>R, GIRK1, GIRK2, and empty vector (no *Dr-VSP*). No significant difference in peak current was observed between 1<sup>st</sup> and 2<sup>nd</sup> applications of either baclofen ( $t_6=0.7$ ;  $P=0.5$ ) or ML297 ( $t_6=0.1$ ;  $P=0.9$ ) groups (n=4 recordings/condition).

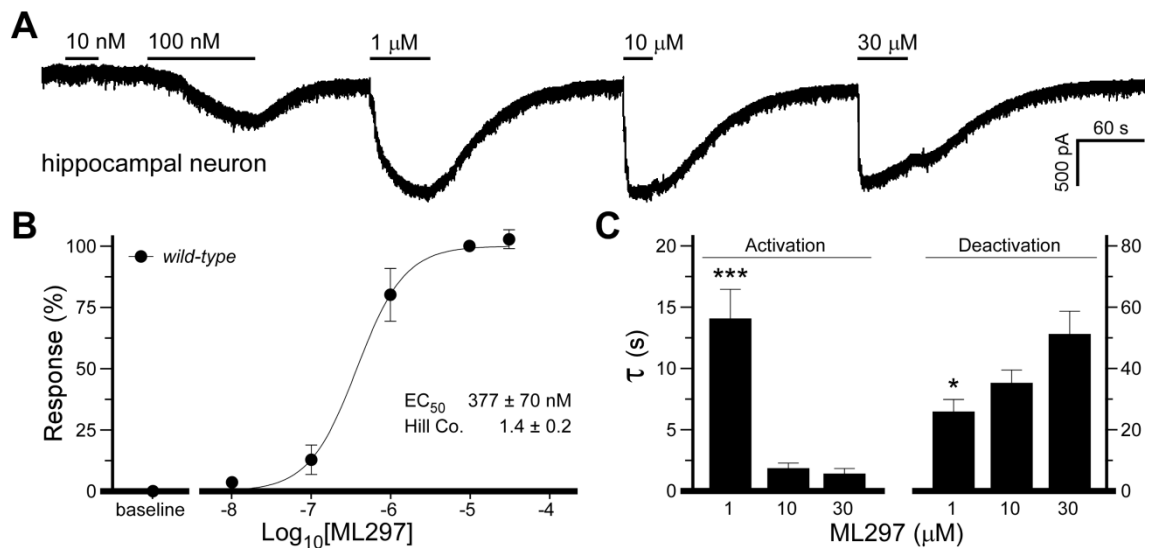


**Figure 3.4. ML297- and baclofen-induced GIRK currents in hippocampal neurons.** (A) Trace showing the effect of increasing concentrations of ML297 on holding current ( $V_{\text{hold}} = -70$  mV) in a wild-type hippocampal neuron. (B) Concentration-response analysis of ML297-evoked currents in hippocampal neurons from wild-type mice. Steady-state currents at each concentration were normalized to the response measured with 10  $\mu$ M ML297 ( $n=5-6$  recordings/concentration). (C) Activation ( $F_{2,16}=30.0$ ;  $P<0.001$ ) and deactivation ( $F_{2,16}=5.0$ ;  $P<0.05$ ) kinetics for the ML297-induced current in hippocampal neurons. \*,\*\*\* $P<0.05$  and 0.001, respectively, vs. 30  $\mu$ M ML297.



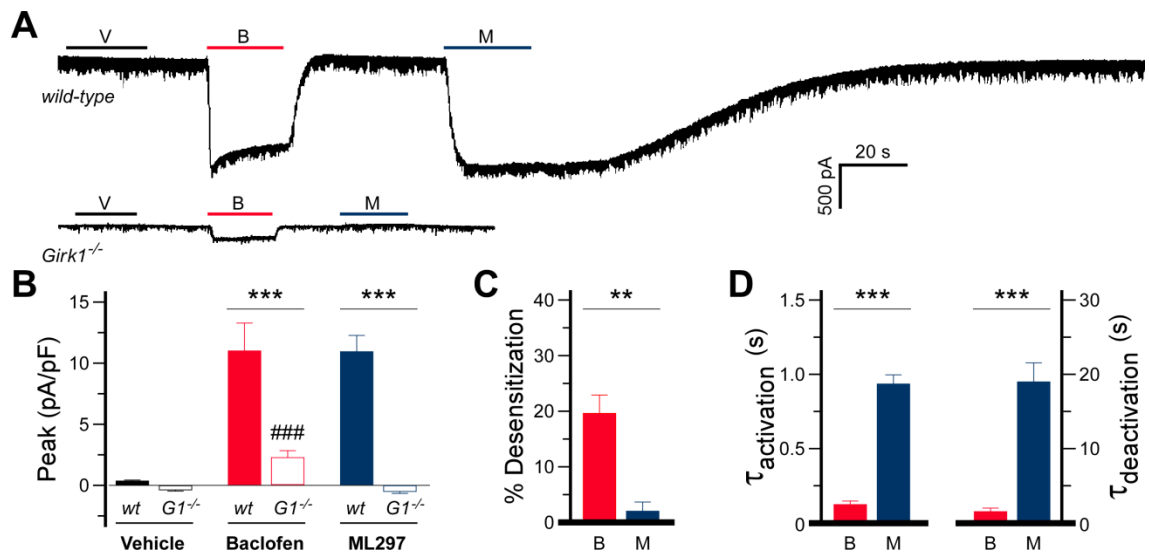


**Figure 3.5. ML297- and baclofen-induced GIRK currents in hippocampal neurons.** (A) Traces showing the relative effects of vehicle (V, 0.1% DMSO), baclofen (B, 100  $\mu$ M), and ML297 (M, 10  $\mu$ M) on holding currents in neurons from wild-type (upper trace) and *Girk1<sup>-/-</sup>* (lower trace) mice. (B) Summary of peak currents evoked by vehicle (0.1% DMSO), baclofen (100  $\mu$ M), and ML297 (10  $\mu$ M) in neurons from wild-type (wt) and *Girk1<sup>-/-</sup>* (*G1<sup>-/-</sup>*) mice; a significant genotype x drug interaction was observed ( $F_{2,43}=16.4$ ;  $P<0.001$ ). \*\*\* $P<0.001$  (within drug); ### $P<0.001$  vs. ML297 (within genotype). (C) Acute desensitization of currents induced by baclofen (100  $\mu$ M) and ML297 (10  $\mu$ M), measured by comparing peak currents with currents measured 20 s after drug application. Baclofen-induced currents showed modest acute desensitization (20%), while ML297-induced currents did not ( $t_{12}=4.2$ ,  $P<0.01$ ). \*\* $P<0.01$ . (D) Activation ( $t_8=12.8$ ,  $P<0.001$ ) and deactivation ( $t_8=6.5$ ,  $P<0.001$ ) kinetics of currents induced by baclofen (B, 100  $\mu$ M) and ML297 (M, 10  $\mu$ M) in hippocampal neurons from wild-type mice. \*\*\* $P<0.001$ .

To identify structural elements in GIRK1 required for ML297-induced channel activation, we used a thallium flux assay to compare responses induced by ML297 and the short-chain alcohol methyl pentanediol (MPD, a non-selective GIRK channel agonist) in cells co-expressing GIRK2 and either GIRK1 or a chimera harboring discrete GIRK1 sub-domains on a GIRK2 backbone (**Fig. 3.6**). We demonstrated previously that these GIRK1/GIRK2 chimeras interact with wild-type GIRK2 and promote levels of GIRK2-containing channels on the cell surface comparable to wild-type GIRK1 [220]. Using this approach, we found that while the non-selective GIRK agonist MPD was efficacious for all constructs evaluated, the P-M2 domain in GIRK1, which contains the pore helix/K<sup>+</sup> selectivity filter and second membrane-spanning domain, was critical for ML297 efficacy (**Fig. 3.6A,B**).

Based on the sequence alignment between GIRK1 and GIRK2 within the P-M2 domain (**Fig. 3.7A**), we next mutated residues in GIRK1 to match the corresponding residues in GIRK2 in an effort to identify specific amino acids required for the ML297-induced activation of GIRK1-containing channels. Two GIRK1 residues (F137 and D173) were identified using this approach (**Fig. 3.6B**). In cells expressing GIRK2 and either GIRK1<sup>F137S</sup> or GIRK1<sup>D173N</sup>, ML297-induced channel activation was virtually absent, while activation by MPD was preserved. Introduction of either of these GIRK1 residues individually into GIRK2 (S148F or N184D) failed to restore ML297 sensitivity. In cells expressing GIRK2 and the GIRK2 mutant harboring both GIRK1 residues (GIRK2<sup>F/D</sup>), ML297-induced channel activation was restored.

To extend these findings, ML297-induced whole-cell currents were compared in cells expressing GIRK2 and either GIRK1, GIRK1<sup>F137S</sup>, GIRK1<sup>D173N</sup>, GIRK1<sup>S/N</sup>,

GIRK2<sup>S148F</sup>, GIRK2<sup>N184D</sup>, or GIRK2<sup>F/D</sup> (**Fig. 3.7B,C**). Similar to the thallium flux results, ML297-induced whole-cell currents were strongly-attenuated or undetectable in cells expressing GIRK2 and either GIRK1<sup>F137S</sup>, GIRK1<sup>D173N</sup>, GIRK1<sup>S/N</sup>, GIRK2<sup>S148F</sup>, or GIRK2<sup>N184D</sup> (**Fig. 3.7C**). ML297-induced currents were normal, however, in cells expressing GIRK2 and GIRK2<sup>F/D</sup> (**Fig. 3.7B,C**). ML297-induced current kinetics were slower for GIRK2<sup>F/D</sup>/GIRK2 channels as compared to GIRK1/GIRK2 channels (**Fig. 3.7D,E**). Finally, the I-V profiles of basal, ML297-induced, and baclofen-induced currents carried by GIRK2<sup>F/D</sup>/GIRK2 channels were comparable to those observed for GIRK1/GIRK2 channels, with ML297 significantly weakening channel inward rectification (**Fig. 3.8A,B**). Thus, GIRK1 residues F137 and D173 are necessary for the ML297-induced activation of GIRK1/GIRK2 channels, and are sufficient to confer ML297 sensitivity to GIRK2.

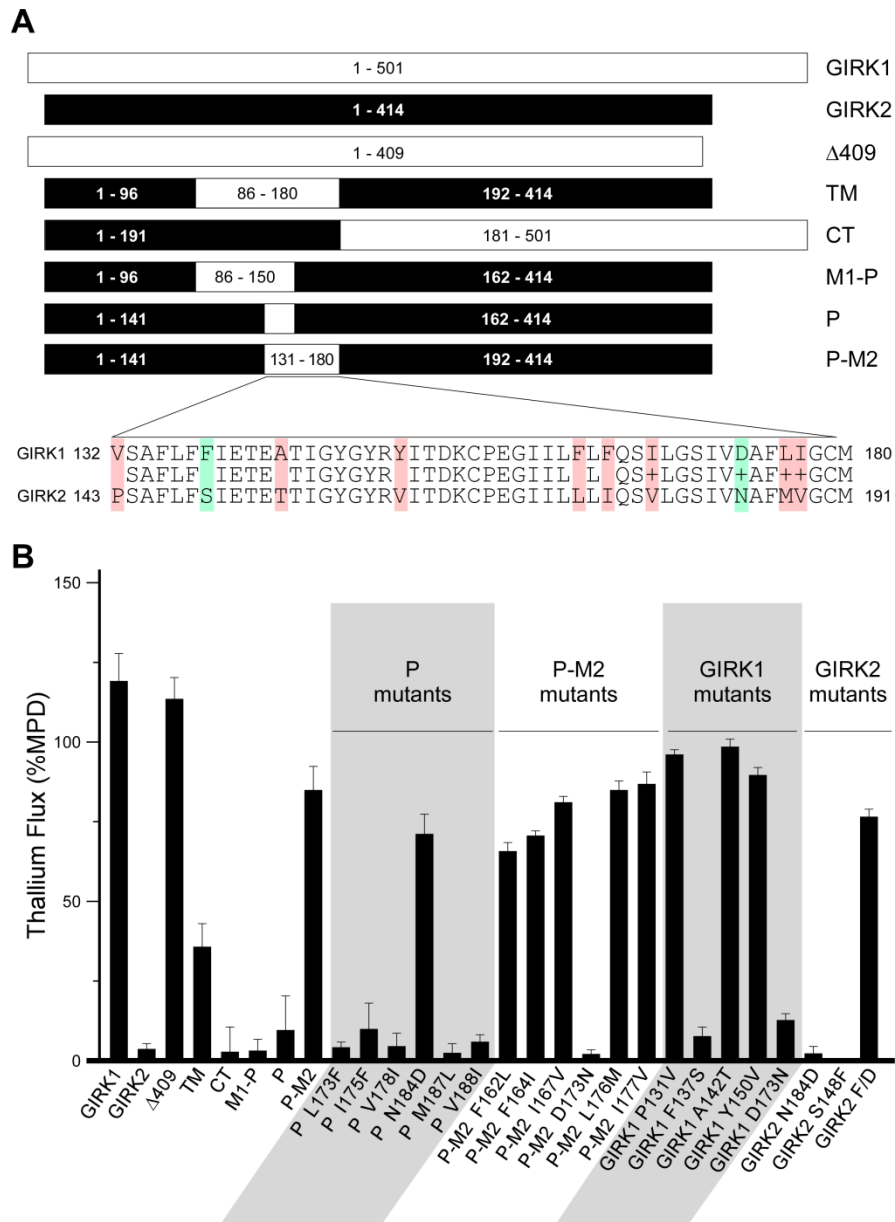


**Figure 3.6. Structural elements of GIRK1 required for ML297 activation.** (A) Schematic depiction of the GIRK1/GIRK2 chimeras used to localize structural elements required for the ML297-induced activation of GIRK1-containing channels. Residues differing between GIRK1 and GIRK2 in the P-M2 region are highlighted, including the two residues required for ML297-induced channel activation. (B) Thallium flux induced by 10  $\mu$ M ML297 in cells expressing GIRK2 and the construct designated below the X-axis, expressed as a percentage of the response of the same cells to MPD (%MPD). Constructs depicted in panel (A) are presented on the left side of the plot, with more selective point mutations introduced into the Pore (P), P-M2, GIRK1, and GIRK2 backbones on the right.

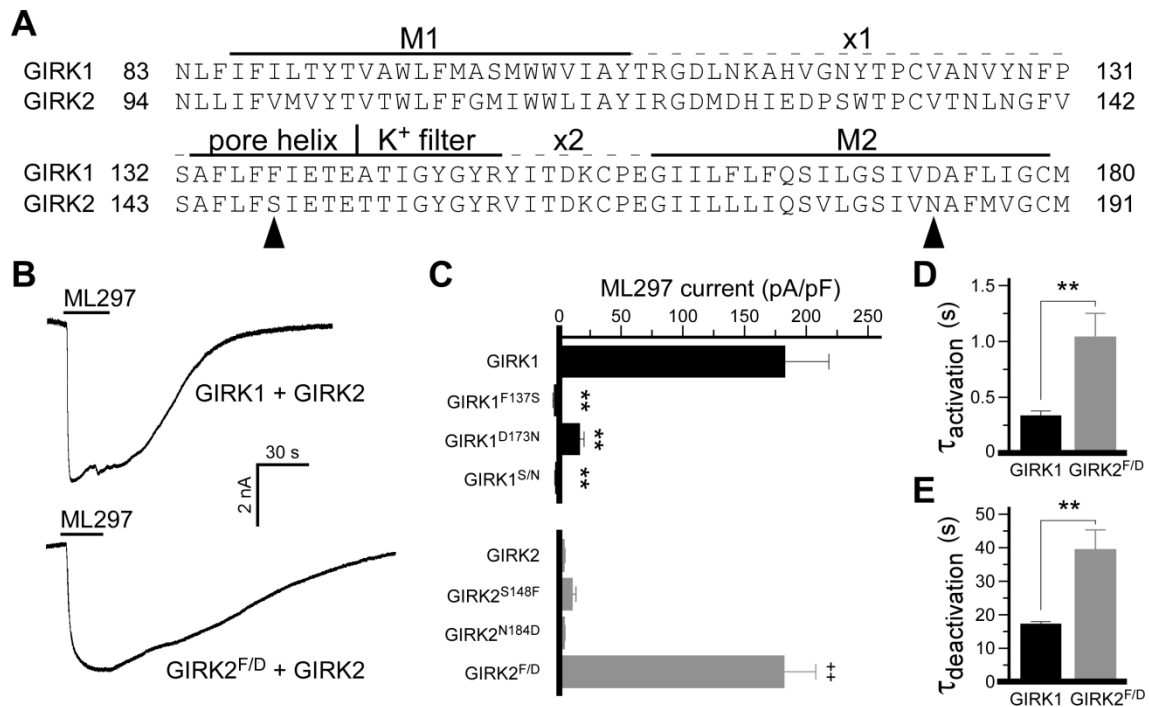


**Figure 3.7. Structural elements in GIRK1 required for ML297 activation.** (A) Alignment of core domains of GIRK1 and GIRK2: M1 (1<sup>st</sup> membrane-spanning domain), x1 (1<sup>st</sup> extracellular loop), pore helix, K<sup>+</sup>-selectivity filter, x2 (2<sup>nd</sup> extracellular domain), M2 (2<sup>nd</sup> transmembrane spanning domain). Arrowheads identify the GIRK1 residues required for ML297 activation. (B) Traces showing currents evoked by ML297 (10  $\mu$ M) in cells expressing GABA<sub>B</sub>R and either GIRK1/GIRK2 or GIRK2<sup>FD</sup>/GIRK2. (C) Summary of ML297-induced peak currents measured in cells expressing GABA<sub>B</sub>R, GIRK2, and either GIRK1, GIRK2, or GIRK mutant (n=4-6/group). A significant impact of group was found for ML297-induced currents for the GIRK1 mutant series (upper/black,  $F_{3,20}=18.9$ ;  $P<0.001$ ), and for the ML297-induced peak currents for the GIRK2 mutant series (lower/gray,  $F_{3,19}=45.4$ ;  $P<0.001$ ). \*\* $P<0.01$  vs. GIRK1; ++ $P<0.01$  vs. GIRK2. Significant differences were found for (D) activation ( $t_{12}=4.3$ ,  $P<0.01$ ) and (E) deactivation kinetics ( $t_{10}=3.6$ ,  $P<0.01$ ) of ML297-induced currents carried by cells expressing GIRK2 and either GIRK1 or GIRK2<sup>FD</sup> (n=6-8/group). \*\* $P<0.01$ .

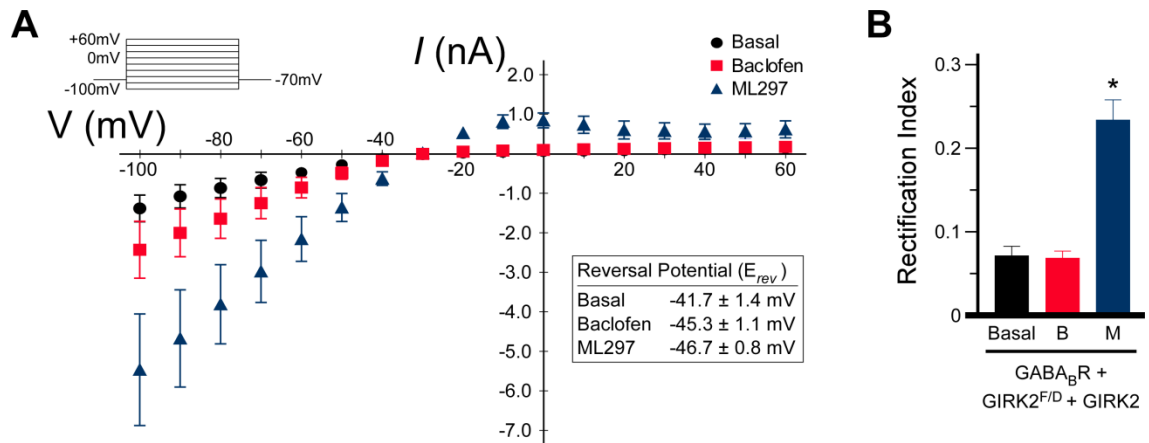


**Figure 3.8. Structural elements in GIRK1 required for ML297 activation.** (A) I-V plots for basal GIRK currents (circles), together with plots for GIRK currents evoked by baclofen (100  $\mu$ M, squares) or ML297 (10  $\mu$ M, triangles), in cells expressing GIRK2 and GIRK2<sup>F/D</sup> (n=3 recordings/condition). (B) Rectification index for basal GIRK currents ('Basal') and GIRK currents evoked by baclofen (B, 100  $\mu$ M) or ML297 (M, 10  $\mu$ M) in cells expressing GABA<sub>B</sub>R, GIRK2, and GIRK2<sup>F/D</sup>. A significant impact of group on rectification index was observed ( $F_{2,8}=45.6$ ;  $P<0.02$ ). \* $P<0.05$  vs. basal and baclofen groups.

Previously, we reported that ML297 was protective in rat epilepsy models [169]. To further investigate the behavioral effects of ML297, we probed its efficacy in tests of motor activity, reward, depression, and anxiety. We began with an open-field motor activity test involving wild-type C57BL/6J mice. We found that at the highest dose tested (60 mg/kg, the dose used in the seizure studies; [169]), ML297 suppressed motor activity (**Fig. 3.9A**). Lower doses (3, 10, and 30 mg/kg), however, had no impact on motor activity. Thus, to avoid the potentially confounding effect of ML297 on motor activity, 30 mg/kg was selected as the maximum dose used in subsequent behavioral tests.

ML297 did not exhibit significant reinforcing effects in wild-type mice as measured using a conditioned place preference (CPP) test (**Fig. 3.9B**), nor did it exhibit anti-depressant efficacy in the forced swim test (FST, **Fig. 3.9C,D**). ML297 did evoke a dose-dependent decrease in anxiety-related behavior in the elevated plus maze (EPM) test, increasing time spent in the open arms of the maze (**Fig. 3.9E**). Similarly, ML297 produced a dose-dependent suppression of stress-induced hyperthermia (SIH; **Fig. 3.9F**), a motor activity-independent physiological stress response blunted by anxiolytic drugs [222].

We repeated EPM and SIH tests using a cohort of wild-type and *Girk1*<sup>-/-</sup> siblings. Consistent with published data for *Girk2*<sup>-/-</sup> mice [223, 224], *Girk1*<sup>-/-</sup> mice exhibited less anxiety-related behavior than wild-type controls in the EPM test (**Fig. 3.9G**). No additional anxiolytic effect of ML297 was observed in *Girk1*<sup>-/-</sup> mice, however, ML297 increased time spent in the open arm in the wild-type group. Similarly, no anxiolytic effect of ML297 was observed in *Girk1*<sup>-/-</sup> mice during the SIH test (**Fig. 3.9H**). Collectively, these results argue that the anxiolytic effect of ML297 observed in wild-

type mice is primarily, if not exclusively, attributable to activation of GIRK1-containing channels.



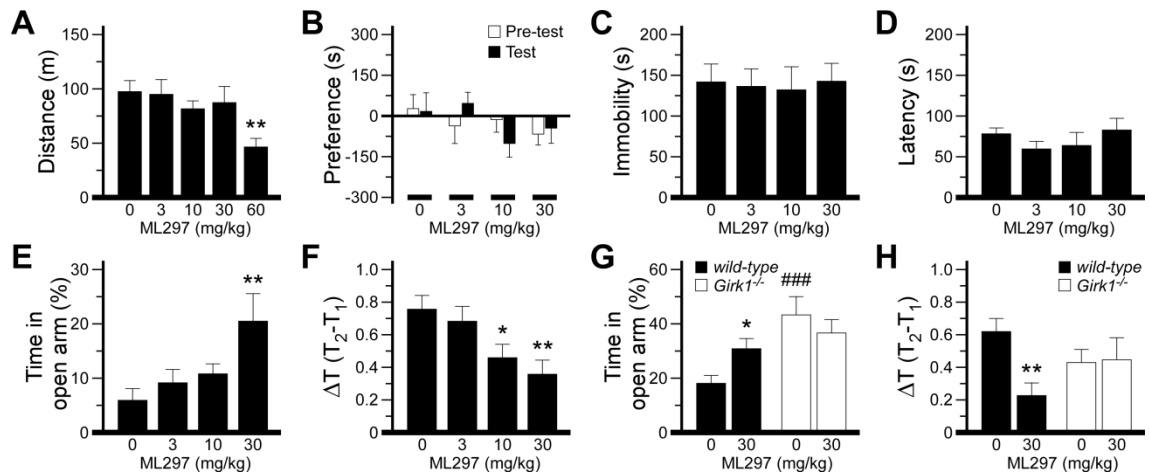


**Figure 3.9. Behavioral impact of ML297.** (A) Total distance traveled (m) by C57BL/6J mice in 1 h in a novel open-field following injection of ML297 (0/vehicle, 3, 10, 30, 60 mg/kg i.p.; n=11-12 mice/dose). A significant effect of dose was observed ( $F_{4,58}=3.2$ ;  $P<0.05$ ). \*\* $P<0.01$  vs. 0/vehicle. (B) Difference in time spent by C57BL/6J mice in the drug-paired and unpaired sides of a CPP chamber, measured on the first day of testing (pre-test, white bars), and after 4 conditioning sessions with ML297 (0/vehicle, 3, 10, or 30 mg/kg i.p.; n=12-13 mice/dose). No significant effect of group was observed for either the pre-test ( $F_{3,48}=0.5$ ;  $P=0.65$ ) or test day ( $F_{3,48}=1.5$ ;  $P=0.24$ ). (C,D) Total immobility time (C,  $F_{3,43}=0.5$ ;  $P=0.70$ ) and latency to first immobility period (D,  $F_{3,43}=0.9$ ;  $P=0.46$ ) measured for C57BL/6J mice during a 6-min forced swim test 30 min following injection of ML297 (0/vehicle, 3, 10, or 30 mg/kg i.p.; n=11 mice/dose). (E) Percent time spent in the open arms ( $F_{3,43}=3.8$ ;  $P<0.05$ ) by C57BL/6J mice in a 5-min elevated plus maze test performed 30 min after injection of ML297 (0/vehicle, 3, 10, or 30 mg/kg i.p.; n=10-12 mice/dose). \*\* $P<0.01$  vs. 0/vehicle. (F) Effect of ML297 on stress-induced hyperthermia response in C57BL/6J mice. Change in temperature ( $\Delta T$ , in °C) from the point of stress (T1) taken 30 min after injection of ML297 (0/vehicle, 3, 10, or 30 mg/kg i.p.; n=12 mice/dose) to 10 min after stress (T2). A significant effect of dose was detected ( $F_{3,47}=4.9$ ;  $P<0.01$ ). \*,\*\*  $P<0.05$ , 0.01, respectively, vs. 0/vehicle. (G) Percent time spent in the open arms by wild-type and congenic *Girk1*<sup>-/-</sup> mice in a 5-min elevated plus maze test performed 30 min after injection of ML297 (0/vehicle or 30 mg/kg i.p.; n=11-16 mice/group). A significant drug x genotype interaction ( $F_{1,52}=7.0$ ;  $P<0.01$ ) was observed. Note the decreased baseline (vehicle group) anxiety-related behavior in *Girk1*<sup>-/-</sup> mice. \* $P<0.05$  vs. 0/vehicle (within genotype); ### $P<0.001$  vs. wild-type (within-dose). (H) Effect of ML297 (0/vehicle or 30 mg/kg i.p.; n=11-16 mice/group) on stress-induced hyperthermia response in wild-type and congenic *Girk1*<sup>-/-</sup> mice. A significant drug x genotype interaction ( $F_{1,36}=4.2$ ;  $P<0.05$ ) was observed. \*\* $P<0.01$  vs. 0/vehicle (within genotype).

## Discussion

The classical mode of GIRK channel activation involves the receptor-induced activation of  $G_{i/o}$  G proteins, which facilitates an interaction between channel and  $G\beta\gamma$ . Several lines of evidence argue that ML297-induced activation of GIRK channels differs mechanistically from this mode of channel activation. For example, ML297 activation of GIRK1-containing channels is not impacted by pertussis toxin, an inhibitor of  $G_{i/o}$  G proteins [169]. In addition, ML297 selectively activates GIRK1-containing channels, whereas  $G\beta\gamma$  activates both GIRK1-containing and GIRK1-lacking channels (*e.g.*, [64]).

Clear resolution of the channel- $G\beta\gamma$  interaction was obtained with the co-crystallization of  $G\beta\gamma$  and a GIRK2 homomer [106].  $G\beta\gamma$  binds to an outward-facing surface created by two adjacent GIRK cytoplasmic domains (the  $\beta$ K,  $\beta$ L,  $\beta$ M, and  $\beta$ N sheets from one subunit, and the  $\beta$ D and  $\beta$ E sheets from the adjacent subunit; **Fig. 3.10A**). GIRK2 residues mediating the GIRK- $G\beta\gamma$  interaction include Q248 and F254 in  $\beta$ D- $\beta$ E, and L342-T343-L344 in  $\beta$ L- $\beta$ M. The GIRK- $G\beta\gamma$  interaction is electrostatic, facilitated by negatively-charged glutamic and aspartic acid residues found in the  $\beta$ L- $\beta$ M loop that attract the electropositive binding face on  $G\beta\gamma$ . Importantly, key elements of this interaction interface are conserved across all GIRK subunits, including GIRK1.

ML297-induced activation of GIRK channels also differs from channel modulation by other known channel activators. Intracellular  $\text{Na}^+$  ( $\text{EC}_{50}$  30-40 mM) activates neuronal and cardiac GIRK channels in a manner dependent on an aspartic acid residue found in the  $\beta$ C- $\beta$ D loop of GIRK2 and GIRK4, respectively [98, 100]. This residue, which contributes to the binding site for  $\text{Na}^+$  [93], is not found in GIRK1. Ethanol activates both GIRK1-containing and lacking channels in a G protein-

independent manner, without altering the strong rectification profile [162, 163]. The hydrophobic alcohol-binding pocket in GIRK2 homomers is formed by a residue in the N-terminus (Y58) and two residues in the  $\beta$ L- $\beta$ M sheet from one subunit (L342 and Y349), together with three residues in the  $\beta$ D- $\beta$ E sheet from the adjacent subunit (I244, P256, L257) [167]. As is the case for structures involved in mediating channel interactions with  $G\beta\gamma$  and  $Na^+$ , the structures mediating channel-alcohol interactions are largely conserved in GIRK1 [162, 163]. Furthermore, we show here that we can eliminate ML297-induced activation of GIRK channels without altering their sensitivity to MPD.

While GIRK channel activation via  $G\beta\gamma$ , ethanol, and  $Na^+$  involves unique structural determinants, these agents (and ML297) require membrane-bound  $PIP_2$  to activate GIRK channels.  $PIP_2$  interacts with lysine residues found at the interface between the transmembrane and cytoplasmic domains of GIRK subunits. Binding of  $G\beta\gamma$ , ethanol, and  $Na^+$  to GIRK channels strengthens channel affinity for  $PIP_2$  [92, 97, 166].  $PIP_2$  binding triggers a rotation of the inner transmembrane helices, displacing the inner helical gate found at the junction of the transmembrane and cytoplasmic domains. With  $PIP_2$  present, GIRK channels are ‘primed’ for activation. Indeed,  $G\beta\gamma$  binding (in the presence of  $PIP_2$ ) leads to opening of the inner-helical gate and the G-loop gate, which is formed by the inner face of the cytosolic domains;  $G\beta\gamma$  in the absence of  $PIP_2$  can only open the G-loop gate [93, 106]. We propose that ML297, like other channel agonists, ultimately activates GIRK channels by opening inner-helical and G loop gates.

Our data argue that ML297 interacts directly with GIRK1-containing channels. Indeed, the observations that one of the GIRK1 residues (D173) required for ML297 agonism has been linked to inward rectification [225] and that ML297 weakens the

inward rectification of the channel are difficult to reconcile with an indirect mechanism of action for ML297. Moreover, the relatively close spatial proximity of the two GIRK1 residues necessary and sufficient for ML297 agonism suggests the possibility that ML297 binds within a pocket formed by one or both residues [93] (**Fig. 3.10B**). We cannot exclude the possibility, however, that ML297 binds to other domains of GIRK1 or to domain(s) conserved across all GIRK subunits. ML297 may bind to both GIRK1/GIRK2 heteromers and GIRK2 homomers, for example, but residues F137 and D173 in GIRK1 translate ML297 binding to enhanced channel activity better than their counterparts in GIRK2. Indeed, these residues were implicated previously in studies aimed at identifying structures in GIRK1 that potentiate basal and receptor-induced activity of heteromeric GIRK channels [114, 220]. Moreover, we show that the deactivation rate of ML297-induced current carried by GIRK2<sup>F/D</sup>/GIRK2 heteromers was substantially slower than that observed for GIRK1/GIRK2 heteromers. Since deactivation rate for a direct-acting channel agonist should largely reflect agonist-channel affinity, these findings support the contention that structures in GIRK2 influence the ML297-GIRK channel interaction. This contention is further supported by the observation that some ML297 derivatives show differential selectivity for GIRK1/GIRK2 and GIRK1/GIRK4 channels [226].

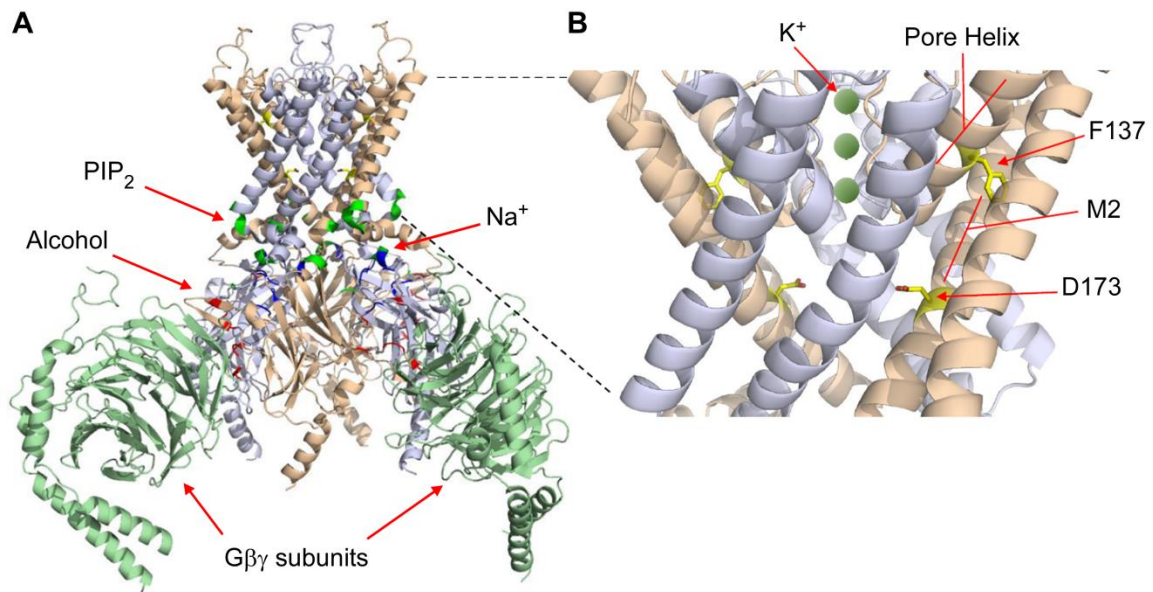


**Figure 3.10. Structural elements involved in GIRK channel activation by Gβγ, PIP<sub>2</sub>, Na<sup>+</sup>, and ML297.** (A) Crystal structure of the GIRK2 homomer bound to Gβγ (Protein Data Bank (PDB) ID code 4KFM), with regions critical for binding PIP<sub>2</sub>, alcohol, and Na<sup>+</sup> denoted by arrows. Note that only 2 bound Gβγ complexes are displayed, in the interest of clarity. The extracellular, transmembrane, and intracellular domains of the four GIRK2 subunits are shown. Specific locations of residues forming binding sites for PIP<sub>2</sub> [93, 106], alcohol [167], and Na<sup>+</sup> [93] are shaded and denoted by arrows. (B) An expanded view of the transmembrane domain depicting the predicted locations of the GIRK1 residues (F137 and D173, shown by arrows) identified as necessary and sufficient for conferring ML297 sensitivity to GIRK channels. The locations of the pore helix (which contains F137) and 2<sup>nd</sup> membrane-spanning domain (which contains D173) are highlighted. Three K<sup>+</sup> ions are shown (spheres) to identify the location of the transmembrane permeation pathway.

ML297 reduced anxiety-related behavior in mice in a GIRK1-dependent manner, without displaying rewarding or sedative effects. Interestingly, genetic ablation of *Girk1* (this study) or *Girk2* also correlated with reduced anxiety-related behavior in mice [223, 224]. The similarity in behavioral outcome for *Girk* ablation and acute systemic pharmacologic GIRK activation is likely attributable to molecular and/or developmental compensation occurring secondary to constitutive gene ablation in knockout studies. Indeed, altered glutamatergic signaling has been documented in multiple neuron populations in *Girk1*<sup>-/-</sup> and *Girk2*<sup>-/-</sup> mice [227, 228].

The sensitivity of GIRK channels to ethanol suggests that GIRK channels are relevant molecular targets for alcohol [162, 163]. In support of this contention, wild-type but not *Girk2*<sup>-/-</sup> mice, developed a conditioned place preference to ethanol [229]. Thus, GIRK channel activation might underlie in part the rewarding effect of ethanol. ML297, however, did not evoke a conditioned place preference in wild-type mice. A possible explanation for the differential reward liability of ethanol and ML297 is that the reward-related, GIRK-dependent effects of ethanol are mediated by GIRK channels lacking GIRK1. In this context, it is noteworthy that dopamine neurons in the ventral tegmental area, a key anatomic substrate of addictive drugs, express GIRK2/GIRK3 heteromers [87].

The lack of potent and selective pharmacologic tools for studying GIRK channels has limited progress on understanding their physiological and pathophysiological relevance. Translational benefits associated with inhibiting or enhancing GIRK signaling are unlikely to be achieved without an ability to manipulate GIRK signaling in a region and/or subunit-selective manner. Here, we show that ML297 selectively activates native

GIRK1-containing channels, decreasing anxiety-related behavior at doses without associated reward or motor liabilities. Thus, ML297 – or perhaps its next-generation derivatives – represents an important step toward realizing the full therapeutic potential of GIRK channel manipulation.

## CHAPTER 4

**RGS6/G $\beta$ 5 complex accelerates I<sub>KACH</sub> gating kinetics in atrial myocytes and modulates parasympathetic regulation of heart rate**

**Posokhova E, Wydeven N, Allen KL, Wickman K\*, Martemyanov KA\*. RGS6/G $\beta$ 5 complex accelerates I<sub>KACH</sub> gating kinetics in atrial myocytes and modulates parasympathetic regulation of heart rate. *Circ. Res.* 2010; 107:1350-4**



## Introduction

Cardiac output is shaped to a great extent by sympathetic and parasympathetic influences. Parasympathetic input tempers heart rate (HR) and counteracts the pro-arrhythmic effects of sympathetic activation, and is mediated by acetylcholine (ACh) [204]. ACh is released from post-ganglionic parasympathetic neurons and binds to  $M_2$  muscarinic receptors ( $M_2R$ ) on pacemaker cells and atrial myocytes, triggering activation of pertussis toxin-sensitive ( $G_{i/o}$ ) heterotrimeric G proteins [51]. Once activated, G proteins dissociate into  $G\alpha$ -GTP and  $G\beta\gamma$  subunits, leading to modulation of adenylyl cyclase and multiple ion channels. Central among these reactions is the binding of  $G\beta\gamma$  to the atrial potassium channel  $I_{KACH}$ , a heterotetramer composed of GIRK1 and GIRK4 subunits [230]. Binding of  $G\beta\gamma$  to  $I_{KACH}$  enhances its gating which leads to cell hyperpolarization and ultimately, decreased HR [205].

The duration of G protein signaling is controlled by members of the Regulator of G protein Signaling (RGS) family [231]. RGS proteins stimulate inactivation of  $G\alpha$ -GTP, facilitating its re-assembly with  $G\beta\gamma$ . RGS proteins play a critical role in shaping bradycardic effects of  $M_2R$  receptor activation [89, 232, 233]. Indeed, eliminating RGS influence by expressing  $G\alpha$  subunits insensitive to RGS action results in a substantial enhancement of  $I_{KACH}$  regulation by  $M_2R$  signaling, via both  $G\alpha_o$  and  $G\alpha_{i2}$  pathways [232, 233]. Although more than 30 RGS proteins have been identified, the involvement of specific RGS proteins in the regulation of parasympathetic input is not fully-understood. Here, we report an unexpected role of the RGS6/ $G\beta5$  complex, previously

thought to be neuron-specific regulator, in the temporal regulation of M<sub>2</sub>R-I<sub>K</sub>ACh signaling.

## **Materials and Methods**

Littermate mice were used for all experiments in this study. All procedures were carried out in accordance with NIH guidelines and were approved by the Institutional Animal Care and Use Committee of the University of Minnesota.

*Antibodies, Recombinant Proteins, DNA Constructs*—Sheep anti-RGS6 antibodies ( $\alpha$ -RGS6-FL) were generated against recombinant fragment containing amino acids 263-472 of mouse RGS6 that was expressed and purified from *E.coli* as described [234]. Antibodies were affinity-purified on the epitope-conjugated column and stored in PBS buffer containing 50% glycerol. Rabbit anti-G $\beta$ 5 (SGS) and rabbit anti-R7BP (TRS) antibodies were a generous gift from Dr. William Simonds, NIDDK. Rabbit polyclonal anti-AU1 tag (GenScript, Piscataway, NJ), mouse monoclonal anti-AU5 (MMS-135R; Covance, Princeton, NJ), goat polyclonal anti-RGS4 (Santa Cruz Biotechnology, Santa Cruz, CA), rabbit polyclonal anti-G $\alpha_{i1/2}$  (Thermo Fisher Scientific, Rochford, IL) and rabbit polyclonal anti-G $\alpha_o$  (K20; Santa Cruz Biotechnology, Santa Cruz, CA) were purchased. All general chemicals were purchased from Sigma Aldrich (St. Louis, MO).

Cloning of full-length mouse G $\beta$ 5S and RGS6 was described previously [235, 236]. The open reading frame of G $\beta$ 5S was subcloned into pcDNA3.1/TOPO (Invitrogen) mammalian expression vector, and RGS6 was cloned into pcDNA3.1NT-GFP-TOPO (Invitrogen) creating an N-terminal fusion with GFP. Cloning of GIRK1-

AU5 and GIRK4-AU1 into mammalian expression vectors has been described [237]. All constructs were propagated using an *E.coli* Top-10 strain (Invitrogen), isolated using Nucleobond kits, (Macherey-Nagel; Bethlehem, PA) and sequenced.

*Mouse Strains*—The generation of *R7bp*<sup>-/-</sup> [137], *Gβ5*<sup>-/-</sup> [238], and *Girk4*<sup>-/-</sup> [205] mice has been described previously. *Gβ5*<sup>-/-</sup> mice were generously provided by Dr. Jason Chen (Virginia Commonwealth University). These three strains of mice were out-bred onto the C57BL/6 background for at least 5 generations. *Rgs6*<sup>-/-</sup> mice were generated by Lexicon Pharmaceuticals using 129SvEvBrd embryonic stem cells. Chimeric offspring were mated with C57BL/6 strain and the resulting heterozygous progeny were inbred to generate null mutant and wild-type littermates. Mice were housed in groups on a 12h light/dark cycle with food and water available *ad libitum*. All procedures were carried out in accordance with the National Institute of Health guidelines and were granted formal approval by the Institutional Animal Care and Use Committee of the University of Minnesota. All efforts were made to minimize the use of animals in this study, as well as their suffering. All animals used in this study were bred on-site.

*Cell culture and transfections*—HEK293FT cells were obtained from Invitrogen (Carlsbad, CA) and cultured at 37°C and 5% CO<sub>2</sub> in DMEM (Dulbecco's Modified Eagle Medium; GIBCO) supplemented with 100 units of penicillin and 100 mg of streptomycin, 10% FBS, 1x MEM non-essential amino acids (GIBCO; Carlsbad, CA), 1 mM sodium pyruvate and 4 mM L-glutamine. Cells were transfected at ~70% confluency, using Lipofectamine LTX (Invitrogen) according to the manufacturer's protocol. The ratio of Lipofectamine to DNA used was 6.25 μl : 2.5 μg per 10 cm<sup>2</sup> cell

surface. Cells were grown for 24-48 hours post-transfection. Equal amounts of each construct were transfected, balanced when necessary by empty pcDNA3.1 vector.

*Immunoprecipitation assays and Western blotting*—Cellular and tissue lysates were prepared in immunoprecipitation (IP) buffer (1XPBS (Fisher Scientific), 150 mM NaCl, 1% Triton X-100, protease inhibitors (Roche; Indianapolis, IN) and centrifuged for 15 min at 14,000 x g. Protein concentration was determined in the resulting extracts using BSA assay (Pierce; Rockford, IL) and equal amounts of protein were incubated with 3 µg of antibodies and 10 µl of protein G beads (GE Healthcare; Waukesha, WI) for 1 h at 4<sup>0</sup>C. After 3 washes with ice-cold IP buffer proteins bound to the beads were eluted with SDS-sample buffer. Eluates were resolved on 12.5% SDS-PAGE gel, transferred onto PVDF membrane (Millipore (Billerica, MA)) and subjected to Western blot analysis using HRP conjugated secondary antibodies and an ECL West Pico (Pierce) detection system. For quantification, samples were analyzed by infrared Western blotting using IRDye680 and IRDye800 labeled secondary antibodies (Li-Cor Biosciences; Lincoln, NE) according to the manufacturer's protocol. Detection and quantification of specific bands was performed on an Odyssey Infrared Imaging System (Li-Cor Biosciences). The integrated intensity of each band of interest was measured in a corresponding channel with a top-bottom background setting.

*Whole-cell electrophysiology*—Primary cultures of atrial myocytes were generated from neonatal mice (P2-4) as described [210, 239], using the Neonatal Cardiomyocyte Isolation System (Worthington Biochemical Corp., Lakewood, NJ). Atrial myocytes were used for electrophysiological analysis after 1-3 d in culture. Sinoatrial nodal cells were isolated from adult mice (3 months) as described [89], and

used within 8 h of isolation. In brief, hearts were excised into Tyrode's solution (in mM): 140 NaCl, 5.4 KCl, 1.2 KH<sub>2</sub>PO<sub>4</sub>, 1.0 MgCl<sub>2</sub>, 1.8 CaCl<sub>2</sub>, 5.5 glucose, 5 HEPES, pH 7.4 with NaOH. The sinoatrial node (SAN) was identified as the narrow band of tissue located on the inner wall of the right atrium, medial to the crista terminalis and between the superior and inferior vena cava. Two incisions were made to the superficial side of the superior and inferior vena cava, followed by a longer cut along the outer atrial wall, to expose the SAN region. SAN-containing tissue was excised into a modified Tyrode's solution containing (in mM): 140 NaCl, 5.4 KCl, 1.2 KH<sub>2</sub>PO<sub>4</sub>, 0.2 CaCl<sub>2</sub>, 50 taurine, 18.5 glucose, 5 HEPES, 0.1% BSA, pH 6.9 with NaOH, with elastase (0.3 mg/ml; Worthington Biochemical Corp.) and collagenase II (0.21 mg/ml; Worthington Biochemical Corp.). SAN tissue was digested at 37°C for 30 min, with occasional inversion, and then washed three times in a solution containing (in mM): 100 L-glutamic acid/potassium salt, 10 L-aspartic acid/potassium salt, 25 KCl, 10 KH<sub>2</sub>PO<sub>4</sub>, 2 MgSO<sub>4</sub>, 20 taurine, 5 creatine, 0.5 EGTA, 20 glucose, 5 HEPES, 0.1% BSA, pH 7.2 with KOH. SAN tissue was then triturated in the wash solution and plated onto poly-L-lysine coated coverslips for electrophysiological studies.

Coverslips containing atrial myocytes or SAN cells were transferred to a chamber containing a low-K<sup>+</sup> bath solution (in mM): 140 NaCl, 4 KCl, 2 CaCl<sub>2</sub>, 2 MgCl<sub>2</sub>, 10 D-glucose, 10 HEPES/NaOH (pH 7.4). Cardiac cells were visualized using an Olympus IX-70 microscope. The dominant population of atrial myocytes with spherical shape (typical capacitance, 10-20 pF) was targeted for this study. SAN cells were identified as the thin striated cells exhibiting spontaneous contractions (typical capacitance, 25-40 pF) (see **Fig. 4.6A**, inset). Membrane potentials and whole-cell currents were measured with

hardware (Axopatch-200B amplifier, Digidata 1320) and software (pCLAMP v. 9.2) from Molecular Devices (Sunnyvale, CA). Borosilicate patch pipettes (3-5 M $\Omega$ ) were filled with (in mM): 130 gluconate, 2 MgCl<sub>2</sub>, 1.1 EGTA/KOH (pH 7.2), 5 HEPES/KOH (pH 7.2), 2 Na<sub>2</sub>ATP, 5 phosphocreatine, 0.3 Na-GTP.

Upon achieving whole-cell access, input resistance, capacitance, and resting membrane potentials were measured. Neonatal atrial *myocytes and SAN cells from wild-type and knockout mice did not differ with respect to these parameters*. CCh-induced currents were measured at a holding potential of -70 mV using a high-K<sup>+</sup> bath solution (in mM): 120 NaCl, 25 KCl, 2 CaCl<sub>2</sub>, 2 MgCl<sub>2</sub>, 10 D-glucose, 10 HEPES/NaOH (pH 7.4). The high-K<sup>+</sup> bath solution (+/-CCh) was applied with an SF-77B rapid perfusion system (Warner Instruments, Inc.; Hamden, CT). In pilot studies, we found no difference in current amplitudes evoked by 10 and 100  $\mu$ M CCh, irrespective of genotype or cell type. As such, 10  $\mu$ M CCh was taken as the saturating CCh concentration for these studies. All currents were low-pass filtered at 1 kHz, sampled at 2 kHz, and stored on computer hard disk for analysis. Steady-state current amplitudes were measured for each experiment by subtracting the baseline current from the current measured just prior to the return to drug-free solution. Activation and deactivation time constants were extracted from appropriate regions of current traces, which were fit with a 1-term Boltzmann equation using the Levenberg-Marquardt search method, sum of squared errors minimization method, and no weighting (**Fig. 4.1**). Only those experiments for which the access resistances were stable and low (<15 M $\Omega$ ) were included in the final analysis.

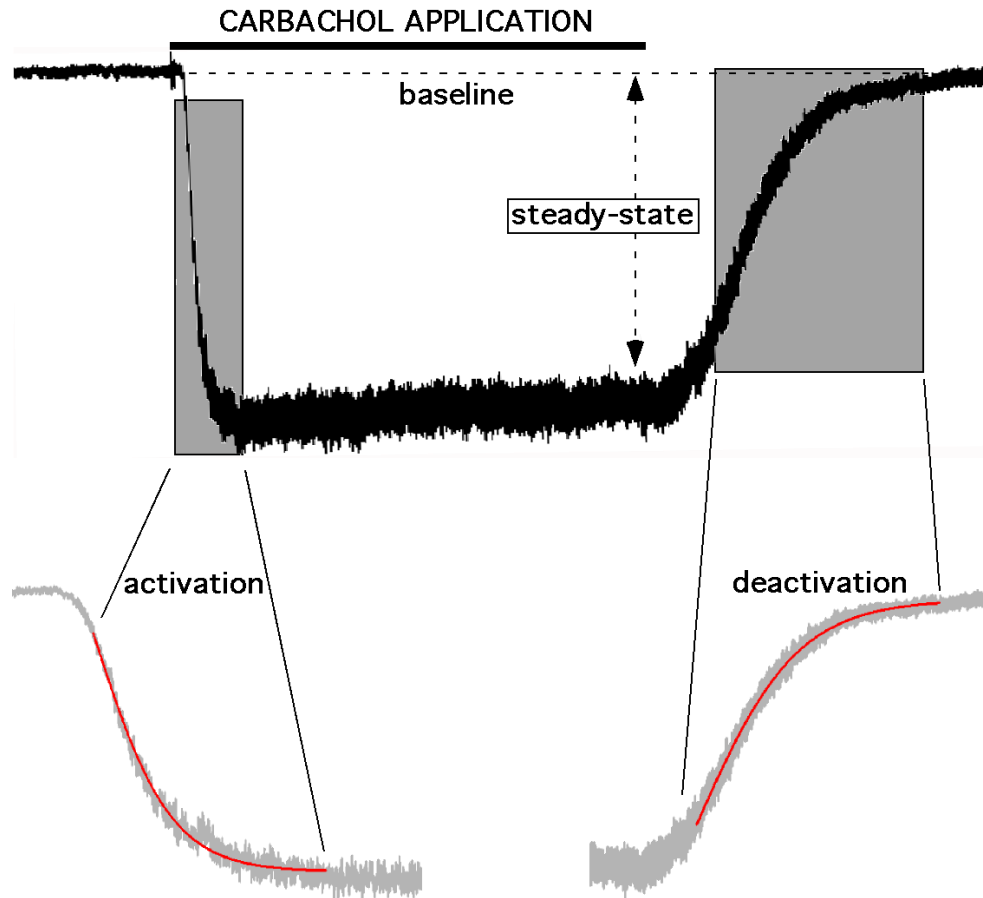


**Figure 4.1. Depiction of measured parameters for the whole-cell CCh-induced current studies.** A typical response of a wild-type neonatal atrial myocyte to 10  $\mu\text{M}$  CCh is shown, with the horizontal line showing the duration of CCh application. Current amplitude and density determinations involved steady-state currents, measured relative to baseline just prior to the removal of CCh. Shaded rectangles identify the regions of the trace used for determination of current activation and deactivation kinetics. The fit curves, derived from a 1-term standard Boltzmann equation, are shown overlaid on the expanded parts of the trace (bottom).

*Telemetry*—Wild-type (n=5) and *Rgs6*<sup>-/-</sup> (n=5) littermates aged 4-5 months were used for *in vivo* ECG monitoring. Biopotential telemetry transmitters ETA-F10 (Data Sciences International; Saint Paul, MN) were implanted intraperitoneally under ketamine/xylazine anesthesia (60 and 12 mg/kg correspondently). ECG leads were externalized and abdominal wall was closed with Prolene 5-0 (Ethicon; Somerville, NJ) incorporating suture rib of the transmitter into the closure. ECG leads were tunneled under the skin into lead II position and sutured to the abdominal wall by Prolene 5-0. Skin incisions were closed using Vicryl 5-0 (Ethicon). Upon termination of anesthesia, animals received a single intraperitoneal injection of ketoprofen (5 mg/kg), followed by administration of ibuprofen and amoxicillin in drinking water during recovery period (days 1-10). Upon recovery, recordings were performed in a scheduled manner, for 20 s each min, following 1-h acclimation using Dataquest ART 4.2 acquisition software (Data Sciences International). On day 11, 6 h of baseline ECG data were recorded. On day 12, after 30 min of baseline recording, animals were injected i.p. with 0.9% saline solution (10 ml/kg) as a vehicle control. Atropine sulfate was injected 2 h later (1 mg/kg, i.p.; Hospira, Lake Forest, IL), followed by 3 h of recording. On day 13, following 30 min of baseline recording, animals were injected first with 0.9% saline solution and 2 h later with CCh (0.1 mg/kg, i.p.; Acros Organics, Geel, Belgium). Recording proceeded for 3 h, after which animals were sacrificed by CO<sub>2</sub> inhalation. Transmitters were explanted, cleaned with 1% Tergazyme enzymatic detergent (Alconox; White Plains, NY), sterilized with Cidex activated dialdehyde solution (Ethicon), and reused.

*Statistical Analysis*—Statistical analyses were performed using Prism (GraphPad Software, Inc.; La Jolla, CA) and SigmaPlot 11 (Systat Software Inc; San Jose, CA).



EC<sub>50</sub> values were calculated with the Hill coefficient set to 1. The impact of genotype on CCh-induced current responses (steady-state current density and kinetics) was evaluated using one-way (single-saturating concentration study) and two-way (concentration-response study) ANOVA. The impact of genotype on CCh- and atropine-induced heart rate response was evaluated using two-way (time-response study) ANOVA. Tukey's Multiple Comparison (one-way ANOVA) and Bonferroni (two-way ANOVA) post hoc tests were used as appropriate. For all analyses, the level of significance was set at  $P < 0.05$ .

## Results

Profiling RGS6 protein expression across mouse tissues revealed its readily detectable levels in the heart in addition to abundant presence in the brain (**Fig. 4.2A and Fig. 4.3**). RGS6 protein was enriched in atria, where it was found predominantly in myocytes (**Fig. 4.4**), consistent with a recent report [240], and similar to the distribution of GIRK1, an integral subunit of I<sub>KACH</sub> (**Fig. 4.2B**). To begin exploring the role of *Rgs6* in cardiac physiology, we obtained *Rgs6*<sup>-/-</sup> mice where exons 5 to 7 encoding the critical N-terminal portion of the protein were eliminated (**Fig. 4.2C,D**). Immunoblotting verified the complete absence of RGS6 protein in the hearts of *Rgs6*<sup>-/-</sup> mice (**Fig. 4.2E**).

RGS6 interacts with the type 5 G protein  $\beta$  subunit (G $\beta$ 5) and the R7 binding protein (R7BP) in the CNS [132] (**Fig. 4.2F**). In the mouse heart, however, only G $\beta$ 5 is available for the interaction with RGS6 (**Fig. 4.2E**). RGS6 was undetectable in hearts from *G $\beta$ 5*<sup>-/-</sup> mice, indicating that the physical association with G $\beta$ 5 is critical for the

expression and/or stability of RGS6 (**Fig. 4.2G**). Similarly, G $\beta$ 5 levels were dramatically reduced in the *Rgs6*<sup>-/-</sup> heart but not brain, indicating that in the heart RGS6 is the predominant RGS bound to G $\beta$ 5. No effect on RGS6 or G $\beta$ 5 levels was observed upon elimination of R7BP or GIRK4. Notably, we detected no compensatory changes in either G $\alpha_{i/o}$  proteins or RGS4, a protein previously implicated in regulation of the *M<sub>2</sub>R-I<sub>KACH</sub>* signaling [89].

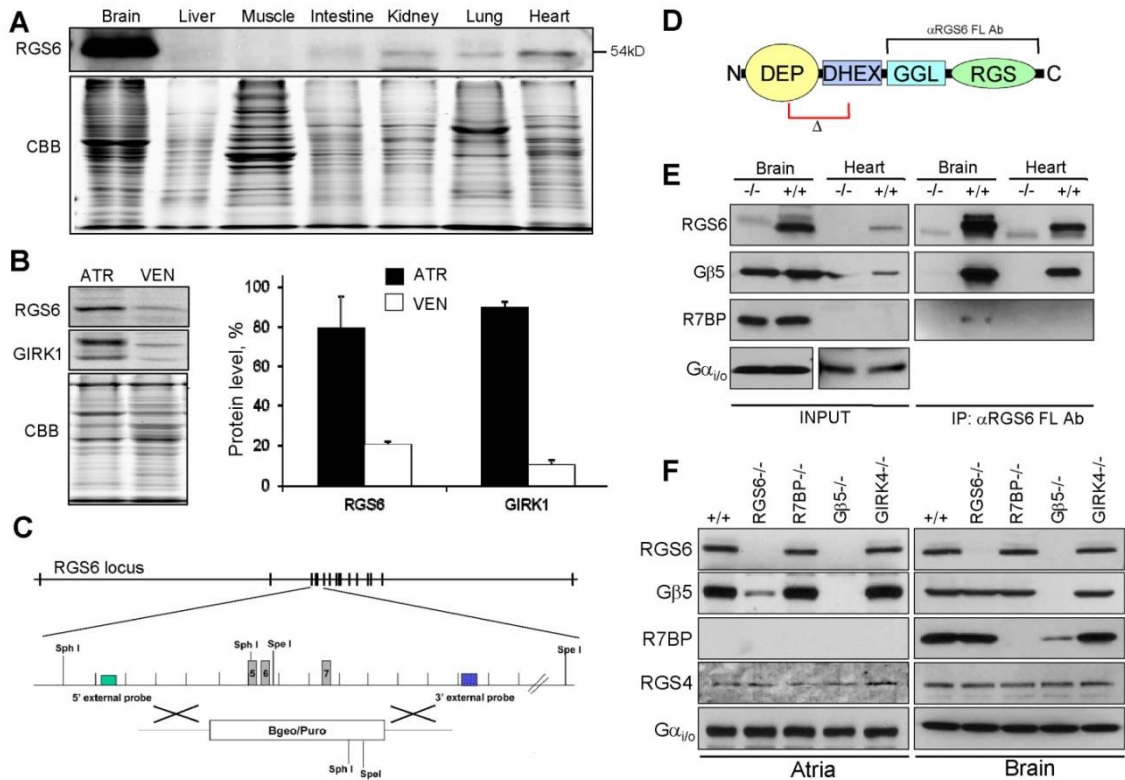


**Figure 4.2. RGS6 protein level and complex formation in the mouse heart.** **A**, RGS6 protein levels across mouse tissues as analyzed by Western blotting. Equal amounts of total protein (20  $\mu$ g) were loaded in each lane. Coomassie staining (CBB) was used as a loading control. **B**, RGS6 is co-enriched with GIRK1 in the atria. Atrial (ATR) and ventricular (VEN) lysates were analyzed by Western blotting (upper panels). CBB staining confirms equal protein loading. *Graph*: Quantification of RGS6 and GIRK1 band densities. **C**, Strategy for *Rgs6* ablation by homologous recombination. **D**, Structural organization of *Rgs6*. Frames designate the deleted region ( $\Delta$ ) and recognition site of the RGS6 FL antibody ( $\alpha$ RGS6 FL Ab) used throughout the study. Boxes designate known structural domains. **E**, Co-immunoprecipitation of RGS6 with G $\beta$ 5 and R7BP from heart and brain tissues. **F**, Co-dependence of RGS6 and G $\beta$ 5 expression in the heart and brain as analyzed by Western blotting.

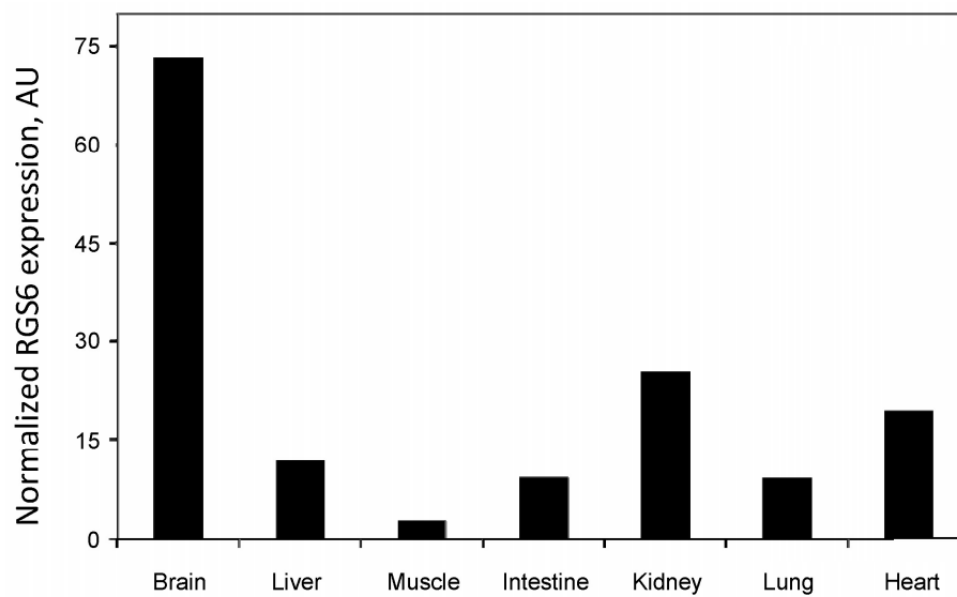


**Figure 4.3. Quantitative analysis of RGS6 distribution across tissues.** RGS6 band densities from Western blot experiment presented in Figure 1A have been determined by densitometry using Image J software and normalized to the total protein content determined from CBB stained gel (Figure 1A). Resulting values representing relative abundance of RGS6 proteins across tissues are plotted as a bar graph.

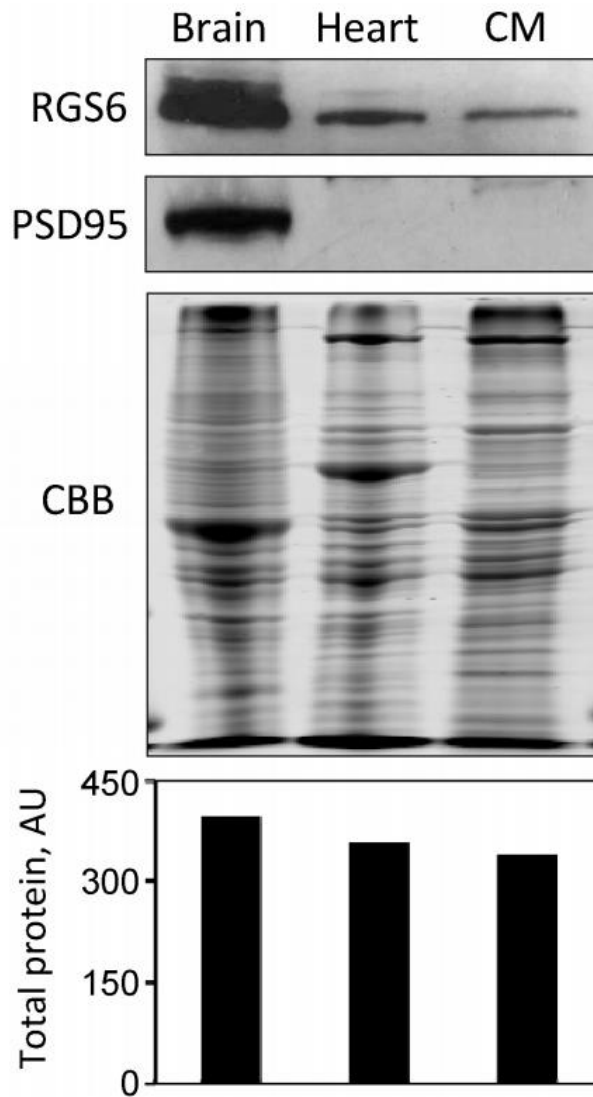


**Figure 4.4. RGS6 is present in isolated atrial cardiomyocytes.** Cardiomyocytes were isolated from adult mice as described in the Materials and Methods section above. Following lysis in SDS sample buffer, 25  $\mu$ g of total protein was loaded on the gel. RGS6 expression was detected by Western blotting with specific anti-RGS6-FL antibodies. Brain tissue was used as a control. The absence of the immunoreactivity for the neuronal specific marker PSD95 in isolated cardiomyocyte fraction (CM) demonstrate that RGS6 is predominantly expressed in the myocytes. Protein loading was verified by Coomassie Brilliant Blue (CBB) following separation on SDS-PAGE gel. Densitometric analysis of the total protein content quantified from the CBB-stained gel is presented in the lower panel.

Given the coenrichment of RGS6 and  $I_{KACH}$  in atria and the role of R7 RGS/G $\beta$ 5 complexes in G protein-coupled receptor-GIRK signaling in the CNS [146], we next measured the impact of *Rgs6* ablation on  $M_2R$ - $I_{KACH}$  signaling in neonatal atrial myocytes, which exhibit robust inward current triggered by the nonselective muscarinic agonist carbachol (CCh). Whereas CCh evoked currents with comparable potency in atrial myocytes from wild-type mice, current deactivation kinetics were notably slower across all CCh concentrations tested in myocytes from *Rgs6*<sup>-/-</sup> mice (**Fig. 4.5**). Current activation kinetics were also delayed in *Rgs6*<sup>-/-</sup> myocytes, although only for the lower CCh concentrations tested.

We next compared CCh-induced currents in sinoatrial node (SAN) cells, the key anatomic substrate for parasympathetic control of heart rate (**Fig. 4.6**). Although some differences in the density and kinetics of CCh-induced responses between adult SAN cells and neonatal atrial myocytes were evident, *Rgs6* ablation correlated with significantly delayed deactivation rates in both cell types. Under the same conditions, no differences in CCh-induced steady-state current density or activation kinetics were observed between genotypes in either atrial myocytes or SAN cells (**Fig. 4.6**). Furthermore, deletion of G $\beta$ 5 replicated prolonged deactivation kinetics seen in *Rgs6*<sup>-/-</sup> myocytes (**Fig. 4.6E**), indicating that regulation of the  $M_2R$ - $I_{KACH}$  signaling in heart atria is mediated by the RGS6/G $\beta$ 5 complex rather than RGS6 by itself.

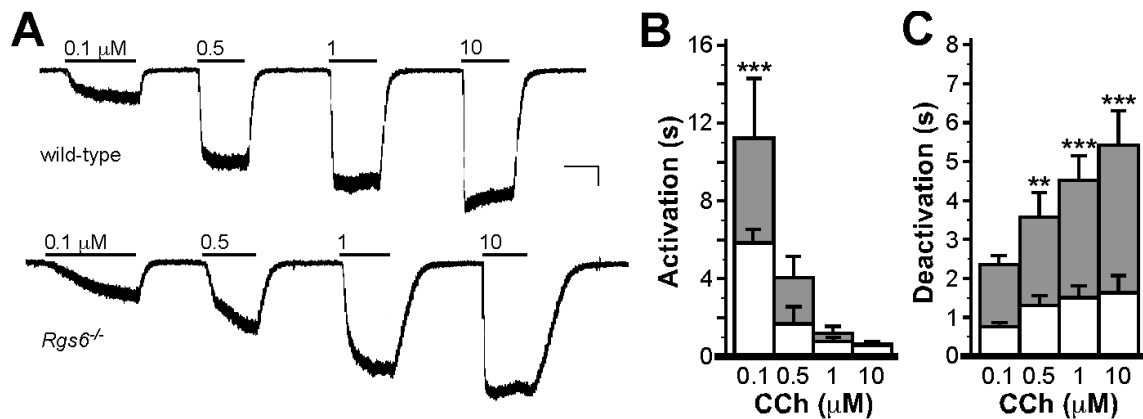


**Figure 4.5. Impact of *Rgs6* ablation on M<sub>2</sub>R-I<sub>KACH</sub> signaling in atrial myocytes.** **A**, Inward currents evoked by CCh (0.1-10 μmol/L) in atrial myocytes from wild-type and *Rgs6*<sup>-/-</sup> mice. Scale bars: 15 s/100 pA. Evoked currents developed gradually at 0.1 μmol/L CCh and saturated at 10 μmol/L CCh (responses to 10 μmol/L CCh are not shown). Steady-state current densities did not differ between *Rgs6*<sup>-/-</sup> (-36±4 pA/pF at 10 μmol/L CCh, n=7) and wild-type (-42±6 pA/pF, n=7) myocytes. **B**, Summary of M<sub>2</sub>R-I<sub>KACH</sub> activation kinetics in atrial myocytes from wild-type and *Rgs6*<sup>-/-</sup> mice. Main effects of concentration (F<sub>3,43</sub>=25.5; P<0.001) and genotype (F<sub>1,43</sub>=13.3; P<0.001) were observed, as well as a concentration x genotype interaction (F<sub>3,43</sub>=4.1; P<0.05). Symbols: \*\*\* P<0.001 vs. wild-type (within dose). **C**, Summary of M<sub>2</sub>R-I<sub>KACH</sub> deactivation kinetics in atrial myocytes from wild-type and *Rgs6*<sup>-/-</sup> mice. Main effects of concentration (F<sub>3,44</sub>=5.5; P<0.01) and genotype (F<sub>1,44</sub>=58.9; P<0.001) were observed, and there was no concentration x genotype interaction (F<sub>3,44</sub>=1.7; P=0.17). Symbols: \*\*\* P<0.05 and 0.01, respectively, vs. wild-type (within dose).

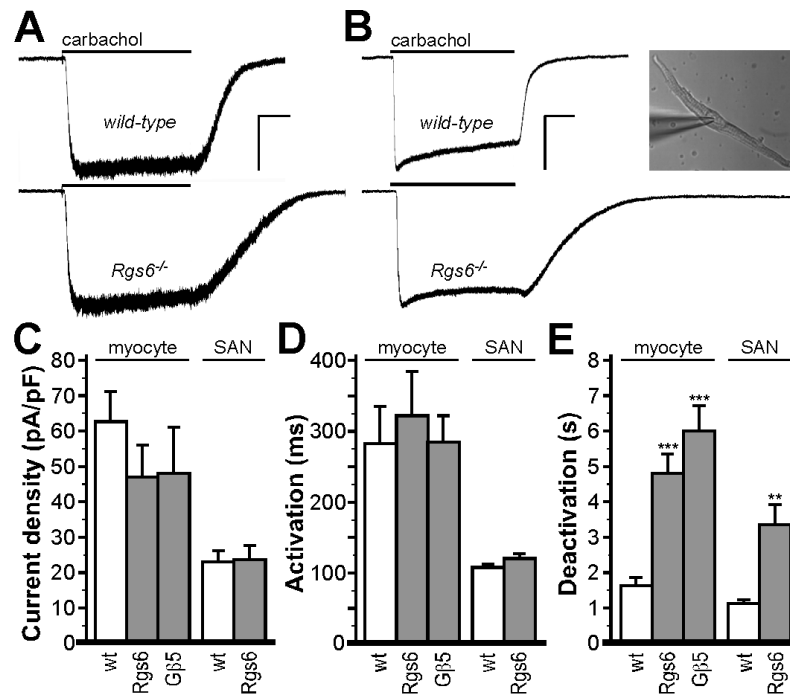


**Figure 4.6. Impact of *Rgs6* ablation on  $M_2R$ - $I_{KACH}$  signaling in atrial myocytes and SAN cells.** **A**, Inward currents evoked by CCh (10  $\mu$ mol/L) in atrial myocytes from wild-type and *Rgs6*<sup>-/-</sup> mice. Scale bars: 5 s/200 pA. **B**, Inward currents evoked by CCh (10  $\mu$ mol/L) in SAN cells from wild-type and *Rgs6*<sup>-/-</sup> mice. Scale bars: 5 s/400 pA. Inset: image of the wild-type SAN cell evaluated in the adjacent trace. Summary of steady-state CCh-induced current density (**C**), activation kinetics (**D**), and deactivation kinetics (**E**) in wild-type, *Rgs6*<sup>-/-</sup>, and *Gβ5*<sup>-/-</sup> atrial myocytes (n=5-11 per group), and in wild-type and *Rgs6*<sup>-/-</sup> SAN cells (n=10-12 per genotype). Genotype did not impact current density (atrial myocytes:  $F_{2,21}=1.9$ ,  $P=0.18$ ; SAN cells:  $t(20)=0.13$ ,  $P=0.90$ ) or activation kinetics (atrial myocytes:  $F_{2,21}=1.0$ ,  $P=0.38$ ; SAN cells:  $t(20)=1.69$ ,  $P=0.11$ ), but did influence deactivation kinetics (atrial myocytes:  $F_{2,21}=24.8$ ,  $P<0.001$ ; SAN cells:  $t(20)=3.71$ ,  $P<0.01$ ). Symbols: \*\* \*\*\*  $P<0.01$  and  $0.001$ , respectively, vs. wild-type (within cell type).



The striking impact of *Rgs6* ablation on M<sub>2</sub>R-I<sub>KACH</sub> signaling kinetics in atrial myocytes and SAN cells prompted us to test whether RGS6/Gβ5 can physically associate with the I<sub>KACH</sub> channel. In transfected HEK293 cells, we detected robust coimmunoprecipitation of the RGS6/Gβ5 complex with GIRK4 but not GIRK1 by both forward and reverse precipitation strategies (**Fig. 4.7**). Thus, the involvement of RGS6/Gβ5 in M<sub>2</sub>R-I<sub>KACH</sub> signaling is likely aided by a direct protein–protein interaction mediated by the cardiac-specific GIRK subunit GIRK4.

The delay in I<sub>KACH</sub> deactivation kinetics triggered by RGS6/Gβ5 elimination is expected to enhance M<sub>2</sub>R-I<sub>KACH</sub> signaling because the channel would stay open longer, which would potentiate the parasympathetic regulation of HR. We addressed this possibility by analyzing cardiac function in mice using ECG telemetry, at baseline and following pharmacological manipulation. Analysis of ECG traces did not reveal gross abnormalities in cardiac physiology in *Rgs6*<sup>-/-</sup> mice (**Fig. 4.8A** and **Fig. 4.9**). *Rgs6*<sup>-/-</sup> mice did, however, display a mild resting bradycardia (511±13 versus 476±4 bpm, P<0.05), consistent with the effect of RGS6/Gβ5 ablation on M<sub>2</sub>R-dependent signaling in atrial myocytes (**Fig. 4.8B**). Although CCh administration (0.1 mg/kg, IP) triggered a rapid decrease in HR in wild-type and *Rgs6*<sup>-/-</sup> animals, the effect was significantly larger and persisted longer in *Rgs6*<sup>-/-</sup> mice (**Fig. 4.8C**). Similarly, parasympathetic blockade with atropine (1 mg/kg, IP) had a positive chronotropic effect in both groups, with a significantly larger effect seen in *Rgs6*<sup>-/-</sup> mice (**Fig. 4.8D**). Importantly, there was no difference in HR immediately following atropine administration, indicating that the bradycardia seen in *Rgs6*<sup>-/-</sup> mice results from enhanced intrinsic M<sub>2</sub>R signaling.

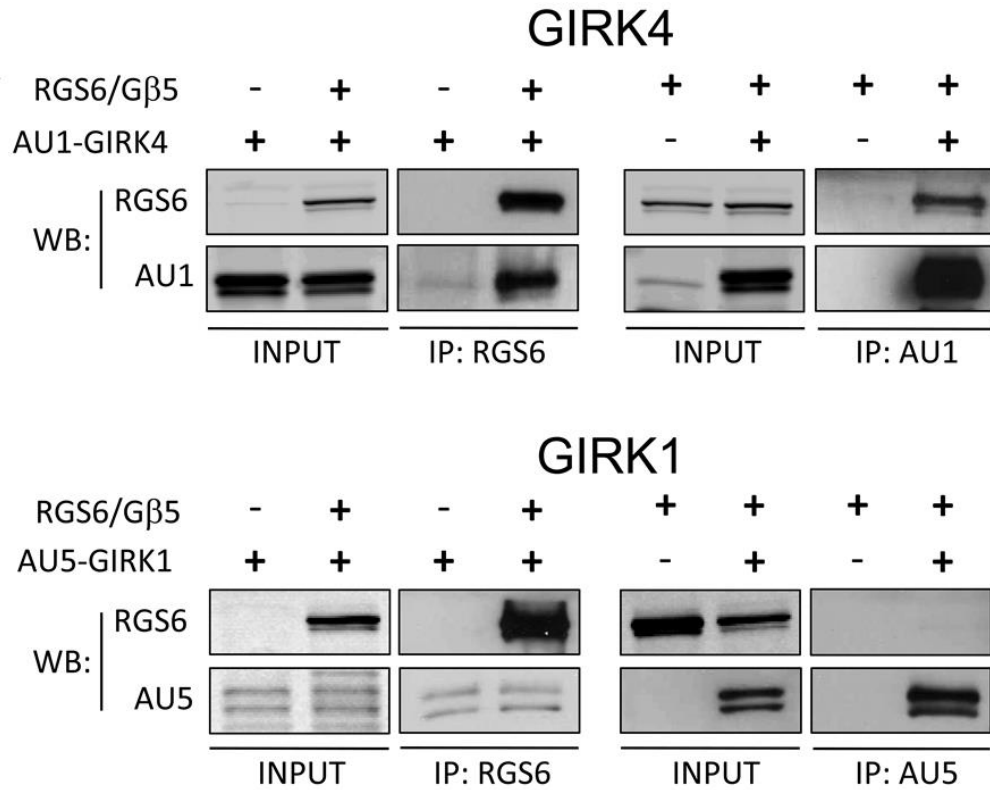


**Figure 4.7. RGS6/Gβ5 forms a complex with GIRK4.** RGS6 and Gβ5 were co-expressed with either AU1-tagged GIRK4 or AU5-tagged GIRK1 in HEK293 cells. Forward and reciprocal co-immunoprecipitation assays were performed as described in the *Methods* using indicated antibodies. Eluates were analyzed using Western blotting.

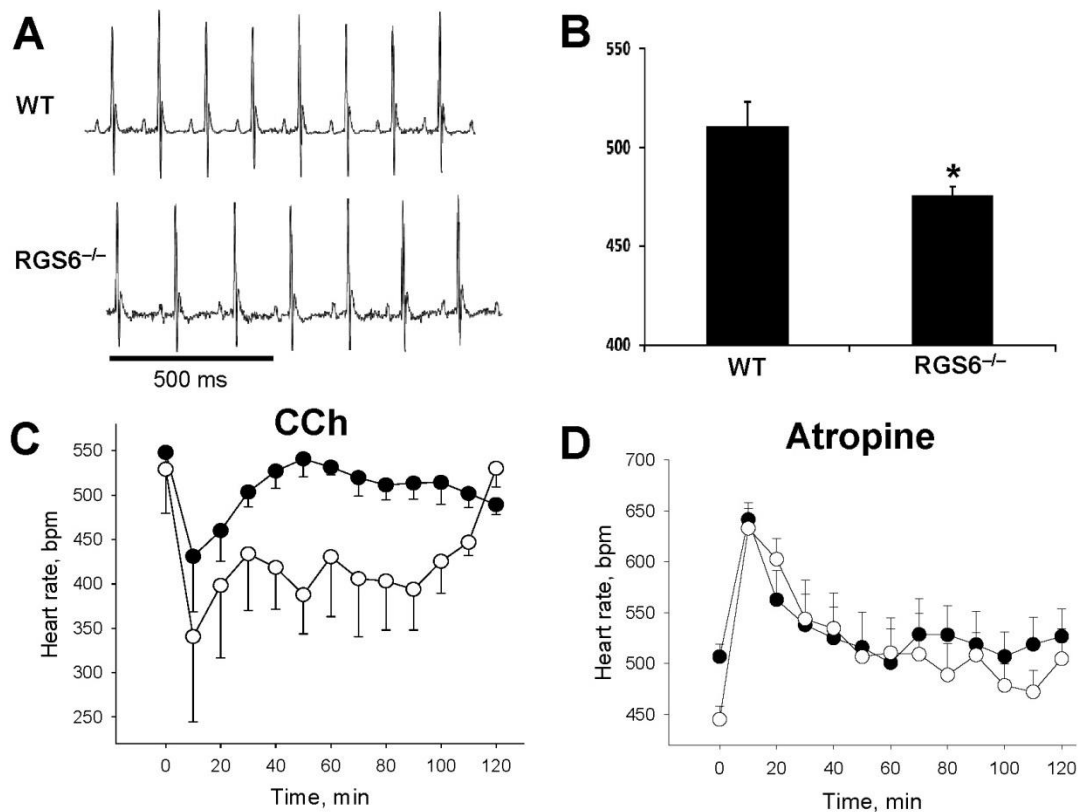
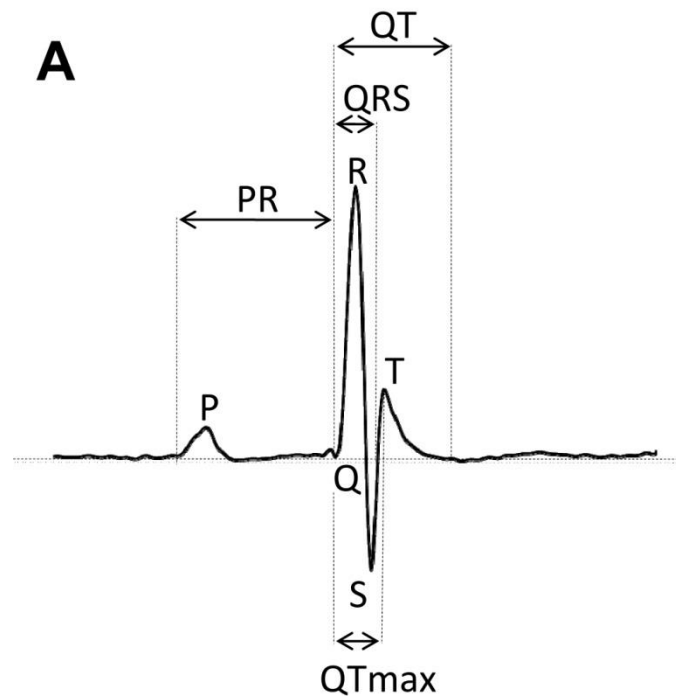


**Figure 4.8. Effect of *Rgs6* ablation on resting HR and muscarinic regulation.** **A**, Baseline ECG recorded during light phase from conscious, unrestrained wild-type (WT,  $n=5$ ) and *Rgs6*<sup>-/-</sup> mice ( $n=5$ ). **B**, Average HR as determined from the analysis of the ECG recordings (6hr). Symbols: \*  $P<0.05$  vs. wild-type. **C**, Effect of CCh (10 mg/kg, i.p.) on HR, analyzed and plotted as simple moving average with a period of 10 min in wild-type (closed circles) and *Rgs6*<sup>-/-</sup> mice (open circles). HR at 0 min corresponds to the 30-min average baseline HR on the day of the experiment. Two-way ANOVA analysis (genotype and time) of the 120-min post-injection interval revealed main effects of genotype ( $F_{1,104}=21.6$ ;  $P<0.001$ ). **D**, Effect of atropine (1 mg/kg, i.p.) on HR, analyzed and plotted as simple moving averages with a period of 10 min in wild-type (closed circles) and *Rgs6*<sup>-/-</sup> mice (open circles). No significant difference in HR was observed during the 60-min post-injection interval ( $F_{1,56}=0.02$ ;  $P=0.89$ ).



**B**

Interval, ms±SEM	RGS6 <sup>+/+</sup>	RGS6 <sup>-/-</sup>
PR	39.41±1.08	40.94±2.12
QRS	9.68±0.49	10.14±0.55
QT	44.12±1.91	38.75±2.08
QTmax	12.06±0.60	11.88±0.29

**Figure 4.9. Quantitative analysis of ECG intervals in *Rgs6*<sup>-/-</sup> mice.** **A**, Representative ECG trace obtained from *Rgs6*<sup>-/-</sup> mice. Peaks and intervals used for the quantitative analysis are annotated. **B**, Quantitative analysis of the ECG traces. Data derived from the analysis of total 500 representative traces from 3 to 5 mice of each genotype. Values were averaged separately for each animal. Group sizes were defined as a number of unique animals used for the analysis (n=3-5). Errors are s.e.m. values.

## Discussion

Here, we report that RGS6/G $\beta$ 5 negatively regulates M<sub>2</sub>R-I<sub>KACH</sub> signaling in atrial myocytes by accelerating I<sub>KACH</sub> deactivation kinetics. These observations, together with the effect of *Rgs6* ablation on HR and responses to pharmacological manipulation, indicate that RGS6/G $\beta$ 5 represents a key node of regulation in the parasympathetic control of cardiac output. Because dysregulation of the parasympathetic tone by deficiencies in I<sub>KACH</sub> function is increasingly accepted as a major factor in the pathogenesis of the atrial fibrillation [204], our study introduces RGS6/G $\beta$ 5 complex as an attractive candidate for better understanding of cardiac pathophysiology and development of corrective therapies.

RGS6 belongs to the R7 family of RGS proteins, members of which were thought to be expressed exclusively in the nervous system, where they play roles in nociception, vision, reward behavior and locomotion [132]. Although RGS6 expression was reported previously in the heart [135, 240, 241], our study documents for the first time the functional relevance of RGS6 to cardiac physiology. In the CNS, RGS6 forms complexes with 2 proteins, G $\beta$ 5 and R7BP, that specify its stability, subcellular distribution, and activity [132]. Here, we show that cardiac RGS6 forms a complex with G $\beta$ 5, but not with R7BP which is undetectable in the heart. The obligate and functionally relevant nature of the RGS6/G $\beta$ 5 interaction was underscored by the mutual dependence of RGS6 and G $\beta$ 5 levels on their coexpression and the phenotypic similarities in M<sub>2</sub>R-I<sub>KACH</sub> signaling in myocytes from *Rgs6*<sup>-/-</sup> and *G $\beta$ 5*<sup>-/-</sup> mice. In neurons, G $\beta$ 5 recruits R7 RGS proteins to GIRK channels, resulting in accelerated channel kinetics associated with GABA<sub>B</sub> receptor activation [146]. Thus, the present work reveals the conservation of this

compartmentalization mechanism by showing that RGS6/G $\beta$ 5 can likewise regulate M<sub>2</sub>R-I<sub>KACH</sub> signaling.

Previous work has identified RGS4 as a critical regulator of M<sub>2</sub>R-I<sub>KACH</sub> signaling in sinoatrial nodal cells [89]. Indeed, the deficiencies in M<sub>2</sub>R-I<sub>KACH</sub> signaling linked to *Rgs6* ablation reported herein are reminiscent of those reported in *Rgs4*<sup>-/-</sup> mice [89]. Therefore, murine sinoatrial nodal cells may use parallel approaches involving RGS4 and RGS6/G $\beta$ 5 to regulate M<sub>2</sub>R-I<sub>KACH</sub> signaling. It is possible, for example, that RGS4 and RGS6/G $\beta$ 5 selectively regulate different G protein subtypes involved in I<sub>KACH</sub> gating. Indeed, studies with knock-in mice expressing RGS-insensitive G proteins reveal a differential contribution of G $\alpha_{i2}$  and G $\alpha_o$  to M<sub>2</sub>R-dependent actions [232, 233]. Furthermore, RGS6/G $\beta$ 5 shows selectivity toward G $\alpha_o$  over G $\alpha_{i2}$  in vitro [242]. However, whereas the role of G $\alpha_{i2}$  in mediating M<sub>2</sub>R-I<sub>KACH</sub> coupling is well established [233], the involvement of G $\alpha_o$  in this process is less certain. Moreover, it remains possible that other proteins of the more than 30-member RGS family also play roles in this regulation. Delineating the mechanisms of the functional involvement of RGS proteins in controlling M<sub>2</sub>R-I<sub>KACH</sub> signaling in the mouse models and their relevance to human physiology will serve as an exciting direction for future research.

## **CHAPTER 5**

**RGS6, but not RGS4, is the dominant regulator of G protein signaling (RGS) modulator of the parasympathetic regulation of mouse heart rate**

**Wydeven N, Posokhova E, Xia Z, Martemyanov K, Wickman K. RGS6, but not RGS4, is the dominant regulator of G protein signaling (RGS) modulator of the parasympathetic regulation of mouse heart rate. J. Biol. Chem. 2014; 289(4):2440-9.**

## Introduction

Cardiac output reflects a balance between input from the parasympathetic and sympathetic branches of the autonomic nervous system. Parasympathetic tone is dominant under resting conditions, slowing heart rate (HR) by decreasing spontaneous pacemaker activity of the sino-atrial node (SAN) [243, 244]. Excessive parasympathetic influence can lead to atrioventricular block, and dysregulation of parasympathetic activity has been linked to sinus node dysfunction and arrhythmia [232, 245, 246]. The importance of parasympathetic regulation to cardiac physiology and pathophysiology has prompted much interest in characterizing the molecular basis of parasympathetic actions in the heart.

The negative chronotropic effect of acetylcholine (ACh) is largely mediated by activation of  $M_2$  muscarinic receptors ( $M_2R$ ) and inhibitory ( $G_{i/o}$ -dependent) G protein signaling in SAN cells [243, 244]. Activated  $G_{i/o}$  G proteins inhibit adenylyl cyclase, leading to suppression of hyperpolarization-activated cyclic nucleotide gated cation channels and L-type  $Ca^{2+}$  channels, while activating the muscarinic-gated atrial  $K^+$  channel  $I_{KACH}$  [243, 244].  $I_{KACH}$  is a tetramer formed by GIRK1/Kir3.1 and GIRK4/Kir3.4 subunits [69], and is found in SAN cells, atrial myocytes, and atrioventricular node cells [243].  $I_{KACH}$  activation accounts for a substantial fraction of the negative chronotropic influence of parasympathetic stimulation on HR in mice [205]. Moreover, loss of this signaling pathway correlates with elevated resting HR, a decrease in heart rate variability (HRV), resistance to pacing-induced arrhythmia, and protracted recovery times from stress, physical activity, and direct sympathetic stimulation [205, 210, 247, 248].



The parasympathetic regulation of HR, and M<sub>2</sub>R-I<sub>KACH</sub> signaling in cardiac myocytes, is negatively-modulated by Regulator of G protein Signaling (RGS) proteins [232, 233, 249, 250]. RGS6, in complex with the atypical Gβ subunit Gβ5 (RGS6/Gβ5), has been implicated in the parasympathetic regulation of HR [251, 252]. Indeed, *Rgs6*<sup>-/-</sup> mice exhibited slower resting HR, enhanced sensitivity to M<sub>2</sub>R-dependent bradycardia, elevated HRV, and enhanced M<sub>2</sub>R-I<sub>KACH</sub> signaling characterized primarily by a prominent slowing of current deactivation [251-253]. Moreover, a loss-of-function mutation in the human *RGS6* gene correlated with elevated HRV [253], and an *RGS6* polymorphism correlated with altered HR recovery after exercise [254].

Interestingly, RGS4 was the first RGS protein implicated in the parasympathetic regulation of HR and modulation of M<sub>2</sub>R-I<sub>KACH</sub> signaling in SAN cells [89, 207]. Indeed, the isolated heart and SAN cell phenotypes reported in *Rgs4*<sup>-/-</sup> and *Rgs6*<sup>-/-</sup> mice related to parasympathetic HR regulation and M<sub>2</sub>R-I<sub>KACH</sub> signaling were virtually identical [251, 252], suggesting the possibility that SAN cells employ parallel RGS4- and RGS6/Gβ5-dependent mechanisms to modulate the parasympathetic regulation of HR. To test this hypothesis, we generated mice lacking both RGS4 and RGS6, and evaluated the impact of single or dual RGS ablation on parasympathetic HR regulation and M<sub>2</sub>R-I<sub>KACH</sub> signaling in SAN cells. Our findings argue that RGS6/Gβ5 provides the dominant RGS influence on parasympathetic regulation of HR in the mouse.

## Materials and Methods

*Animals*—*Rgs4*<sup>-/-</sup> mice (B6;129P2-*Rgs4*<sup>tm1Dgen</sup>/J) were purchased from Jackson Labs (Bar Harbor, ME). The generation of *Rgs6*<sup>-/-</sup> mice was described previously [252].

Mice were housed in groups on a 12-h light/dark cycle with food and water available *ad libitum*. All procedures were approved by Institutional Animal Care and Use Committees of the University of Minnesota and The Scripps Research Institute.

*qRT-PCR*—RGS4 expression in the SAN and hippocampus from wild-type and *Rgs4*<sup>-/-</sup> mice was compared using quantitative RT-PCR. Intact hippocampi were extracted from freshly-isolated brain tissue, and total RNA was isolated using Trizol, according to manufacturer's recommendations (Invitrogen; Carlsbad, CA), and treated with recombinant DNase I (Roche; Indianapolis, IN). Total RNA from mouse heart (SAN and left atria) was isolated using RNeasy Fibrous Tissue Mini Kit (Qiagen; Germantown, Maryland). Reverse transcription was performed using iScript™ cDNA Synthesis Kit (Bio-Rad Laboratories; Hercules, CA). The qPCR was performed on a LightCycler® 480 II in a final volume of 20 µL, with LightCycler® 480 SYBR Green I Master kit (Roche Applied Science; Indianapolis, IN). After pre-incubation at 95°C for 5 min, amplification consisted of 45 cycles of 10 s denaturation at 95°C, followed by annealing (30 s) at 60°C and extension (10 s) at 72°C. Intron-spanning RGS4 primer sets were as follows: set A (A+: 5'-gtcgaatacagcgaggagaac-3', A-: 5'-ggaag gattggcagggtcaagatag-3'), set B (B+: 5'-ttcaccatgaa tgtggactggca-3', B-: 5'-gtccaggttcacctctttgtgc-3'). All samples were tested in triplicate; the average of replicates was used in the data analysis. GAPDH (Mm\_Gapd\_2\_SG QuantiTect primers; Qiagen) was used as internal control in each test.

*Quantitative immunoblotting*—Preparation of hippocampal neuron cultures was described previously [220]. After 10 days, cultures were treated with vehicle (DMSO) or 50 µM MG132 (American Peptide Company; Sunnyvale, CA) for 6 h. Neurons were lysed in RIPA buffer containing protease inhibitors (10 mg/mL pepstatin A, 10 mg/mL

aprotinin, 10 mg/mL PMSF, 1 mg/mL leupeptin, and 50  $\mu$ M MG132) and incubated on ice for 20 min. Lysates were centrifuged for 15 min at 16,000 x g at 4°C. The supernatant was mixed with 4X SDS sample buffer, heated to 75°C, and then stored at 4°C. DTT was added to each sample to a final concentration of 0.2 M. Samples were then heated at 75°C for 10 min, loaded onto 12% Bis-Tris gels, and run in a Tris-glycine buffer. Samples were transferred to nitrocellulose membranes and blocked in 5% milk for 1 h. Primary antibodies against RGS4 (EMD Millipore; Billerica, MA) and  $\beta$ -actin (Abcam; Cambridge, MA) were diluted in 5% milk to 1:200 and 1:10,000, respectively, and then incubated overnight at 4°C with shaking. Blots were washed 3X with PBS+0.1% Tween-20 and then incubated with IRDye 680CW donkey anti-rabbit and IRDye 800CW donkey anti-mouse secondary antibodies (Li-Cor Biosciences; Lincoln, NE), diluted 1:2000 and 1:5000 in 5% milk, respectively, for 1 h at room temperature with shaking. After 3 more washes in PBS+0.1% Tween-20, blots were developed using an Odyssey Infrared Imaging System (Li-Cor Biosciences); integral band intensities were measured using Li-Cor Odyssey software.

*Ex vivo cardiac physiology*—Mice (8-12 wks) were heparinized (100 IU) and anesthetized using isoflurane (Halocarbon; River Edge, NJ). Hearts were rapidly excised and immediately cannulated for retrograde aortic perfusion in a constant pressure mode (60 mmHg) with modified Krebs-Henseleit buffer containing (in mM): 118.5 NaCl, 25 NaHCO<sub>3</sub>, 4.7 KCl, 1.2 KH<sub>2</sub>PO<sub>4</sub>, 11 D-glucose, 1.2 MgSO<sub>4</sub>, 1.8 CaCl<sub>2</sub>, 2 sodium pyruvate. The buffer solution was filtered (0.22  $\mu$ m) and saturated with 95% O<sub>2</sub>-5% CO<sub>2</sub> at 38°C. Hearts were allowed to stabilize for 30 min, and were excluded from pharmacological experiments and HRV analysis if any of the following was present: (i)

persistent arrhythmia >5 min, (ii) HR below 250 bpm, (iii) stable steady-state HR not attained within the first 20 min. Hearts with signs of ischemia upon dismounting from the apparatus were also excluded. *Ex vivo* data were acquired using the PowerLab data acquisition system (ADInstruments; Colorado Springs, CO) and digitized at a sampling rate of 2 kHz. LabChart Pro v.7 software with HRV and dose-response plug-ins (ADInstruments) was used for all data analysis. Basal HRs were quantified within a 10 min window using the HRV plug-in of LabChart Pro v7 as described below. The HR response to various doses of CCh was measured as the 7-min average following the beginning of drug application. Effect of CCh in isoproterenol (Iso)-treated hearts was evaluated in a similar manner. After stabilizing the hearts with Krebs-Henseleit buffer perfusion they were treated with 50 nM Iso alone (to establish the appropriate baseline) or in combination with increasing doses of CCh. All drugs were added to the perfusate immediately prior to the start of the treatment to minimize effects on stability and concentration. The HR response was measured as the 7-min average following the beginning of drug application (CCh+Iso) or the beginning of the response plateau (Iso alone).

*HRV analysis*—A “maximum after threshold” algorithm was used for R peak detection. Noisy data segments and ectopic beats were manually excluded from analysis. Signal pre-processing, threshold and retrigger delay values were altered when necessary to ensure all the peaks within the selected window were labeled correctly. All HRV parameters were analyzed in the 5-min interval preceding drug treatment for isolated hearts, or over a 5 min total of appended consecutive intervals of telemetry recording (baseline), or within the last 5-min window of drug application for isolated hearts. For

time domain analysis, the following parameters were calculated: mean normal-to-normal interval (NN, ms), standard deviation of all NN intervals (SDNN, ms), and square root of the mean square of successive differences between adjacent NN intervals (RMSSD, ms). Frequency domain analysis was done with FFT (Fast Fourier Transformation) size of 1024 and a Welch window with half overlap. Frequency bands were defined as follows: 0.4-1.5 Hz, low frequency (LF); 1.5-5 Hz, high frequency (HF). Power in each band and total power (TP, 0.0-10 Hz;  $\text{ms}^2$ ) were calculated. LF and HF were also expressed in normalized units (nu;  $(\text{LF or HF}) \times 100 / (\text{TP} - \text{VLF})$ ), and LF/HF ratio was determined.

*SAN preparation and electrophysiology*—SAN cells were isolated from adult mice (2-3 months) as described [89], and used within 8 h of isolation. In brief, hearts were excised into Tyrode's solution (in mM): 140 NaCl, 5.4 KCl, 1.2  $\text{KH}_2\text{PO}_4$ , 1.0  $\text{MgCl}_2$ , 1.8  $\text{CaCl}_2$ , 5.5 glucose, 5 HEPES, pH 7.4 with NaOH. The SAN was identified as the narrow band of tissue located on the inner wall of the right atrium, medial to the crista terminalis and between the superior and inferior vena cava. Two incisions were made to the superficial side of the superior and inferior vena cava, followed by a longer cut along the outer atrial wall, to expose the SAN region. SAN-containing tissue was excised into a modified Tyrode's solution containing (in mM): 140 NaCl, 5.4 KCl, 1.2  $\text{KH}_2\text{PO}_4$ , 0.2  $\text{CaCl}_2$ , 50 taurine, 18.5 glucose, 5 HEPES, 0.1% BSA, pH 6.9 with NaOH, with elastase (0.3 mg/mL; Worthington Biochemical Corp., Lakewood, NJ) and collagenase II (0.21 mg/mL; Worthington). SAN tissue was digested at 37°C for 30 min and then washed three times in a solution containing (in mM): 100 L-glutamic acid/potassium salt, 10 L-aspartic acid/potassium salt, 25 KCl, 10  $\text{KH}_2\text{PO}_4$ , 2  $\text{MgSO}_4$ , 20 taurine, 5 creatine, 0.5 EGTA, 20 glucose, 5 HEPES, 0.1% BSA, pH 7.2 with KOH. SAN tissue was then

triturerated in wash solution and plated onto poly-L-lysine coated coverslips. Coverslips containing SAN cells were transferred to a perfusion chamber and electrophysiological recordings were conducted as described [252, 253]. SAN cells targeted for electrophysiological characterization were spindle-shaped, striated, and in most cases, exhibited spontaneous beating. Most experiments used a fast-step perfusion system to allow for fast application and removal of CCh (within 100 ms) and have been described previously [252, 253]. A small subset of experiments was done with gravity-flow perfusion of CCh (within 10-20 s).

*Analysis*—Statistical analyses were performed using Prism 5 (GraphPad Software, Inc.; La Jolla, CA) and SigmaPlot 11 (Systat Software Inc; San Jose, CA). Non-linear fitting of dose-response data, Hill co-efficient analysis, and EC<sub>50</sub> analysis were all done with Prism 5 software using the least squares fitting method. The impact of genotype on CCh-induced current responses (steady-state current density and kinetics) was evaluated using 1-way (single-saturating concentration study) and 2-way (concentration-response study) ANOVA. The impact of genotype on CCh-induced HR response was evaluated using two-way (time-response study) ANOVA. Activation and deactivation kinetics were determined by fitting regions of current traces with a 1-term Boltzmann equation as described previously [252]. Newman-Keuls Multiple Comparison (one-way ANOVA) and Bonferroni (two-way ANOVA) post hoc tests were used as appropriate. The level of significance was set at  $P < 0.05$ .

## Results

### *Characterization of Rgs4<sup>-/-</sup> mice*

We acquired the *Rgs4* mutant strain B6;129P2-*Rgs4*<sup>tm1Dgen</sup>/J (The Jackson Laboratory; Bar Harbor, ME) used previously to implicate RGS4 in the parasympathetic regulation of heart rate (HR) [89]. This strain harbors a lacZ-containing insert (LacO-SA-IRES-lacZ-Neo555G/Kan) that spans part of exons 1 and 2, resulting in the loss of 58 base pairs of coding sequence (and intervening intronic sequence), predicted to result in a frame shift and early truncation of RGS4 (**Fig. 5.1A,B**). Sequencing of the amplicon generated in mutant mice using the supplier's genotyping conditions confirmed the presence of a foreign DNA element positioned between exon 1 and 2 in the *Rgs4* gene (not shown).

We probed the levels of residual RGS4-like mRNAs in tissue samples from the heart (SAN and left atria) and brain (hippocampus) from RGS4 mutant mice. We used two distinct intron-spanning primer pairs targeting sequence in exons 3-5, which encodes the catalytic domain of RGS4, including one pair ("A") used previously to characterize RGS4 expression in B6;129P2-*Rgs4*<sup>tm1Dgen</sup>/J mice [89]. Residual RGS4 expression levels were 10-100-fold lower in tissue samples from B6;129P2-*Rgs4*<sup>tm1Dgen</sup>/J mice than in corresponding wild-type samples (**Fig. 5.1C**).

RGS4 protein is difficult to detect in cells as it is efficiently degraded via the ubiquitin-dependent N-end rule pathway [255, 256]. Indeed, we were unable to detect recombinant RGS4 by immunoblotting in HEK cells transfected with RGS4 unless cells were pre-treated with the proteasome inhibitor MG132 (not shown). Thus, we used MG132 pre-treatment to probe for RGS4 protein in hippocampal cultures from wild-type

and B6;129P2-*Rgs4*<sup>tm1Dgen</sup>/J mice. While RGS4 was observed in MG132-treated wild-type cultures, no immunoreactive band was seen in cultures from RGS4 mutant mice (**Fig. 5.1D,E**). Collectively, these data indicate that the *Rgs4* gene is targeted as described B6;129P2-*Rgs4*<sup>tm1Dgen</sup>/J mice (hereafter referred to as *Rgs4*<sup>-/-</sup> mice), yielding a dramatic reduction in mRNA levels and no detectable residual RGS4 protein. *Rgs4*<sup>-/-</sup> mice were bred with *Rgs6*<sup>-/-</sup> mice to generate mice lacking both RGS4 and RGS6 (*Rgs4*<sup>-/-</sup>:*Rgs6*<sup>-/-</sup>); *Rgs4*<sup>-/-</sup>:*Rgs6*<sup>-/-</sup> mice were viable and did not display obvious phenotypic abnormalities.



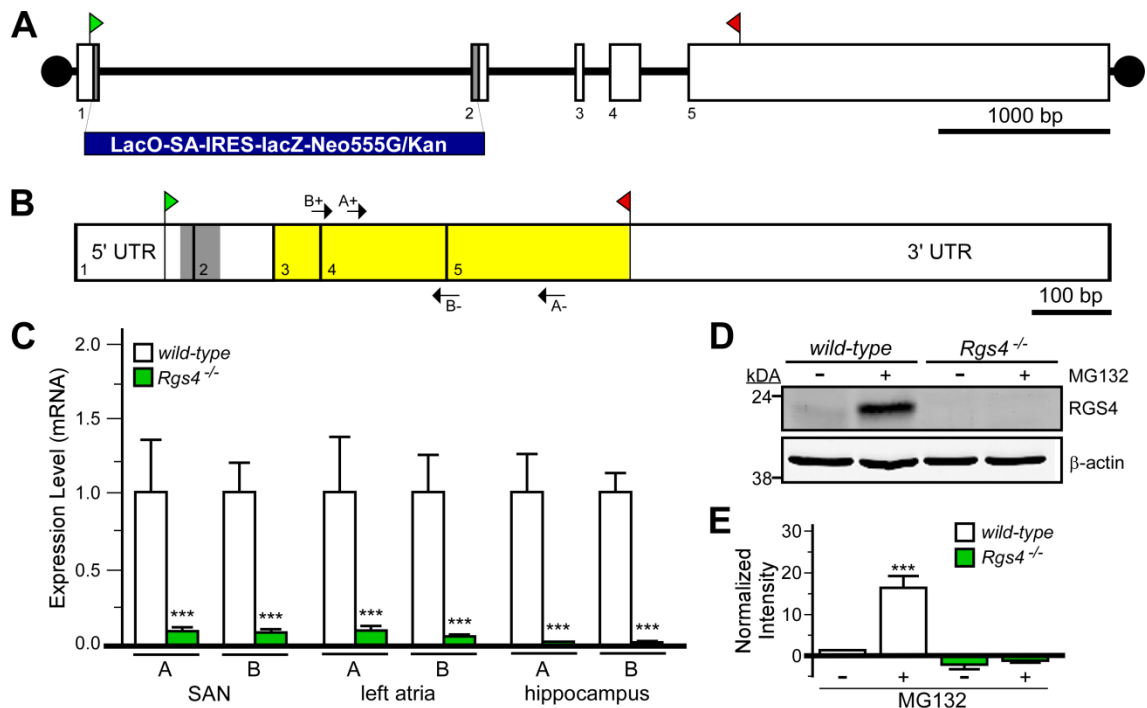


**Figure 5.1. Characterization of *Rgs4*<sup>-/-</sup> mice.** **A)** Schematic depiction of the *Rgs4* gene, which consists of 5 exons (rectangles, with corresponding number labels below). The translation initiation (ATG) and termination (STOP) codons are shown as forward (▶) and reverse (◀) flags, respectively. The gray shaded regions in exons 1 and 2 (along with intervening intronic sequence) was replaced with the LacZ-containing cassette (LacO-SA-IRES-LacZ-Neo555G/Kan) to generate B6;129P2-*Rgs4*<sup>tm1Dgen</sup>/J mice. **B)** Schematic depiction of RGS4 mRNA, with exon boundaries denoted by vertical lines and numbers. The gray shaded domain between boxes 1 and 2 corresponds to the 58-bp fragment of coding sequence missing in the RGS4 mutant mice. Highlighting across boxes 3-5 shows the location of coding sequence for the catalytic (RGS) domain of RGS4. Arrows denote the positions and identities of the primer sets (A+/-, B+/-) used for qRT-PCR. **C)** qRT-PCR analysis of RGS4 expression in cardiac tissue (SAN and left atria) and hippocampus from wild-type and B6;129P2-*Rgs4*<sup>tm1Dgen</sup>/J mice, using the primer sets depicted in **B**. Expression levels were normalized within samples to GAPDH (levels of which were comparable in all tissues examined), and to wild-type samples for each primer set. Symbols: \*\*\* *P*<0.001 vs. wild-type (within tissue and primer set by t-test). **D)** Immunoblotting for RGS4 in primary hippocampal cultures (10 DIV) from wild-type and B6;129P2-*Rgs4*<sup>tm1Dgen</sup>/J mice. Cultures were pre-treated with MG132 (50 μM) for 6 h prior to protein isolation. **E)** Quantification of RGS4 immunoblotting data (n=3 separate experiments). A significant impact of group was observed ( $F_{3,11}=29.8$ ; *P*<0.001). Symbols: \*\*\**P*<0.001 vs. wild-type (untreated).

### *Impact of RGS ablation: isolated hearts*

We first compared the contributions of RGS4 and RGS6 to automaticity and HRV using a retrogradely-perfused Langendorff heart preparation. Basal HR in hearts from *Rgs6*<sup>-/-</sup> mice was significantly lower than measured in wild-type counterparts, consistent with published observations [252, 253], while HR in hearts from *Rgs4*<sup>-/-</sup> mice was normal (**Fig. 5.2A**). Interestingly, HR measured in hearts from *Rgs4*<sup>-/-</sup>:*Rgs6*<sup>-/-</sup> was also normal. Using time- and frequency-based analyses to compare HRV across genotypes [253], we observed that HRV was significantly elevated in hearts from *Rgs6*<sup>-/-</sup> mice (**Table 5.1**), whereas all HRV measures in *Rgs4*<sup>-/-</sup> mice were normal. Similar to the effect on HR, concurrent RGS4 ablation rescued in part the HRV abnormalities seen in hearts from *Rgs6*<sup>-/-</sup> mice.

We next evaluated the impact of RGS ablation on the bradycardic effects of the cholinergic agonist carbachol (CCh) (**Fig. 5.2B**). CCh suppressed HR in all genotypes, though differences in sensitivity were evident (**Fig. 5.2C**). The IC<sub>50</sub> for CCh-induced bradycardia was nearly 10-fold lower in *Rgs6*<sup>-/-</sup> hearts (31±6 nM) compared to wild-type (219±24 nM). In contrast, CCh sensitivity was normal in hearts from *Rgs4*<sup>-/-</sup> mice. The dose-response relationship in *Rgs4*<sup>-/-</sup> mice was shallower, however, than in other genotypes. Finally, the CCh sensitivity of hearts from *Rgs4*<sup>-/-</sup>:*Rgs6*<sup>-/-</sup> mice was significantly lower than wild-type and higher than in *Rgs6*<sup>-/-</sup> mice, indicating that RGS4 ablation partially rescued the enhanced CCh sensitivity seen in *Rgs6*<sup>-/-</sup> mice.

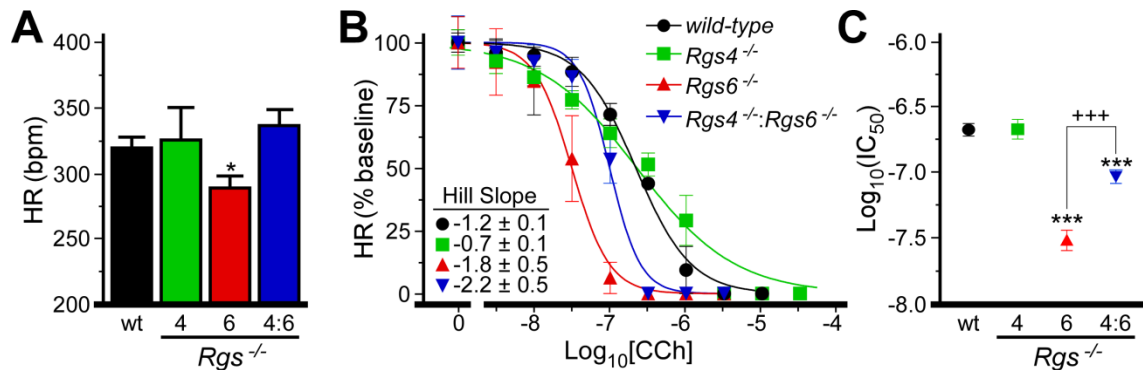


**Figure 5.2. Impact of RGS ablation on HR and CCh-induced bradycardia.** **A)** HR in isolated hearts from wild-type (wt) and *Rgs*<sup>-/-</sup> mice. A significant effect of genotype on HR was observed ( $F_{3,94}=2.7$ ,  $P<0.05$ ;  $n=4-12/\text{genotype}$ ). **B)** Impact of CCh on HR in wild-type and *Rgs*<sup>-/-</sup> hearts ( $n=4-8/\text{genotype}$ ); data are normalized to baseline HR. A significant impact of genotype was observed for normalized HR ( $F_{3,101}=21.0$ ,  $P<0.001$ ). Hill coefficients for each curve are listed. A significant impact of genotype was observed for Hill coefficients ( $F_{3,135}=3.7$ ,  $P=0.013$ ). Specifically, *Rgs4*<sup>-/-</sup> was significantly different from *Rgs4*<sup>-/-</sup>:*Rgs6*<sup>-/-</sup> ( $*P>0.05$ ). **C)** IC<sub>50</sub> values calculated from dose-response curves in **B** ( $F_{3,135}=38.1$ ,  $P<0.001$ ). Symbols: \*,\*\*\* $P<0.05$  and  $0.001$ , respectively, vs. wild-type; +++ $P<0.001$ .

HRV Parameter	Genotype				ANOVA
	<i>wild-type</i>	<i>Rgs4</i> <sup>-/-</sup>	<i>Rgs6</i> <sup>-/-</sup>	<i>Rgs4::6</i> <sup>-/-</sup>	
NN range, ms	16.2 ± 1.6	18.2 ± 3.7	30.2 ± 4.8 <sup>a</sup>	22.6 ± 7.2	F <sub>3,30</sub> =3.0; P<0.05
SDNN, ms	2.70 ± 0.20	3.20 ± 0.43	5.22 ± 0.87 <sup>a</sup>	4.06 ± 1.28	F <sub>3,30</sub> =3.4; P<0.05
RMS-SD, ms	1.35 ± 0.28	1.20 ± 0.29	3.90 ± 1.13	2.31 ± 1.30	F <sub>3,30</sub> =2.7; P=0.06
TP, ms <sup>2</sup>	5.2 ± 0.9	8.7 ± 2.2	29.0 ± 8.5 <sup>a</sup>	17.5 ± 10.0	F <sub>3,30</sub> =3.8; P<0.05
VLF, ms <sup>2</sup>	4.2 ± 0.8	7.7 ± 1.9	18.2 ± 5.8	11.5 ± 5.5	F <sub>3,30</sub> =2.7; P=0.06
LF, ms <sup>2</sup>	0.48 ± 0.17	0.68 ± 0.39	4.50 ± 1.94	3.53 ± 3.25	F <sub>3,30</sub> =2.1; P=0.12
LF norm	49.9 ± 3.8	51.7 ± 8.0	48.6 ± 5.4	46.5 ± 5.1	F <sub>3,30</sub> =0.1; P=0.96
HF, ms <sup>2</sup>	0.54 ± 0.17	0.32 ± 0.11	6.26 ± 3.49	2.54 ± 2.25	F <sub>3,30</sub> =1.7; P=0.19
HF norm	50.1 ± 3.8	48.2 ± 8.0	51.4 ± 5.4	51.2 ± 4.5	F <sub>3,30</sub> =0.1; P=0.98
LF/HF	1.13 ± 0.17	1.82 ± 0.86	1.44 ± 0.54	1.00 ± 0.17	F <sub>3,30</sub> =0.4; P=0.75

**Table 5.1. HRV analysis of wild-type and *Rgs*<sup>-/-</sup> hearts.** Baseline HRV analysis of 5-min recordings from 4-12 mice per genotype (8-16 wk). Abbreviations: NN range, range of intervals between successive heart beats; SDNN, standard deviation of NN intervals; RMS-SD, square root of the mean squared difference of successive NNs; TP, total power (0-10 Hz); VLF, very low frequency (0-0.4 Hz); LF, low frequency (0.4-1.5 Hz); LF norm, 100\*[LF/(TP-VLF)]; HF, high frequency (1.5-5 Hz); HF norm, 100\*[HF/(TP-VLF)]; LF/HF, ratio of LF to HF. Results of corresponding ANOVAs are indicated in the right column; pair-wise comparisons were made using Tukey's HSD test, when appropriate. Symbols: <sup>a</sup>P<0.05 vs. wild-type.

*Impact of RGS ablation: M<sub>2</sub>R-I<sub>KACH</sub> signaling in SAN cells*

We next examined the impact of RGS ablation on M<sub>2</sub>R-I<sub>KACH</sub> signaling in SAN cells (**Fig. 5.3**). Previous studies have shown that *Girk4* gene ablation completely eliminated the whole-cell inward currents induced by CCh in SAN cells, confirming the I<sub>KACH</sub>-dependence of the response [248, 253]. No significant genotype-dependent differences in peak or steady-state CCh-induced I<sub>KACH</sub> currents were observed in response to a saturating CCh concentration (10 μM) (**Fig. 5.3A,B**), though responses seen in cells from *Rgs4*<sup>-/-</sup> mice tended to be larger. Similarly, no genotype-dependent difference in acute desensitization was found (**Fig. 5.3E**). Consistent with previous reports [251, 252], M<sub>2</sub>R-I<sub>KACH</sub> current deactivation rate was profoundly slower in *Rgs6*<sup>-/-</sup> SAN cells, and a modest but significant slowing of current activation was also seen (**Fig. 5.3C,D**). In alignment with results from the isolated heart study, CCh-induced I<sub>KACH</sub> currents in *Rgs4*<sup>-/-</sup> cells exhibited normal activation and deactivation kinetics, and concurrent RGS4 ablation partially rescued M<sub>2</sub>R-I<sub>KACH</sub> kinetic deficits seen in *Rgs6*<sup>-/-</sup> cells.

We also evaluated the sensitivity of M<sub>2</sub>R-I<sub>KACH</sub> signaling in SAN cells from wild-type and *Rgs*<sup>-/-</sup> mice. The EC<sub>50</sub> values for I<sub>KACH</sub> activation by CCh in wild-type and *Rgs4*<sup>-/-</sup> SAN cells were indistinguishable (**Fig. 5.3F,G**). In contrast, the M<sub>2</sub>R-I<sub>KACH</sub> signaling pathway in SAN cells from *Rgs6*<sup>-/-</sup> mice was ~5-fold more sensitive to CCh. The EC<sub>50</sub> measured in *Rgs4*<sup>-/-</sup>:*Rgs6*<sup>-/-</sup> SAN cells was slightly larger than that of *Rgs6*<sup>-/-</sup> cells, but the difference was not significant. Genotype- and dose-dependent differences in M<sub>2</sub>R-I<sub>KACH</sub> activation and deactivation kinetics were also observed (**Fig. 5.3H,I**), and these differences were consistent with outcomes from the saturating CCh experiments (**Fig. 5.3C,D**).

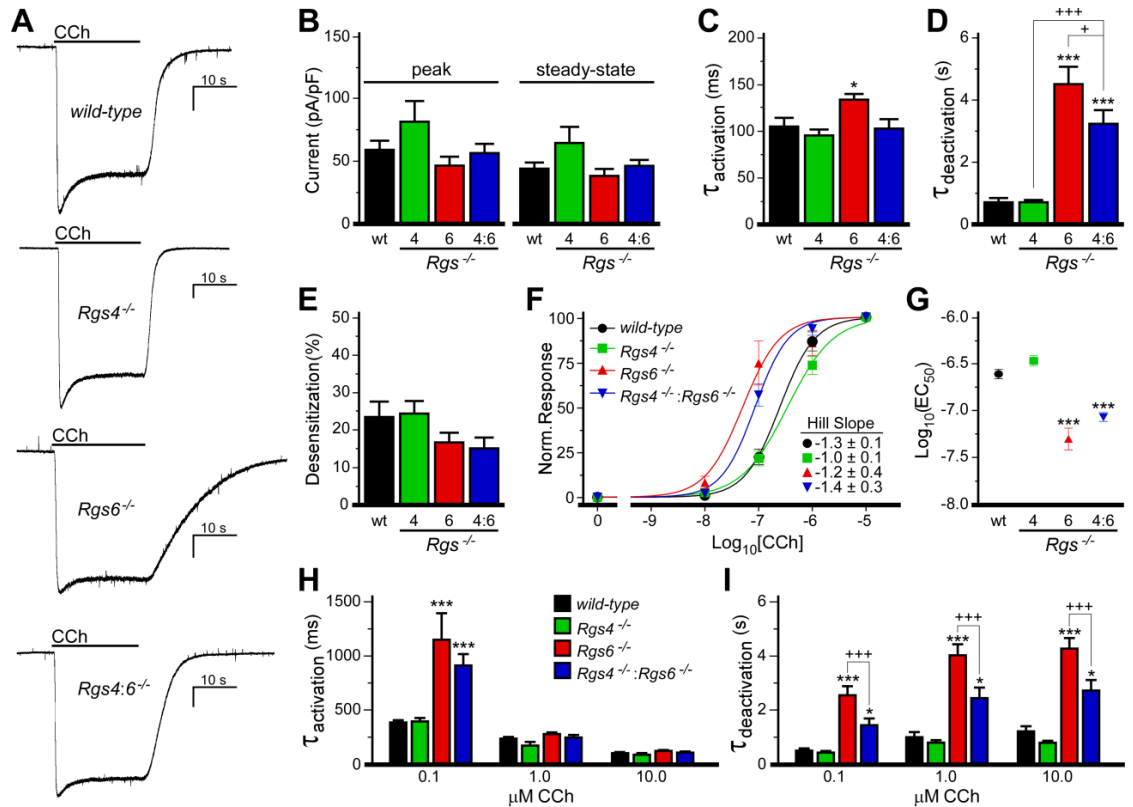


**Figure 5.3. Impact of RGS ablation on M<sub>2</sub>R-I<sub>KACH</sub> signaling in SAN cells.** **A)** I<sub>KACH</sub> currents evoked by CCh (10  $\mu$ M) in SAN cells from wild-type and *Rgs*<sup>-/-</sup> mice. Peaks were normalized to allow for comparison of deactivation kinetics. Scale bars: 10 s/400 pA. **B)** No impact of genotype on peak ( $F_{3,36}=2.0$ ,  $P=0.13$ ) or steady-state ( $F_{3,36}=2.2$ ,  $P=0.10$ ) current densities was observed ( $n=8-16$ /genotype). **C,D)** A significant impact of genotype was observed for activation ( $F_{3,35}=5.0$ ,  $P<0.01$ ) and deactivation ( $F_{3,36}=29.1$ ,  $P<0.001$ ) kinetics of the CCh-induced current in wild-type and *Rgs*<sup>-/-</sup> SAN cells. **E)** There was no impact of genotype on the acute desensitization of the CCh-induced I<sub>KACH</sub> current ( $F_{3,36}=1.3$ ,  $P=0.29$ ). **F)** Concentration-response curves for CCh-induced I<sub>KACH</sub> activation (steady-state current amplitudes normalized to response measured with 10  $\mu$ M CCh) in wild-type and *Rgs*<sup>-/-</sup> mice ( $n=6-8$  per group). Hill coefficients for each curve are listed. No significant impact of genotype was observed for Hill coefficients ( $F_{3,151}=0.4$ ,  $P=0.8$ ). **G)** EC<sub>50</sub> values calculated from concentration-response curves shown in **F** ( $F_{3,151}=24.8$ ,  $P<0.0001$ ). **H,I)** Activation and deactivation kinetics of the CCh-induced currents in wild-type and *Rgs*<sup>-/-</sup> SAN cells. An interaction of genotype and dose was observed for activation kinetics ( $F_{6,95}=7.4$ ,  $P<0.001$ ) but not deactivation kinetics ( $F_{6,95}=1.5$ ,  $P=0.18$ ). However, a significant impact of group on deactivation kinetics was observed for both genotype ( $F_{3,95}=66.2$ ,  $P<0.001$ ) and concentration ( $F_{2,95}=15.3$ ,  $P<0.001$ ), so within-concentration comparisons were performed by one-way ANOVA. Symbols: \*, \*\*\*,  $P<0.05$  and  $0.001$ , respectively, vs. wild-type; +++  $P<0.001$ .

### *Influence of another R7 RGS protein*

The partial rescue of RGS6-dependent phenotypes seen with concurrent ablation of RGS4 suggested that another cardiac RGS protein(s) is present that can modulate parasympathetic signaling when RGS4 is absent. To test this hypothesis, and to explore the possibility that adaptations secondary to constitutive RGS4 ablation played a role in these phenomena, we employed a pharmacologic strategy involving CCG-63802, a compound that inhibits RGS4 (and likely other RGS and non-RGS proteins) by forming a covalent adduct to cysteine residues [257, 258]. With CCG-63802 (50  $\mu$ M) included in the pipette solution, M<sub>2</sub>R-I<sub>KACH</sub> deactivation rate was significantly accelerated in SAN cells from *Rgs6*<sup>-/-</sup> mice, similar to the effect of concurrent genetic ablation of RGS4 and RGS6 (**Fig. 5.4A,B**). There was no effect of CCG-63802 on activation kinetics, and while peak and steady-state current responses tended to be larger than in control cells, this difference was not significant (**Fig. 5.4C-E**).

As RGS6 belongs to the R7 sub-family of RGS proteins (which consists of RGS6, RGS7, RGS9, and RGS11 [132]), we next asked whether the unusual influence of genetic ablation of RGS4 or acute CCG-63802 application on M<sub>2</sub>R-I<sub>KACH</sub> signaling seen in SAN cells from *Rgs6*<sup>-/-</sup> mice was attributable to another R7 RGS family member. We exploited the observation that all four R7 RGS proteins are undetectable in *G $\beta$ 5*<sup>-/-</sup> mice [238]. Consistent with the involvement of multiple R7 RGS proteins, CCh-induced I<sub>KACH</sub> current deactivation was significantly longer in *G $\beta$ 5*<sup>-/-</sup> SAN cells than in *Rgs6*<sup>-/-</sup> SAN cells ( $t_{13}=2.30$ ,  $P<0.05$ ). Moreover, while CCG-63802 accelerated M<sub>2</sub>R-I<sub>KACH</sub> deactivation rate in *Rgs6*<sup>-/-</sup> SAN cells, it had no such effect in SAN cells from *G $\beta$ 5*<sup>-/-</sup>

mice (**Fig. 5.4A,B**). The differential impact of RGS4 inhibition (genetic or pharmacologic) on M<sub>2</sub>R-I<sub>KACH</sub> signaling in SAN cells from *Rgs6*<sup>-/-</sup> and *Gβ5*<sup>-/-</sup> mice argues that RGS4 suppresses the influence of another R7 RGS family member when RGS6 is absent.



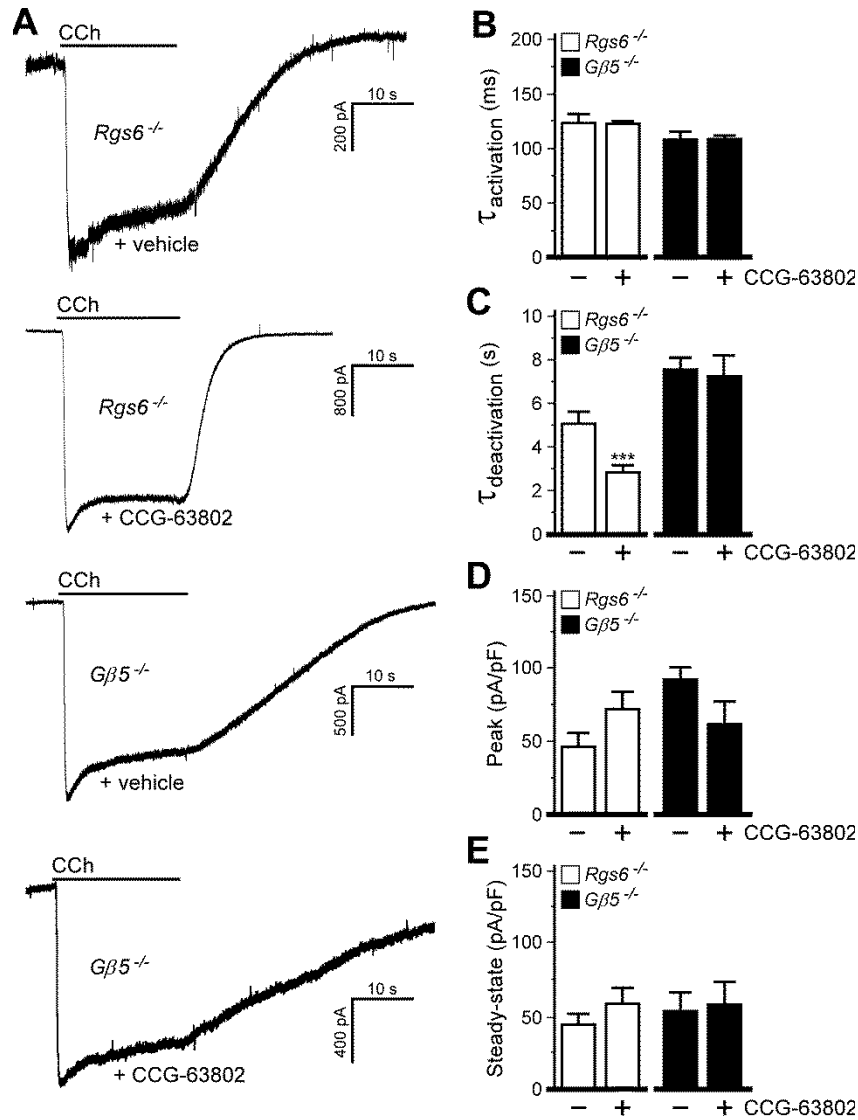


**Figure 5.4. Influence of another R7 RGS protein revealed by *Rgs4* ablation.** **A)**  $I_{KACH}$  currents evoked by CCh (10  $\mu$ M) in  $Rgs6^{-/-}$  and  $G\beta5^{-/-}$  SAN cells treated with vehicle or CCG-63802 (50  $\mu$ M, delivered via the pipette). Peak currents were normalized for comparison. **B)** Activation kinetics of the CCh-induced current in  $Rgs6^{-/-}$  ( $t_{14}=0.1$ ,  $P=0.9$ ) or  $G\beta5^{-/-}$  ( $t_8=0.2$ ,  $P=1.0$ ) SAN cells. **C)** Deactivation kinetics of the CCh-induced current in  $Rgs6^{-/-}$  ( $t_{18}=3.0$ ,  $P<0.01$ ) or  $G\beta5^{-/-}$  ( $t_6=0.3$ ,  $P=0.8$ ) SAN cells. **D)** Peak  $I_{KACH}$  current densities in  $Rgs6^{-/-}$  ( $t_{15}=1.7$ ,  $P=0.1$ ) or  $G\beta5^{-/-}$  ( $t_9=0.4$ ,  $P=0.7$ ) SAN cells. **E)** Steady-state  $I_{KACH}$  current densities in  $Rgs6^{-/-}$  ( $t_{16}=1.1$ ,  $P=0.3$ ) or  $G\beta5^{-/-}$  ( $t_8=0.2$ ,  $P=0.8$ ) SAN cells. Note that only within-genotype comparisons were made. n=4-12/genotype. Symbols: \*\*\* $P<0.001$  vs. vehicle for each genotype.

## Discussion

Our findings extend the previously-reported roles for RGS6 in the parasympathetic regulation of HR and M<sub>2</sub>R-I<sub>KACH</sub> signaling in SAN cells [251-253]. RGS6 ablation correlates with decreased HR (*in vivo* and *ex vivo*), increased HRV, enhanced sensitivity to the negative chronotropic effects of CCh, and multiple effects on M<sub>2</sub>R-I<sub>KACH</sub> signaling in SAN cells that should collectively enhance the influence of this signaling pathway on cardiac output. Under equivalent conditions, no similar impact of RGS4 ablation was observed.

To the contrary, we did observe that the ablation of RGS4 seemed to enhance slightly M<sub>2</sub>R-I<sub>KACH</sub> signaling in SAN cells rather than disrupt it. While these effects were not statistically significant, the loss of RGS4 (by either genetic or pharmacologic manipulation) tended to correlate with larger peak CCh-induced responses, higher EC<sub>50</sub> value for CCh-induced I<sub>KACH</sub> activation, and exhibited faster activation and deactivation kinetics. In addition, isolated heart experiments from *Rgs4*<sup>-/-</sup> mice revealed a shallower CCh dose-response curve compared to wild-type despite that the IC<sub>50</sub> was the same for both genotypes. Collectively, these observations suggest that RGS4 can impact parasympathetic regulation of HR and underlying signaling pathways, albeit in manner distinct from that proposed previously. Furthermore, the mild effect observed with RGS4 ablation appears to be exacerbated with the concurrent ablation of RGS6, leading to the partial rescue of the prominent phenotypes linked to RGS6 ablation in both single cell and isolated heart assays.

The lack of negative influence of RGS4 on parasympathetic signaling was unexpected in light of a previous report involving the same mice [89]. While some of the

cardiac phenotypes in *Rgs4*<sup>-/-</sup> mice reported previously could be due to an influence of RGS4 in the central nervous system (*e.g.*, the enhanced negative chronotropic effect of CCh seen in conscious *Rgs4*<sup>-/-</sup> mice), there are few differences between studies with respect to the design of the isolated heart experiments. In this context, it is worth noting that we also examined the influence of RGS4 ablation on CCh-induced bradycardia under conditions of sympathetic (isoproterenol) stimulation. While the previous study reported that CCh-induced bradycardia was more pronounced in isoproterenol-treated hearts from *Rgs4*<sup>-/-</sup> mice as compared to wild-type controls [89], we observed no genotype-dependent difference in this assay (**Fig. 5.5A-C**). Interestingly, baseline HR of retrogradely-perfused hearts was slower (300-350 bpm) in our hands than in the previous study (>400 bpm). This may be due to the difference in the perfusion protocol used in the *ex vivo* heart studies, which involved constant pressure (our study) or constant flow (previous study). Moreover, while the CCh sensitivity of hearts from *Rgs4*<sup>-/-</sup> mice was apparently similar in both studies, hearts from wild-type mice appeared to be slightly more sensitive to CCh-induced bradycardia in our study.

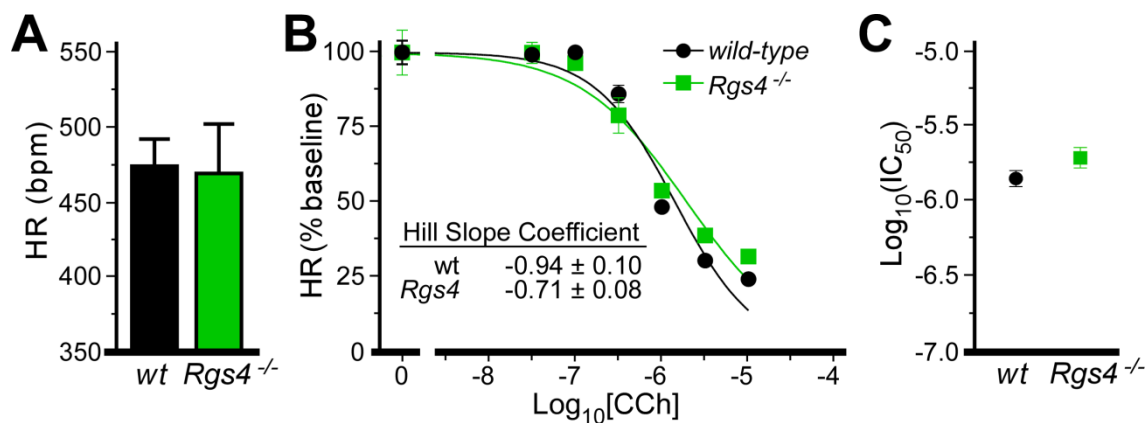


**Figure 5.5. *Rgs4* ablation in isoproterenol-stimulated hearts.** **A)** HR in isolated hearts from wild-type (wt) and *Rgs4*<sup>-/-</sup> mice stimulated with isoproterenol. HR from isoproterenol-treated wild-type and *Rgs4*<sup>-/-</sup> hearts were not significantly different ( $t_4=0.14$ ,  $P=0.9$ ). **B)** Impact of CCh on HR in wild-type and *Rgs4*<sup>-/-</sup> hearts ( $n=3$ /genotype); data are normalized to baseline HR. There was no significant impact of genotype observed for normalized HR ( $F_{2,37}=2.4$ ,  $P=0.1$ ). Hill coefficients for each curve are listed and were not significantly different ( $t_{37}=1.8$ ,  $P=0.09$ ). **C)** IC<sub>50</sub> values calculated from dose-response curves in **B** were not significant ( $t_{37}=1.6$ ,  $P=0.12$ ).

With respect to the measurement of  $M_2R$ - $I_{KACH}$  signaling in SAN cells, there were also few study design-related differences that might explain the divergent outcomes. We used a rapid solution-exchange system to apply and remove CCh to/from SAN cells. Accordingly, the rates of current activation and deactivation were ~100-fold faster in our study. Rapid solution exchange (complete solution exchange in <100 ms) ensures that the time-course of  $I_{KACH}$  activation and deactivation is controlled by G protein cycling rather than gradually changing levels of agonist and/or the potentially confounding influence of signaling pathway desensitization. This difference in experimental design, however, is unlikely to explain the discrepancy between studies. Indeed, using a slower gravity-flow perfusion approach to deliver and remove CCh, we found no difference in CCh-induced  $I_{KACH}$  current densities, desensitization, or kinetics in SAN cells from wild-type and  $Rgs4^{-/-}$  mice (**Fig. 5.6A-D**).

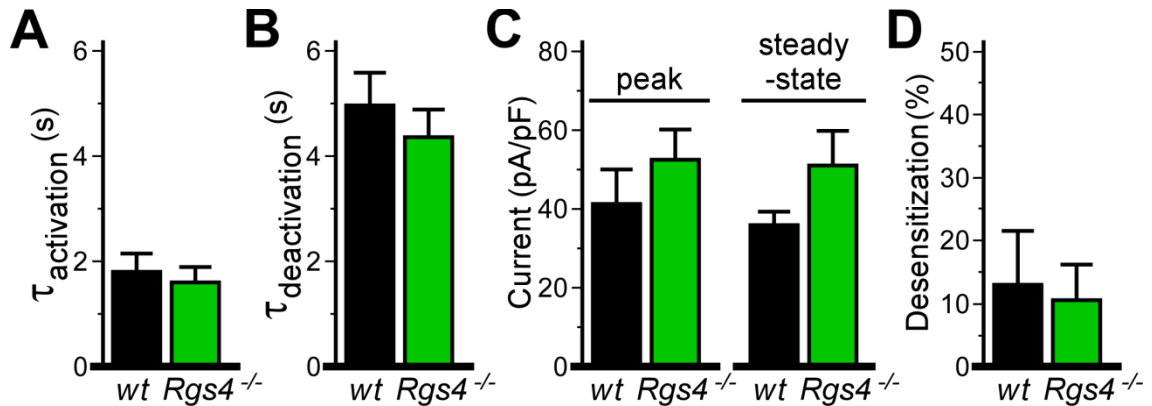


**Figure 5.6.  $M_2R$ - $I_{KACH}$  signaling evaluated by slow perfusion of CCh.** Summary data of  $I_{KACH}$  currents evoked by CCh (10  $\mu$ M) in wild-type and *Rgs4*<sup>-/-</sup> SAN cells, taken from experiments in which CCh was allowed to slowly fill the recording chamber by gravity flow, and was washed out of the chamber by gravity flow of CCh-free bath solution. While responses in SAN cells from *Rgs4*<sup>-/-</sup> mice showed slightly faster kinetics and larger current densities, there were no significant genotype-dependent differences in any of the following parameters: **A**) Activation rate ( $t_8=0.4$ ,  $P=0.7$ ) and **B**) deactivation rate ( $t_7=0.7$ ,  $P=0.5$ ), **C**) Peak ( $t_8=0.9$ ,  $P=0.4$ ) or steady-state ( $t_7=1.5$ ,  $P=0.2$ ) CCh-induced current densities, or **D**) Acute desensitization of the CCh-induced  $I_{KACH}$  current ( $t_8=0.2$ ,  $P=0.8$ ;  $n=4-6$ /genotype).

While we did not observe a marked influence of RGS4 on the parasympathetic regulation of HR or M<sub>2</sub>R-I<sub>KACH</sub> signaling in SAN cells, our data suggest that RGS4 could influence such signaling under certain circumstances. Indeed, while the sensitivity of the isolated heart to CCh-induced bradycardia was normal in *Rgs4*<sup>-/-</sup> mice, the slope of curve was shallower. Moreover, M<sub>2</sub>R-I<sub>KACH</sub> current densities tended to be higher with inhibition of RGS4. While the mechanisms underlying these observations are unclear, RGS4 can serve as a GAP for G $\alpha_q$  [259-261], which should enhance the activity of PLC $\beta$  and increase the levels of phosphoinositol-4,5-bisphosphate (PIP<sub>2</sub>), a required co-factor for GIRK channel gating [57, 217]. As RGS4 is up-regulated in the failing human heart [262], a more robust influence of RGS4 on parasympathetic HR regulation and related signaling might be expected in this setting.

Studies with embryonic stem cell-derived cardiomyocytes expressing RGS-insensitive G proteins implicated G $\alpha_{i2}$  and G $\alpha_o$  in M<sub>2</sub>R-dependent signaling [233]. RGS6/G $\beta_5$  strictly acts on members of the G $\alpha_{i/o}$  family [242], while RGS4 can serve as a GAP for G $\alpha_o$  and G $\alpha_{i1}$ , G $\alpha_{i2}$ , G $\alpha_{i3}$ , and G $\alpha_q$  [131, 263, 264]. Since RGS4 can regulate M<sub>2</sub>R-GIRK signaling mediated by G $\alpha_{i2}$  and G $\alpha_o$  in expression systems [265, 266], some compartmentalization mechanism in SAN cells must facilitate the interaction between RGS6/G $\beta_5$  and M<sub>2</sub>R-I<sub>KACH</sub> and/or preclude the interaction between RGS4 and M<sub>2</sub>R-GIRK. Macromolecular complex formation may play a role in this process, as RGS/G $\beta_5$  can interact directly with cardiac and neuronal GIRK channels [146, 252]. In contrast, while RGS4 can interact with receptor-GIRK complexes [199, 266], the association appears to be driven by an interaction between RGS4 and the receptor.

Our data suggest that another member of the R7 RGS protein family, whose influence on  $M_2R$ - $I_{K_{ACh}}$  signaling is masked by RGS4 in the absence of RGS6, can partially compensate for the loss of RGS6. RGS7 and/or RGS9 may be the compensatory factor(s), as expression of both RGS proteins has been detected in the heart [262, 267]. The presence of another R7 RGS protein would explain the comparably larger impact of  $G\beta 5$  ablation on  $I_{K_{ACh}}$  deactivation kinetics in SAN cells than is seen in SAN cells from  $Rgs6^{-/-}$  mice. It remains unclear how RGS4 masks its influence on  $M_2R$ - $I_{K_{ACh}}$  activity. It is possible that RGS4 is expressed at levels sufficiently higher than the compensatory R7 RGS protein(s) in SAN cells, which allows it to out-compete residual RGS/ $G\beta 5$  complexes for binding to receptor and/or channel.

Enhanced parasympathetic input to the heart facilitates the induction of atrial fibrillation (AF), while decreased parasympathetic influence (and decreased  $I_{K_{ACh}}$ ) confers resistance to atrial fibrillation [249]. A mutation in the human *GIRK4/KCNJ5* gene that yields reduced surface expression of  $I_{K_{ACh}}$  has been linked to long QT syndrome [178, 180]. Furthermore, loss-of-function mutations in RGS6 that increase  $I_{K_{ACh}}$  function result in elevated HRV and increased susceptibility to AF induction [253]. These observations suggest directly that certain arrhythmias may be effectively treated or prevented by decreasing (AF) or enhancing (long QT syndrome)  $M_2R$ - $I_{K_{ACh}}$  signaling. While direct-acting  $I_{K_{ACh}}$  agonists and antagonists may eventually prove useful in these settings, data presented herein argue that RGS6/ $G\beta 5$  should be considered as a novel target for the treatment or prevention of arrhythmias.



## **CHAPTER 6**

### **DISCUSSION**

## General summary and significance

GIRK channels are involved in the control and maintenance of cellular excitability in the brain through regulating synaptic transmission and in the heart by modulating heart rate [50, 51]. Alterations or disruptions to GIRK signaling processes may contribute to a number of cardiac and CNS disorders, including arrhythmia, epilepsy, depression, anxiety, schizophrenia, and drug addiction [57]. GIRK channels are one set of downstream effectors in inhibitory  $G_{i/o}$  protein signaling cascades, which are activated by a plethora of GPCRs. GPCRs are popular drug targets, but often have adverse or unwanted effects as they activate G proteins that have several downstream effectors. This has created a need for pharmacotherapies that directly target individual downstream effectors to elicit a desired effect. One such effector, GIRK channels, represents an important target for pharmacotherapeutic treatment of cardiac and neurological disorders.

Findings in this dissertation contribute to current understandings of GIRK channel structure and function within the CNS and modulation in the heart. Within the CNS, we identify key GIRK1 residues that are necessary for receptor-induced channel activation and characterize a new drug class that selectively targets these channels. Further, we demonstrate that the novel GIRK agonist, ML297, has an anxiolytic effect in mice, suggesting that it may be a potential therapeutic in the treatment of anxiety-related disorders. This work also demonstrates that RGS6, and not RGS4, regulates  $M_2R-I_{KACH}$  signaling and is the key modulator of parasympathetic activity of the heart, making it a

potential therapeutic target in the treatment of cardiac disorders, such as arrhythmias, long-QT syndrome, and fibrillation.

There were a few challenges associated with the work presented here. First, the constitutive knockdown of genes can often result in compensatory mechanisms that can sometimes mask the full effect of a complete loss-of-function of a gene of interest. Second, preferred knockout lines, such as a double knockout of  $G\beta 5^{-/-}$  and  $Rgs4^{-/-}$ , were not viable, leading us to pursue pharmacological approaches instead. Third, hippocampal and sinoatrial node cell culture models employed throughout this work are a heterogeneous mix of cell types, creating potential confounds when using assays that analyze entire cell populations such as immunoblotting techniques. Finally, the study of heteromeric channels in a reconstituted system produces certain qualitative and quantitative confounds. For example, we are unable to strictly control the order and stoichiometry of GIRK subunits in a given heteromeric channel. Furthermore, it is impossible to control how much of the transfected material forms GIRK1/GIRK2 heteromers versus GIRK2 homomers, which is particularly problematic when studying heteromers of GIRK2 mutant and wild-type GIRK2. Despite these confounds, it is important to study the native GIRK1/GIRK2 heteromer because it displays fundamentally different channel properties compared to a native GIRK2 homomer or engineered GIRK1 homomer.

## **Key functional domains in GIRK1**

Our initial studies sought to expand upon previous published deletion and chimera work within the context of a GIRK1-containing heteromeric channel by identifying a specific amino acid residue or residues that would account for the robust currents associated with GIRK1-containing heteromers. Previous work demonstrated the necessity of both GIRK1 core and distal C-terminal regions in the facilitation of M<sub>2</sub>R-induced signaling via GIRK1-containing heteromeric channels [110]. Our work has also been studied at the level of receptor-facilitated GIRK activation. Consistent with previous findings, we also observed that the GIRK1 distal C-terminus was dependent on the presence of the GIRK1 core region. Further, we have linked GIRK1 residues F137, A142, Y150, and Q404 to the robust GABA<sub>B</sub>R-induced activity associated with GIRK1-containing heteromeric channels.

### *GIRK1 C-terminus and residue Q404*

Q404, a residue within the distal C-terminal domain, was found to significantly influence the magnitude of basal and GPCR-dependent GIRK currents. When compared to GIRK1, GIRK1 Q404A demonstrated a 30% reduction in GABA<sub>B</sub>R-induced current. This reduction could be linked to altered channel gating, Gβγ sensitivity, or an inherent property of the channel, as there is neither a difference in expression between GIRK1 and GIRK1 Q404A nor a difference in GIRK2A surface expression when coexpressed with either GIRK1 or GIRK1 Q404A. Most likely, this residue strengthens the channel–Gβγ interaction. However, it is also possible that Q404 strengthens the allosteric coupling that

translates G $\beta\gamma$  binding to an increase in channel gating. Future experiments should be aimed at defining the physical interactions between G $\beta\gamma$  and GIRK1 Q404, with the expectation that the Q404A mutant would display significantly less co-immunoprecipitation with G $\beta\gamma$  compared to wild-type GIRK1 if it is responsible for facilitating the physical protein-protein interaction.

We demonstrated that the CT/GIRK2 heteromer has small basal and receptor-induced currents similar to that of a GIRK2 homomer. On the contrary, previous work in oocytes suggests that the distal C-terminus of GIRK1 (359-501) is responsible for elevated basal and M<sub>2</sub>R-induced channel activity associated with GIRK1, while GIRK1 residues 190-501 also elevate receptor-induced channel activity [112, 113]. A number of experimental differences may contribute to the disparity of GIRK1 C-terminal functionality between CT chimera data and previously reported work. First, the chimera containing GIRK4 (1-365) and GIRK1 (359-501) was evaluated as a homomeric channel [113]. Heteromeric overlapping of GIRK1 NT with GIRK2 CT and vice versa may play a large role in how the channel passes current [268, 269]. Second, the intracellular milieu, e.g., endogenous proteins, can be distinctly different across expression systems and potentially altering signaling cascades in oocytes that are not present in HEK cells. For example, these cell types have since been identified to contain an endogenous GIRK-like subunit: GIRK5 [270]. Finally, previous studies only explored the distal region and excluded the first 10 amino acids of the C-terminus, suggesting the possibility of a site in the proximal GIRK1 C-terminus inhibiting channel activity [112, 113]. Any one or more

of these experimental differences may contribute to the lack of GIRK1-like function seen with our CT/GIRK2 heteromeric channel.

Basal activity of GIRK1-containing channels is significantly greater than that of non-GIRK1-containing counterparts, and substantial basal activity of GIRK channels is seen in neurons [52, 158, 213, 271-273]. While structures that enhance single-channel properties such as conductance and mean open time should increase basal (and GPCR-induced) activity, the most significant determinants identified in our study were the domains between 180-328 and 409-462, as deletion of the latter domain reduced basal activity by 50% while sparing GABA<sub>B</sub>R-dependent signaling. While further refinement of these domains is necessary, it is tempting to speculate that the different affinities observed for GIRK1 (higher) and GIRK2 (lower) for PIP<sub>2</sub>, which binds between residues 61-81, 183-189, and 219-229 of GIRK1 [111, 274], contributes to this phenomenon. Interestingly, a specific interaction between the unique distal C-terminus of GIRK1 and Gα<sub>i3</sub> has been shown to reduce basal activity and increase Gβγ activity in GIRK1 F137S homomeric channels, while GIRK2 homomeric channels were independent of Gα<sub>i3</sub> modulation [275]. Although this regulation of GIRK1 was not studied in a wild-type GIRK1/GIRK2 heteromeric context, it does provide insight into potential functions of the GIRK1 distal C-terminus. For example, it is possible that binding Gα<sub>i3</sub> enhances coupling of the GIRK1/GIRK2 heteromer to the GPCR over that of a GIRK2 homomer, giving rise to augmented GPCR-induced channel activity in GIRK1-containing heteromeric channels.

The difference in affinity of GIRK1 and GIRK2 for PIP<sub>2</sub> is an interesting phenomenon for which a mechanism of action has yet to be discovered. Similar to other residues found in this study, there is likely a residue or small domain unique to GIRK1 that is responsible for the increased affinity and resulting increased sensitivity of GIRK1 to PIP<sub>2</sub>. In order to find this domain, future experiments should employ a similar mutagenic strategy and the voltage-sensing phosphatase (Dr-VSP) described in Chapter 5. Mutants would be tested for their GABA<sub>B</sub>R-induced activity both prior to and during the activation of Dr-VSP. If indeed a GIRK1 structure is responsible, the loss of GABA<sub>B</sub>R-induced activity through GIRK2 during Dr-VSP activation would be partially rescued by inserting GIRK1 residues.

*GIRK1 core domain and residues F137, A142, Y150*

Previous work first identified GIRK1 F137 as a key determinant in the slow voltage-dependent activation kinetics typical of GIRK1-containing channels [225]. Later work showed GIRK1 F137 as an enhancer of basal and GPCR-dependent currents carried by the GIRK1/GIRK4 heteromer [114]. Likewise, GIRK2 (S148F) was the only single point mutant tested in our study to significantly enhance GABA<sub>B</sub>R-induced current when expressed with GIRK2. The phenylalanine substitution at this position introduces an aromatic side chain into the space between the pore and inner helices. While the precise impact of this substitution on the selectivity filter and/or the inner (M1) and pore helices is unknown, it is clear that manipulations at this site influence a wide spectrum of GIRK channel properties. Indeed, substitution of the serine residue in GIRK2 (S148) and

GIRK4 (S143) for threonine yields homomeric channels exhibiting significantly higher activity than their wild-type counterparts [215, 276]. Further, the GIRK1 (F137S) mutant expresses on the cell surface and makes functional homomeric channels, despite the lack of an ER export signal that normally precludes trafficking of GIRK1 to cell surface [68], indicating that single channel properties are not dramatically affected, even across GIRK1/GIRK2 vs. GIRK2 and that influence of GIRK1 on heteromers is in enhancing open probability (gating).

The current understanding is that GIRK channels possess two gates: the inner helix gate and the G loop gate [93]. The former consists of the inner helices of the transmembrane spanning domains [277, 278], while the latter is formed by the G loop at the top of the cytoplasmic domain [103, 105]. Recent crystal structures of the GIRK2 homomer demonstrate that  $G\beta\gamma$  only opens the G loop in the absence of  $PIP_2$ , but the presence of  $PIP_2$  causes the inner helix gate to couple to the G loop gate so that both open upon  $G\beta\gamma$  activation [93]. These gates are highly conserved across GIRK subunits, yet there are discrete differences in amino acids surrounding these regions that suggest potential changes to the molecular structure of these gates when comparing GIRK1 and GIRK2. For example, there has been some indication from previous work that GIRK1 is more sensitive to  $PIP_2$  than GIRK2 [111]; whereas  $Na^+$  enhances the open state of GIRK2 homomeric channels but GIRK1 subunits are  $Na^+$  insensitive [98]. The pore residues of GIRK1 (F137, A142, and Y150) explored in this work will most likely cause slight changes and movements to the molecular architecture of the pore loop and selectivity filter. Perhaps these GIRK1 pore residues better facilitate the coactivation of these



heteromeric channels by PIP<sub>2</sub> and Gβγ. It is, however, unclear how GIRK1 Q404A fits into this picture because the distal C-terminus of GIRK1 has yet to be crystallized. It is possible that it facilitates (directly or indirectly) a higher level of PIP<sub>2</sub> binding or an interaction with Gα<sub>i/o</sub>-GTP to facilitate GPCR coupling.

### *Summary*

Using electrophysiological and biochemical approaches, we sought to better understand how GIRK1 potentiates basal and receptor-dependent activity of the prototypical neuronal GIRK channel, GIRK1/GIRK2. We established that GIRK1 does not enhance the surface trafficking of GIRK2-containing channels, arguing that GIRK1 confers unique functionality to heteromeric GIRK channels. Indeed, we identified four amino acids in GIRK1 that promote enhanced basal and/or GABA<sub>B</sub>R-GIRK signaling. One residue (Q404) is found in the unique, unresolved C-terminal domain of GIRK1, within a region that has been linked to high affinity interactions between the GIRK1 C-terminus and Gβγ [214, 268]. The other three amino acids (F137, A142, Y150) are located near the K<sup>+</sup> selectivity filter, where they work together to enhance channel mean open time and single channel conductance. Through this work, we have provided new structural insights of subunit-dependent differences that GIRK1 contributes to basal and GABA<sub>B</sub>R-facilitated GIRK channel activity.

## **Mechanisms of ML297 activation and selectivity**

Recently, a novel family of small molecule modulators of GIRK channels was discovered using a high-throughput screen [169]. Preliminary functional characterization of the prototypical agonist ML297, which relied heavily on an indirect thallium flux assay, suggested that it selectively activated GIRK1-containing channels in a G protein-independent manner, however the exact mechanism of action remained unclear. Using a combination of mutagenesis, thallium flux screening, and electrophysiology, we successfully determined that two GIRK1 residues are responsible for the selectivity of ML297: F137 and D173. Further experiments demonstrated that ML297-induced GIRK channel activation is dependent upon PIP<sub>2</sub> and has fundamental differences compared to the canonical receptor-induced activation of GIRK channels. Importantly, we demonstrated that ML297 has anxiolytic properties in wild-type mice that were absent upon constitutive knockout of *Girk1*.

### *Mechanism of ML297 activation*

One focus of this work was to determine the mechanism that underlies the ML297 activation of GIRK channels. We investigated the dependence of ML297 on the presence of PIP<sub>2</sub> and found that PIP<sub>2</sub> is required to maximally activate GIRK channels. This finding was expected given that PIP<sub>2</sub> is necessary for complete activation of the channel by endogenous Gβγ, intracellular Na<sup>+</sup>, and ethanol [92, 97, 166]. Activation of GIRK channels via Gβγ, ethanol, or ML297, all hinge on the presence of membrane-bound PIP<sub>2</sub>. Yet, it appears that ML297 agonism is structurally distinct, as previously known

channel activators do not exhibit a strong GIRK1-dependence. Binding sites for PIP<sub>2</sub>, Gβγ, and ethanol are mostly conserved across all GIRK subunits. The hydrophobic alcohol binding pocket is made up of the N-terminus (GIRK2 residue Y56) and the βL-βM sheet (GIRK2 residues L340, Y347) from one subunit and the βD-βE sheet (GIRK2 residues I242, P254, L254) from the adjacent subunit [167]. Ethanol, like ML297, can activate GIRK channels in the presence of PTX, indicating that GPCR-mediated activation of G<sub>i/o</sub> proteins is not involved in either compounds mechanism of action [162, 169]. Further, ethanol activation of GIRK channels was shown to be insensitive to alterations in cellular levels of Gβγ, indicating that it does not require channel-bound Gβγ to activate GIRK current [166].

While it has been established that ML297 can activate GIRK channels in the presence of PTX [169], it is still unclear if ML297 is completely independent of G protein signaling. PTX acts on Gα<sub>i/o</sub> by locking it in the inactive GDP-bound state through ADP-ribosylation [36, 39]. It is unclear as to whether the ADP-ribosylation of Gα<sub>i/o</sub> occludes the Gβγ binding site leaving it free to interact with downstream targets or still allows it to sequester Gβγ. Further, G proteins other than G<sub>i/o</sub> are unaffected by PTX and are still able to release Gβγ. Therefore, more experiments need to be done to assess the dependence of ML297 on free Gβγ. This would be done by looking at reconstituted GABA<sub>B</sub>R-GIRK1/GIRK2 signaling in HEK cells in the presence and absence of co-transfected phosducin, a protein that scavenges free Gβγ. In this paradigm, baclofen-induced GIRK currents through the GABA<sub>B</sub> receptor would be reduced by the presence of phosducin. If ML297 acts independently of Gβγ, then the presence of phosducin would

not affect ML297-induced GIRK currents. Understanding the dependence or independence of ML297 on the presence of G $\beta$  $\gamma$  is important to further elucidating the mechanism of ML297 activation of GIRK channels.

*Mechanism of ML297 selectivity and the GIRK1/GIRK2 heteromeric channel*

The most attractive feature of ML297 is that it is highly selective for GIRK1-containing channels, while having no effect on GIRK2 homomers. We sought to identify the structural determinants in GIRK1 that make it an effective target of ML297. Work in Chapter 3 clearly demonstrates that ML297 is dependent upon two residues unique to the GIRK1 subunit, F137 and D173. F137 is located in the pore-helix and D173 is located in the M2 domain. As previously demonstrated in Chapter 2, GIRK1 residue F137 is a critical determinant of robust basal- and GABA<sub>B</sub>R-induced GIRK channel activity. Previous mutagenic studies have shown this residue to play a role in kinetics of activation, GIRK1 surface trafficking, and enhancement of GIRK current [68, 114, 225]. In the context of the P chimera discussed in Chapter 2, D173 enhanced GABA<sub>B</sub>R-induced GIRK current when compared to GIRK2 residue N184. Interestingly, GIRK1 residue D173 has been previously identified as is a critical determinant for the inward rectification of K<sup>+</sup> channels. Removing the negative charged aspartate residue and replacing it with an uncharged glutamine weakened the inward-rectification properties associated with GIRK1 [225]. This aspartic residue is conserved across several other Kir channels, but is not in GIRK2, GIRK3, or GIRK4. D173 has been implicated as an interaction site for Mg<sup>2+</sup>, polyamines, and cation blockade. In mutating a homologous

residue in IRK1 (Kir2.1) (D172N), blockade by  $\text{Cs}^+$  and  $\text{Rb}^+$  were abolished [279]. Having an aspartate residue at this position is associated with strong rectification and a high affinity for blockade by  $\text{Mg}^{2+}$  and polyamines [280, 281]. By mutating this aspartate residue to asparagine (D to N), the channel affinity for  $\text{Mg}^{2+}$  and polyamines and strong rectification are both diminished [60, 282, 283]. GIRK activation by ML297 is dependent upon the presence of an aspartate at this position (GIRK1 D173) but our experiments also show that ML297 weakens inward rectification. This relationship suggests a direct interaction of ML297 with the channel and perhaps residue D173 itself, and that, through binding of ML297, the position of D173 is altered to cause a weakened rectification profile.

The work presented in this dissertation falls short of identifying the physical binding site of ML297 on GIRK channels. There are two binding theories that would be supported by the data shown here. The first is that ML297 could directly interact with GIRK1 residues F137 and D173. The fact that the mutation of either of these residues in GIRK1 disrupts activation by ML297 supports this theory but more experiments are needed. There is an alternate possibility that ML297 can bind GIRK1/GIRK2 channels or GIRK2 homomers and that F137 and D173 are simply required for enhanced channel activity. It is possible that ML297 could bind GIRK2 homomeric channels without activating them. Perhaps ML297 binds in a manner that mimics activation by  $\text{G}\beta\gamma$ , similar to  $\text{Na}^+$  and short chain alcohols [93, 106, 167]. However, ML297 differs from these compounds in its complete dependence on the presence of GIRK1.

The mechanism of GIRK activation by ML297 is further complicated by the ability of ML297 to switch its function depending on the composition of the GIRK channel. ML297 has no effect on GIRK2 homomeric channels, is an effective agonist on GIRK1/GIRK2 and GIRK2<sup>S148F/N184D</sup>/GIRK2 heteromeric channels, and, surprisingly, acts as an antagonist on GIRK2<sup>S148F/N184D</sup> homomers or GIRK2<sup>S148F/N184D</sup> coexpressed with GIRK1 (data not shown). These results suggest that the organization of the GIRK channel pore is an extremely important determinant of ML297 activity. Similarly, other studies have observed differences in channel activity between heteromeric and homomeric pore conformations of GIRK channels [284]. Further, set configurations and stoichiometry of GIRK1/GIRK4 heterotetramers have been proposed [65, 285, 286]. Also, several groups suggest that a heteromeric GIRK1/GIRK4 pore is necessary for high K<sup>+</sup> selectivity and robust channel activity [48, 69, 209, 284]. While some consider studying heteromeric channels as a caveat, it would seem that a heteromeric GIRK channel, and particularly a heteromeric pore, can be fundamentally different from a homomeric GIRK channel.

### **Therapeutic potential of ML297**

The drug metabolism and pharmacokinetic (DMPK) properties of ML297 were characterized previously [169]. ML297 was found to have one inactive metabolite “ML397-M1” after being metabolized by cytochrome P450. *In vitro* assays found that ML297 has modest solubility, plasma protein binding, and hepatic clearance. *In vivo* assays found that ML297 is able to cross the blood brain barrier in mice with a

brain:plasma ratio of 0.2 at 30 minutes post I.P. injection of 60 mg/kg ML297. Despite the relatively short half-life and only modest brain penetration of ML297, a positive effect of ML297 was observed in two models of epilepsy [169]. In both models of epilepsy, ML297 treatment was found to be as, if not more, effective than sodium valproate, an antiepileptic compound in clinical use. In a maximal electroshock epilepsy model, 60 mg/kg ML297 resulted in a significant increase in the latency of seizure onset. In the chemically-induced epilepsy model (PTZ-treatment), pretreatment with 60 mg/kg ML297 resulted in a significant level of prevention of both convulsions and death [169].

The full therapeutic potential associated with inhibiting or enhancing GIRK signaling will likely not be achieved without regional and/or GIRK subunit-selective manipulation because they are so widely expressed. In Chapter 3, we demonstrate the therapeutic potential that results from the selectivity of ML297. ML297, by activating GIRK1/2 channels, is able to elicit an anxiolytic phenotype without developing a conditioned place preference, meaning that ML297 achieves selective anxiolytic efficacy without a significant rewarding liability in mice. There is a need for anxiolytics with fewer side effects, rapid onset, with no abuse potential or motor dysfunction, and ML297 poses to be a good therapeutic candidate. Given the importance of GIRK signaling to the proper function of the heart and brain, ML297 and derivatives represent the most promising class of pharmacologic tools currently available to study GIRK-dependent signaling. Their availability will transform this field, allowing us to break the species barrier and begin examining in rigorous detail the therapeutic potential of GIRK manipulation in more clinically-relevant settings.

## **RGS influence on parasympathetic heart rate regulation**

Activation of the parasympathetic branch of the autonomic nervous system decreases heart rate via the neurotransmitter acetylcholine. Acetylcholine stimulates M<sub>2</sub> muscarinic receptors (M<sub>2</sub>R) on sinoatrial nodal cells and atrial myocytes, leading to the G protein-dependent activation of the potassium channel I<sub>KACH</sub> [51, 69]. Temporal regulation of the M<sub>2</sub>R-I<sub>KACH</sub> signaling cascade can impact heart rate [205, 206]. In Chapter 4, we found that the RGS6/Gβ5 protein complex is an essential modulator of M<sub>2</sub>R-I<sub>KACH</sub> signaling in cardiac myocytes and sinoatrial node cells. Furthermore, inactivation of the *Rgs6* gene in mice results in a mild bradycardia and an enhanced effect of drug-induced parasympathetic stimulation. Thus, RGS6/Gβ5 may contribute to, or represent a novel therapeutic target for, pathological conditions characterized by abnormal regulation of cardiac output.

At the same time the work in Chapter 4 was published, another study about the role of RGS6 in parasympathetic regulation was also published [251]. Both studies demonstrated high levels of RGS6 expressed in atrial tissue via immunoblotting, particularly compared to RGS4 levels, which were higher in the brain than in the heart. Using immunohistochemistry, RGS6 was demonstrated to be specifically expressed in the SAN and AVN regions [251]. In our study we observed a slight but significant decrease in resting HR in *Rgs6*<sup>-/-</sup> mice compared to wild-type mice as well as enhanced bradycardia during carbachol administration in *Rgs6*<sup>-/-</sup> mice. Other work also observed enhanced carbachol induced bradycardia in *Rgs6*<sup>-/-</sup> mice [251]. Furthermore, an exaggerated CCh-induced inhibition of spontaneous action potential firing in SAN cells



isolated from *Rgs6*<sup>-/-</sup> mice was observed [251]. Both studies identify RGS6 as a key modulator of the M<sub>2</sub>R-I<sub>KACH</sub> cascade and, subsequently, of the parasympathetic regulation of heart rate.

An interesting finding of this study was that R7BP is not expressed in atrial tissue of wild-type mice. In the CNS, both Gβ5 and R7BP are necessary for the functionality of the R7 RGS family, including RGS6 [135-138]. While we demonstrated that the presence of Gβ5 is necessary for the stability and function of atrial RGS6, we don't observe any deficits in RGS6 expression in the absence of R7BP. In the CNS, R7BP anchors RGS6 to the membrane so that it can interact with G<sub>i/o</sub> protein signaling complexes. The mechanism by which RGS6 is anchored to the membrane in cardiomyocytes is still unknown. We demonstrated that RGS6/Gβ5 has a protein-protein interaction with GIRK4, but this interaction is likely through Gβ5 and not the DEP/DHEX domain of RGS6. It is possible that there is a different anchoring protein expressed in cardiomyocytes that fills the role of R7BP. Another possibility is that the RGS6/Gβ5 complex is regulating the M<sub>2</sub>R-I<sub>KACH</sub> cascade from the cytosol and not the membrane. One approach to answering this question would be to perform a proteomic screen of RGS6/Gβ5 binding partners. Another approach would be to look at the intracellular localization of RGS6/Gβ5 with a live cell imaging assay.

A study in 2008 identified RGS4 as a regulator of parasympathetic M<sub>2</sub>R-I<sub>KACH</sub> signaling and heart rate, very similar to our findings for RGS6 [89]. It was demonstrated, albeit indirectly, that RGS4 is expressed in the SAN [89]. *Rgs4*<sup>-/-</sup> mice displayed both significantly reduced resting heart rate and significantly enhanced CCh-induced

inhibition of spontaneous action potential firing compared to wild-type mice [89]. Further, *Rgs4*<sup>-/-</sup> SAN cells had significantly slower activation and deactivation kinetics of CCh-induced I<sub>KACH</sub> activity [89]. Our original hypothesis concerning this work was that RGS4 and RGS6/Gβ5 were acting in parallel to regulate M<sub>2</sub>R-I<sub>KACH</sub> signaling. However, we failed to see an upregulation of RGS4 in the atrial tissue taken from *Rgs6*<sup>-/-</sup> mice, which we would expect to see if RGS4 were to exert a compensatory effect in these knockout animals. The goal of our next study (Chapter 5) was aimed at testing this hypothesis.

The work in Chapter 5 sought to clarify the molecular basis of the parasympathetic regulation of heart rate, dysregulation of which underlies multiple forms of arrhythmia and sudden cardiac death. Both RGS4 and RGS6 have been implicated in the temporal regulation of M<sub>2</sub>R-I<sub>KACH</sub> signaling and in the parasympathetic regulation of heart rate. We found that RGS4 does not make a significant contribution to the parasympathetic regulation of HR or related signaling in the SAN, under recording conditions where a prominent impact of RGS6 is observed. Interestingly, concurrent ablation of *Rgs4* rescued, in part, many of the phenotypes observed in *Rgs6*<sup>-/-</sup> mice. It appears that another member of the R7 RGS protein subfamily is present in SAN cells and can modulate muscarinic signaling, but its influence is masked by RGS6 and RGS4. This is an intriguing form of molecular compensation that may suggest an efficacious form of pharmacotherapy (i.e., RGS4 antagonism) that could be used to treat disorders linked to loss-of-function *Rgs6* mutations.

In reconstituted expression systems, RGS4 has been shown to regulate GIRK channel kinetics [145, 287]. RGS4 was demonstrated to have GAP activity on members of both  $G\alpha_{i/o}$  and  $G\alpha_q$  protein families [145, 259, 262]. Furthermore, RGS4 has been shown to be upregulated in myocardial tissue taken from failing human hearts [262]. In that study, they found that the upregulation of RGS4 corresponded to a reduction in  $G\alpha_q$  protein signaling. In our study, *Rgs4* ablation trended in faster kinetics and larger GIRK responses through  $M_2$  activation. It is possible that RGS4 is acting on  $G\alpha_q$  in the SAN in our study. If this is the case, the loss of RGS4 would result in less regulation of excitatory G protein signaling. GIRK signaling has been shown to be enhanced by excitation through feedback mechanisms, particularly by increases in intracellular  $Na^+$  [73, 93, 97-101]. Taken together, RGS4 may be acting on  $G\alpha_q$  to regulate excitatory sympathetic inputs in the SAN.

Another explanation as to why we did not observe an effect of *Rgs4* ablation is that different signaling cascades might be compartmentalized within the atria, perhaps even within the SAN. Both adenosine and acetylcholine have been demonstrated to signal through  $I_{KACH}$  in atrial myocytes [288]. In Chapter 4, we demonstrate that *Rgs6* ablation causes enhanced CCh-induced bradycardia but there was no enhancement of adenosine-induced bradycardia. This would suggest that while RGS6 is the key regulator of  $M_2R$ - $I_{KACH}$  signaling, the same may not be true for adenosine receptor- $I_{KACH}$  signaling. Perhaps the roles of RGS4 and RGS6 within the heart depend on the identity of GPCR upstream of the  $I_{KACH}$  channel. Further, both signaling cascades may not be present in the SAN. While we've demonstrated robust  $M_2R$ - $I_{KACH}$  activity in SAN cells by applying both CCh

and ACh, we have not observed an  $I_{KACH}$  response in SAN cells to maximal doses of adenosine (data not shown). In order to get at this question, comparisons of electrophysiology responses to CCh and adenosine are needed from both SAN cells and atrial cardiomyocytes. These experiments could be done in cells taken from wild-type, *Rgs4*<sup>-/-</sup>, and *Rgs6*<sup>-/-</sup> mice to further explore the compartmentalization of RGS proteins by cell population and GPCR identity.

## **Future Directions**

### *Crystallization of the GIRK1/GIRK2 heteromer*

Many of the questions that remain unanswered in Chapters 2 and 3 point to the need to resolve the structure of the GIRK1/GIRK2 heteromeric channel. First, the functionality and structure of the distal C-terminus region unique to GIRK1 are still unknown. Some studies suggest that it may participate in binding  $G\beta\gamma$  or even  $G\alpha_{i/o}$  subunits [275, 289, 290]. Second, the shape and configuration of the GIRK1/GIRK2 heteromeric pore has yet to be resolved and compared with the GIRK2 homomeric pore. Third, GIRK1 residue Q404 alters the sensitivity of GIRK channels for  $G\beta\gamma$  but the underlying mechanism remains unknown. Resolving the GIRK1/GIRK2 heteromer in the absence and presence of  $G\beta\gamma$  would give insight into whether Q404 alters the structural conformation of the channel's cytosolic regions or if this residue is directly involved with a stronger physical interaction with  $G\beta\gamma$ . Finally, the location of the physical binding site of ML297 and how the channel rearranges in the presence of ML297 needs to be elucidated to further understand the mechanism of action of this new drug class.

Unfortunately, crystallizing a natively formed heteromer is not possible, as a subset of formed-channel would be GIRK2 homomers, giving a non-uniform organization of protein. To fix this issue a concatamer of GIRK1 and GIRK2 fused together could be used instead. When expressed, this concatamer would form a dimer with another concatamer forcing uniform expression of GIRK1/GIRK2 heteromeric protein. This protein would be crystallized by itself, in the presence of PIP<sub>2</sub> and Gβγ, and in the presence of ML297. Point mutations of GIRK1, such as Q404A, could be made on the concatamer and crystallized as well. This set of crystal structures would give much needed insight into the unresolved questions from Chapters 2 and 3.

*Mechanism of selectivity for GIRK2- and GIRK4-containing channels*

An interesting observation in the characterization of ML297 is that, while it has a robust effect on GIRK1/GIRK2 heteromeric channels, it induces less current from GIRK1/GIRK4 heteromeric channels. Some drugs from this new class demonstrate even more preference for GIRK2 over GIRK4 than ML297, while others are able to activate GIRK1/GIRK2 and GIRK1/GIRK4 equally. VU0466553 is completely selective for GIRK1/GIRK2 channels, and actually antagonizes GIRK1/GIRK4 channels (data not shown). As this drug class undergoes development, it would have enormous therapeutic potential if drugs completely selective in their activation of either GIRK1/GIRK2 or GIRK1/GIRK4 could be designed or identified in a high-throughput screen. GIRK1/GIRK4 channels make up the I<sub>KACH</sub> channel in the heart and, as discussed previously, play a role in the modulation of heart rate. A targeted GIRK1/GIRK4 agonist,

with no activity on GIRK1/GIRK2 channels, could be used to treat arrhythmias without having adverse effects on cognitive functions. Alternately, a completely GIRK1/GIRK2 selective drug could be used in the treatment of anxiety, epilepsy, and perhaps pain, without the concern of adverse effects on cardiac function.

In order to test compounds for their selectivity between GIRK2- and GIRK4-containing channels, we would first apply them in electrophysiology experiments in different cell types. By taking advantage of the endogenous expression of different heteromeric GIRK channels in hippocampal neurons (GIRK1/GIRK2) and sinoatrial node cells (GIRK1/GIRK4), we would apply these compounds to both types and see if they are able to evoke a response in one and not the other. In doing so, this assay would assess their selectivity for GIRK1/GIRK2 and GIRK1/GIRK4. Behavioral tests, such as motor activity, elevated plus maze, stress-induced hyperthermia, and physiological tests, including ECG telemetry and ex vivo perfused-heart rate measurements (also referred to as Langendorff perfusion), would be further used to look at the efficacy and selectivity of compounds that show promise in the electrophysiology assays.

The other side of this project would be to identify the structural determinant(s) in GIRK2 and GIRK4 that cause this difference in selective activation by this new drug class. Out of all the GIRK channels, GIRK2A and GIRK4 are the most similar in sequence and structure but differ in their distribution [50, 70, 291]. Using a chimeric approach, similar to the approach used in Chapter 2, and the high-throughput thallium flux assay, we would be able to test different regions for their role in this mechanism of selectivity. Once a region (or regions) was isolated, site-directed mutagenesis would

allow us to pinpoint the exact residues responsible for this difference. In discovering the structural determinant(s) of selectivity between GIRK2 and GIRK4, we may also gain insight into the physical binding site of compounds in this new drug class.

By understanding the mechanism of selectivity between GIRK2- and GIRK4-containing channels, we would have new potential therapeutic compounds that could selectively treat cardiac and CNS diseases. GIRK1/GIRK2 selective agonists and antagonists would allow for new pharmacotherapies against anxiety, epilepsy, neuropathic pain, depression, addiction, schizophrenia, and Down's syndrome [57, 170]. GIRK1/GIRK4 selective agonists and antagonists could offer new pharmacotherapies for cardiac arrhythmias, hyperaldosteronism, and obesity [170]. Together, this new drug class will have an important impact on how GIRK channels are studied and will greatly change how many excitatory diseases are treated.

## **REFERENCES**



1. Schlyer, S. and R. Horuk, *I want a new drug: G-protein-coupled receptors in drug development*. Drug discovery today, 2006. **11**(11-12): p. 481-93.
2. Oldham, W.M. and H.E. Hamm, *Heterotrimeric G protein activation by G-protein-coupled receptors*. Nature reviews. Molecular cell biology, 2008. **9**(1): p. 60-71.
3. Schmidt, C.J., et al., *Specificity of G protein beta and gamma subunit interactions*. The Journal of biological chemistry, 1992. **267**(20): p. 13807-10.
4. Downes, G.B. and N. Gautam, *The G protein subunit gene families*. Genomics, 1999. **62**(3): p. 544-52.
5. Hermans, E., *Biochemical and pharmacological control of the multiplicity of coupling at G-protein-coupled receptors*. Pharmacology & therapeutics, 2003. **99**(1): p. 25-44.
6. Senogles, S.E., et al., *Specificity of receptor-G protein interactions. Discrimination of Gi subtypes by the D2 dopamine receptor in a reconstituted system*. The Journal of biological chemistry, 1990. **265**(8): p. 4507-14.
7. Simon, M.I., M.P. Strathmann, and N. Gautam, *Diversity of G proteins in signal transduction*. Science, 1991. **252**(5007): p. 802-8.
8. Trumpp-Kallmeyer, S., et al., *Modeling of G-protein-coupled receptors: application to dopamine, adrenaline, serotonin, acetylcholine, and mammalian opsin receptors*. Journal of medicinal chemistry, 1992. **35**(19): p. 3448-62.
9. Hearing, M.C., A.N. Zink, and K. Wickman, *Cocaine-induced adaptations in metabotropic inhibitory signaling in the mesocorticolimbic system*. Reviews in the neurosciences, 2012. **23**(4): p. 325-51.
10. Lambright, D.G., et al., *Structural determinants for activation of the alpha-subunit of a heterotrimeric G protein*. Nature, 1994. **369**(6482): p. 621-8.
11. Coleman, D.E., et al., *Structures of active conformations of Gi alpha 1 and the mechanism of GTP hydrolysis*. Science, 1994. **265**(5177): p. 1405-12.
12. Mixon, M.B., et al., *Tertiary and quaternary structural changes in Gi alpha 1 induced by GTP hydrolysis*. Science, 1995. **270**(5238): p. 954-60.
13. Smotrys, J.E. and M.E. Linder, *Palmitoylation of intracellular signaling proteins: regulation and function*. Annual review of biochemistry, 2004. **73**: p. 559-87.
14. Chen, C.A. and D.R. Manning, *Regulation of G proteins by covalent modification*. Oncogene, 2001. **20**(13): p. 1643-52.
15. Sondek, J., et al., *Crystal structure of a G-protein beta gamma dimer at 2.1A resolution*. Nature, 1996. **379**(6563): p. 369-74.
16. Wall, M.A., et al., *The structure of the G protein heterotrimer Gi alpha 1 beta 1 gamma 2*. Cell, 1995. **83**(6): p. 1047-58.
17. Zhang, F.L. and P.J. Casey, *Protein prenylation: molecular mechanisms and functional consequences*. Annual review of biochemistry, 1996. **65**: p. 241-69.
18. Bjarnadottir, T.K., et al., *Comprehensive repertoire and phylogenetic analysis of the G protein-coupled receptors in human and mouse*. Genomics, 2006. **88**(3): p. 263-73.

19. Fredriksson, R., et al., *The G-protein-coupled receptors in the human genome form five main families. Phylogenetic analysis, paralogon groups, and fingerprints*. *Molecular pharmacology*, 2003. **63**(6): p. 1256-72.
20. Kristiansen, K., *Molecular mechanisms of ligand binding, signaling, and regulation within the superfamily of G-protein-coupled receptors: molecular modeling and mutagenesis approaches to receptor structure and function*. *Pharmacology & therapeutics*, 2004. **103**(1): p. 21-80.
21. Javitch, J.A., *The ants go marching two by two: oligomeric structure of G-protein-coupled receptors*. *Molecular pharmacology*, 2004. **66**(5): p. 1077-82.
22. Milligan, G., *G protein-coupled receptor dimerization: function and ligand pharmacology*. *Molecular pharmacology*, 2004. **66**(1): p. 1-7.
23. Baneres, J.L. and J. Parello, *Structure-based analysis of GPCR function: evidence for a novel pentameric assembly between the dimeric leukotriene B4 receptor BLT1 and the G-protein*. *Journal of molecular biology*, 2003. **329**(4): p. 815-29.
24. Pin, J.P., T. Galvez, and L. Prezeau, *Evolution, structure, and activation mechanism of family 3/C G-protein-coupled receptors*. *Pharmacology & therapeutics*, 2003. **98**(3): p. 325-54.
25. George, S.R., B.F. O'Dowd, and S.P. Lee, *G-protein-coupled receptor oligomerization and its potential for drug discovery*. *Nature reviews. Drug discovery*, 2002. **1**(10): p. 808-20.
26. Brinkerhoff, C.J., J.R. Traynor, and J.J. Linderman, *Collision coupling, crosstalk, and compartmentalization in G-protein coupled receptor systems: can a single model explain disparate results?* *Journal of theoretical biology*, 2008. **255**(3): p. 278-86.
27. Challiss, R.A. and J. Wess, *Receptors: GPCR-G protein preassembly?* *Nature chemical biology*, 2011. **7**(10): p. 657-8.
28. Gales, C., et al., *Probing the activation-promoted structural rearrangements in preassembled receptor-G protein complexes*. *Nature structural & molecular biology*, 2006. **13**(9): p. 778-86.
29. Alves, I.D., et al., *Phosphatidylethanolamine enhances rhodopsin photoactivation and transducin binding in a solid supported lipid bilayer as determined using plasmon-waveguide resonance spectroscopy*. *Biophysical journal*, 2005. **88**(1): p. 198-210.
30. Alves, I.D., et al., *Direct observation of G-protein binding to the human delta-opioid receptor using plasmon-waveguide resonance spectroscopy*. *The Journal of biological chemistry*, 2003. **278**(49): p. 48890-7.
31. Qin, K., et al., *Inactive-state preassembly of G(q)-coupled receptors and G(q) heterotrimers*. *Nature chemical biology*, 2011. **7**(10): p. 740-7.
32. Nobles, M., A. Benians, and A. Tinker, *Heterotrimeric G proteins precouple with G protein-coupled receptors in living cells*. *Proceedings of the National Academy of Sciences of the United States of America*, 2005. **102**(51): p. 18706-11.
33. Hall, R.A., R.T. Premont, and R.J. Lefkowitz, *Heptahelical receptor signaling: beyond the G protein paradigm*. *The Journal of cell biology*, 1999. **145**(5): p. 927-32.

34. Wickman, K. and D.E. Clapham, *Ion channel regulation by G proteins*. *Physiological reviews*, 1995. **75**(4): p. 865-85.
35. Burns, D.L., et al., *Biochemical properties of pertussis toxin*. *The Tokai journal of experimental and clinical medicine*, 1988. **13 Suppl**: p. 181-5.
36. Burns, D.L., *Subunit structure and enzymic activity of pertussis toxin*. *Microbiological sciences*, 1988. **5**(9): p. 285-7.
37. Katada, T. and M. Ui, *ADP ribosylation of the specific membrane protein of C6 cells by islet-activating protein associated with modification of adenylate cyclase activity*. *The Journal of biological chemistry*, 1982. **257**(12): p. 7210-6.
38. Kurose, H., et al., *Specific uncoupling by islet-activating protein, pertussis toxin, of negative signal transduction via alpha-adrenergic, cholinergic, and opiate receptors in neuroblastoma x glioma hybrid cells*. *The Journal of biological chemistry*, 1983. **258**(8): p. 4870-5.
39. Mangmool, S. and H. Kurose, *G(i/o) protein-dependent and -independent actions of Pertussis Toxin (PTX)*. *Toxins*, 2011. **3**(7): p. 884-99.
40. Carter, B.D. and F. Medzihradsky, *Go mediates the coupling of the mu opioid receptor to adenylyl cyclase in cloned neural cells and brain*. *Proceedings of the National Academy of Sciences of the United States of America*, 1993. **90**(9): p. 4062-6.
41. Wittpoth, C., et al., *Regions on adenylyl cyclase that are necessary for inhibition of activity by beta gamma and G(ialpha) subunits of heterotrimeric G proteins*. *Proceedings of the National Academy of Sciences of the United States of America*, 1999. **96**(17): p. 9551-6.
42. Johnson, D.A., et al., *Dynamics of cAMP-dependent protein kinase*. *Chemical reviews*, 2001. **101**(8): p. 2243-70.
43. Chen, H. and N.A. Lambert, *Inhibition of dendritic calcium influx by activation of G-protein-coupled receptors in the hippocampus*. *Journal of neurophysiology*, 1997. **78**(6): p. 3484-8.
44. Jeong, S.W. and S.R. Ikeda, *Effect of G protein heterotrimer composition on coupling of neurotransmitter receptors to N-type Ca(2+) channel modulation in sympathetic neurons*. *Proceedings of the National Academy of Sciences of the United States of America*, 2000. **97**(2): p. 907-12.
45. Herlitze, S., et al., *Modulation of Ca<sup>2+</sup> channels by G-protein beta gamma subunits*. *Nature*, 1996. **380**(6571): p. 258-62.
46. Wickman, K.D., et al., *Recombinant G-protein beta gamma-subunits activate the muscarinic-gated atrial potassium channel*. *Nature*, 1994. **368**(6468): p. 255-7.
47. Reuveny, E., et al., *Activation of the cloned muscarinic potassium channel by G protein beta gamma subunits*. *Nature*, 1994. **370**(6485): p. 143-6.
48. Krapivinsky, G., et al., *G beta gamma binds directly to the G protein-gated K<sup>+</sup> channel, IKACH*. *The Journal of biological chemistry*, 1995. **270**(49): p. 29059-62.
49. Inanobe, A., et al., *G beta gamma directly binds to the carboxyl terminus of the G protein-gated muscarinic K<sup>+</sup> channel, GIRK1*. *Biochemical and biophysical research communications*, 1995. **212**(3): p. 1022-8.

50. Karschin, C., et al., *IRK(1-3) and GIRK(1-4) inwardly rectifying K<sup>+</sup> channel mRNAs are differentially expressed in the adult rat brain*. The Journal of neuroscience : the official journal of the Society for Neuroscience, 1996. **16**(11): p. 3559-70.
51. Wickman, K., et al., *Structure, G protein activation, and functional relevance of the cardiac G protein-gated K<sup>+</sup> channel, IKACH*. Annals of the New York Academy of Sciences, 1999. **868**: p. 386-98.
52. Luscher, C., et al., *G protein-coupled inwardly rectifying K<sup>+</sup> channels (GIRKs) mediate postsynaptic but not presynaptic transmitter actions in hippocampal neurons*. Neuron, 1997. **19**(3): p. 687-95.
53. Lacey, M.G., N.B. Mercuri, and R.A. North, *Dopamine acts on D2 receptors to increase potassium conductance in neurones of the rat substantia nigra zona compacta*. The Journal of physiology, 1987. **392**: p. 397-416.
54. Newberry, N.R. and R.A. Nicoll, *Comparison of the action of baclofen with gamma-aminobutyric acid on rat hippocampal pyramidal cells in vitro*. The Journal of physiology, 1985. **360**: p. 161-85.
55. Dutar, P., H.M. Vu, and D.J. Perkel, *Pharmacological characterization of an unusual mGluR-evoked neuronal hyperpolarization mediated by activation of GIRK channels*. Neuropharmacology, 1999. **38**(4): p. 467-75.
56. Sun, Q.Q., J.R. Huguenard, and D.A. Prince, *Somatostatin inhibits thalamic network oscillations in vitro: actions on the GABAergic neurons of the reticular nucleus*. The Journal of neuroscience : the official journal of the Society for Neuroscience, 2002. **22**(13): p. 5374-86.
57. Luscher, C. and P.A. Slesinger, *Emerging roles for G protein-gated inwardly rectifying potassium (GIRK) channels in health and disease*. Nature reviews. Neuroscience, 2010. **11**(5): p. 301-15.
58. Nichols, C.G. and A.N. Lopatin, *Inward rectifier potassium channels*. Annual review of physiology, 1997. **59**: p. 171-91.
59. Fakler, B., et al., *Strong voltage-dependent inward rectification of inward rectifier K<sup>+</sup> channels is caused by intracellular spermine*. Cell, 1995. **80**(1): p. 149-54.
60. Lopatin, A.N., E.N. Makhina, and C.G. Nichols, *Potassium channel block by cytoplasmic polyamines as the mechanism of intrinsic rectification*. Nature, 1994. **372**(6504): p. 366-9.
61. Yamada, M. and Y. Kurachi, *Spermine gates inward-rectifying muscarinic but not ATP-sensitive K<sup>+</sup> channels in rabbit atrial myocytes. Intracellular substance-mediated mechanism of inward rectification*. The Journal of biological chemistry, 1995. **270**(16): p. 9289-94.
62. Yamada, M., A. Inanobe, and Y. Kurachi, *G protein regulation of potassium ion channels*. Pharmacological reviews, 1998. **50**(4): p. 723-60.
63. Liao, Y.J., Y.N. Jan, and L.Y. Jan, *Heteromultimerization of G-protein-gated inwardly rectifying K<sup>+</sup> channel proteins GIRK1 and GIRK2 and their altered expression in weaver brain*. The Journal of neuroscience : the official journal of the Society for Neuroscience, 1996. **16**(22): p. 7137-50.

64. Jelacic, T.M., et al., *Functional and biochemical evidence for G-protein-gated inwardly rectifying K<sup>+</sup> (GIRK) channels composed of GIRK2 and GIRK3*. The Journal of biological chemistry, 2000. **275**(46): p. 36211-6.
65. Tucker, S.J., M. Pessia, and J.P. Adelman, *Muscarine-gated K<sup>+</sup> channel: subunit stoichiometry and structural domains essential for G protein stimulation*. The American journal of physiology, 1996. **271**(1 Pt 2): p. H379-85.
66. Kofuji, P., N. Davidson, and H.A. Lester, *Evidence that neuronal G-protein-gated inwardly rectifying K<sup>+</sup> channels are activated by G beta gamma subunits and function as heteromultimers*. Proceedings of the National Academy of Sciences of the United States of America, 1995. **92**(14): p. 6542-6.
67. Dascal, N., *Signalling via the G protein-activated K<sup>+</sup> channels*. Cellular signalling, 1997. **9**(8): p. 551-73.
68. Ma, D., et al., *Diverse trafficking patterns due to multiple traffic motifs in G protein-activated inwardly rectifying potassium channels from brain and heart*. Neuron, 2002. **33**(5): p. 715-29.
69. Krapivinsky, G., et al., *The G-protein-gated atrial K<sup>+</sup> channel IKACH is a heteromultimer of two inwardly rectifying K(+)-channel proteins*. Nature, 1995. **374**(6518): p. 135-41.
70. Jelacic, T.M., S.M. Sims, and D.E. Clapham, *Functional expression and characterization of G-protein-gated inwardly rectifying K<sup>+</sup> channels containing GIRK3*. The Journal of membrane biology, 1999. **169**(2): p. 123-9.
71. Wischmeyer, E., et al., *Subunit interactions in the assembly of neuronal Kir3.0 inwardly rectifying K<sup>+</sup> channels*. Molecular and cellular neurosciences, 1997. **9**(3): p. 194-206.
72. Lesage, F., et al., *Cloning provides evidence for a family of inward rectifier and G-protein coupled K<sup>+</sup> channels in the brain*. FEBS letters, 1994. **353**(1): p. 37-42.
73. Lesage, F., et al., *Molecular properties of neuronal G-protein-activated inwardly rectifying K<sup>+</sup> channels*. The Journal of biological chemistry, 1995. **270**(48): p. 28660-7.
74. Isomoto, S., et al., *A novel ubiquitously distributed isoform of GIRK2 (GIRK2B) enhances GIRK1 expression of the G-protein-gated K<sup>+</sup> current in Xenopus oocytes*. Biochemical and biophysical research communications, 1996. **218**(1): p. 286-91.
75. Nehring, R.B., et al., *Neuronal inwardly rectifying K(+)-channels differentially couple to PDZ proteins of the PSD-95/SAP90 family*. The Journal of neuroscience : the official journal of the Society for Neuroscience, 2000. **20**(1): p. 156-62.
76. Inanobe, A., et al., *Molecular cloning and characterization of a novel splicing variant of the Kir3.2 subunit predominantly expressed in mouse testis*. The Journal of physiology, 1999. **521 Pt 1**: p. 19-30.
77. Nelson, C.S., J.L. Marino, and C.N. Allen, *Cloning and characterization of Kir3.1 (GIRK1) C-terminal alternative splice variants*. Brain research. Molecular brain research, 1997. **46**(1-2): p. 185-96.

78. Steinecker, B., C. Rosker, and W. Schreibmayer, *The GIRK1 brain variant GIRK1d and its functional impact on heteromultimeric GIRK channels*. Journal of receptor and signal transduction research, 2007. **27**(5-6): p. 369-82.
79. Wagner, V., et al., *Cloning and characterisation of GIRK1 variants resulting from alternative RNA editing of the KCNJ3 gene transcript in a human breast cancer cell line*. Journal of cellular biochemistry, 2010. **110**(3): p. 598-608.
80. Wickman, K., et al., *Brain localization and behavioral impact of the G-protein-gated K<sup>+</sup> channel subunit GIRK4*. The Journal of neuroscience : the official journal of the Society for Neuroscience, 2000. **20**(15): p. 5608-15.
81. Perry, C.A., et al., *Predisposition to late-onset obesity in GIRK4 knockout mice*. Proceedings of the National Academy of Sciences of the United States of America, 2008. **105**(23): p. 8148-53.
82. Koyrakh, L., et al., *Molecular and cellular diversity of neuronal G-protein-gated potassium channels*. The Journal of neuroscience : the official journal of the Society for Neuroscience, 2005. **25**(49): p. 11468-78.
83. Slesinger, P.A., et al., *Defective gamma-aminobutyric acid type B receptor-activated inwardly rectifying K<sup>+</sup> currents in cerebellar granule cells isolated from weaver and Girk2 null mutant mice*. Proceedings of the National Academy of Sciences of the United States of America, 1997. **94**(22): p. 12210-7.
84. Torrecilla, M., et al., *G-protein-gated potassium channels containing Kir3.2 and Kir3.3 subunits mediate the acute inhibitory effects of opioids on locus ceruleus neurons*. The Journal of neuroscience : the official journal of the Society for Neuroscience, 2002. **22**(11): p. 4328-34.
85. Cruz, H.G., et al., *Absence and rescue of morphine withdrawal in GIRK/Kir3 knock-out mice*. The Journal of neuroscience : the official journal of the Society for Neuroscience, 2008. **28**(15): p. 4069-77.
86. Labouebe, G., et al., *RGS2 modulates coupling between GABAB receptors and GIRK channels in dopamine neurons of the ventral tegmental area*. Nature neuroscience, 2007. **10**(12): p. 1559-68.
87. Cruz, H.G., et al., *Bi-directional effects of GABA(B) receptor agonists on the mesolimbic dopamine system*. Nature neuroscience, 2004. **7**(2): p. 153-9.
88. Inanobe, A., et al., *Characterization of G-protein-gated K<sup>+</sup> channels composed of Kir3.2 subunits in dopaminergic neurons of the substantia nigra*. The Journal of neuroscience : the official journal of the Society for Neuroscience, 1999. **19**(3): p. 1006-17.
89. Cifelli, C., et al., *RGS4 regulates parasympathetic signaling and heart rate control in the sinoatrial node*. Circulation research, 2008. **103**(5): p. 527-35.
90. Iwanir, S. and E. Reuveny, *Adrenaline-induced hyperpolarization of mouse pancreatic islet cells is mediated by G protein-gated inwardly rectifying potassium (GIRK) channels*. Pflugers Archiv : European journal of physiology, 2008. **456**(6): p. 1097-108.
91. Yi, Y.J., et al., *Sperm GIRK2-containing K<sup>+</sup> inward rectifying channels participate in sperm capacitation and fertilization*. Systems biology in reproductive medicine, 2011. **57**(6): p. 296-308.

92. Huang, C.L., S. Feng, and D.W. Hilgemann, *Direct activation of inward rectifier potassium channels by PIP2 and its stabilization by Gbetagamma*. *Nature*, 1998. **391**(6669): p. 803-6.
93. Whorton, M.R. and R. MacKinnon, *Crystal structure of the mammalian GIRK2 K<sup>+</sup> channel and gating regulation by G proteins, PIP2, and sodium*. *Cell*, 2011. **147**(1): p. 199-208.
94. Suh, B.C. and B. Hille, *PIP2 is a necessary cofactor for ion channel function: how and why?* *Annual review of biophysics*, 2008. **37**: p. 175-95.
95. Somlyo, A.P. and A.V. Somlyo, *Signal transduction and regulation in smooth muscle*. *Nature*, 1994. **372**(6503): p. 231-6.
96. Lopes, C.M., et al., *Alterations in conserved Kir channel-PIP2 interactions underlie channelopathies*. *Neuron*, 2002. **34**(6): p. 933-44.
97. Zhang, H., et al., *Activation of inwardly rectifying K<sup>+</sup> channels by distinct PtdIns(4,5)P2 interactions*. *Nature cell biology*, 1999. **1**(3): p. 183-8.
98. Ho, I.H. and R.D. Murrell-Lagnado, *Molecular determinants for sodium-dependent activation of G protein-gated K<sup>+</sup> channels*. *The Journal of biological chemistry*, 1999. **274**(13): p. 8639-48.
99. Ho, I.H. and R.D. Murrell-Lagnado, *Molecular mechanism for sodium-dependent activation of G protein-gated K<sup>+</sup> channels*. *The Journal of physiology*, 1999. **520 Pt 3**: p. 645-51.
100. Sui, J.L., K.W. Chan, and D.E. Logothetis, *Na<sup>+</sup> activation of the muscarinic K<sup>+</sup> channel by a G-protein-independent mechanism*. *The Journal of general physiology*, 1996. **108**(5): p. 381-91.
101. Sui, J.L., J. Petit-Jacques, and D.E. Logothetis, *Activation of the atrial KACH channel by the betagamma subunits of G proteins or intracellular Na<sup>+</sup> ions depends on the presence of phosphatidylinositol phosphates*. *Proceedings of the National Academy of Sciences of the United States of America*, 1998. **95**(3): p. 1307-12.
102. Nishida, M. and R. MacKinnon, *Structural basis of inward rectification: cytoplasmic pore of the G protein-gated inward rectifier GIRK1 at 1.8 Å resolution*. *Cell*, 2002. **111**(7): p. 957-65.
103. Pegan, S., et al., *Cytoplasmic domain structures of Kir2.1 and Kir3.1 show sites for modulating gating and rectification*. *Nature neuroscience*, 2005. **8**(3): p. 279-87.
104. Inanobe, A., et al., *Structural diversity in the cytoplasmic region of G protein-gated inward rectifier K<sup>+</sup> channels*. *Channels*, 2007. **1**(1): p. 39-45.
105. Nishida, M., et al., *Crystal structure of a Kir3.1-prokaryotic Kir channel chimera*. *The EMBO journal*, 2007. **26**(17): p. 4005-15.
106. Whorton, M.R. and R. MacKinnon, *X-ray structure of the mammalian GIRK2-betagamma G-protein complex*. *Nature*, 2013. **498**(7453): p. 190-7.
107. Lunn, M.L., et al., *A unique sorting nexin regulates trafficking of potassium channels via a PDZ domain interaction*. *Nature neuroscience*, 2007. **10**(10): p. 1249-59.

108. Hibino, H., et al., *Anchoring proteins confer G protein sensitivity to an inward-rectifier K(+) channel through the GK domain*. The EMBO journal, 2000. **19**(1): p. 78-83.
109. Leaney, J.L., *Contribution of Kir3.1, Kir3.2A and Kir3.2C subunits to native G protein-gated inwardly rectifying potassium currents in cultured hippocampal neurons*. The European journal of neuroscience, 2003. **18**(8): p. 2110-8.
110. Slesinger, P.A., et al., *Identification of structural elements involved in G protein gating of the GIRK1 potassium channel*. Neuron, 1995. **15**(5): p. 1145-56.
111. Thomas, A.M., et al., *Differential phosphoinositide binding to components of the G protein-gated K+ channel*. The Journal of membrane biology, 2006. **211**(1): p. 43-53.
112. Stevens, E.B., et al., *Identification of regions that regulate the expression and activity of G protein-gated inward rectifier K+ channels in Xenopus oocytes*. The Journal of physiology, 1997. **503 ( Pt 3)**: p. 547-62.
113. Chan, K.W., et al., *Specific regions of heteromeric subunits involved in enhancement of G protein-gated K+ channel activity*. The Journal of biological chemistry, 1997. **272**(10): p. 6548-55.
114. Chan, K.W., et al., *Control of channel activity through a unique amino acid residue of a G protein-gated inwardly rectifying K+ channel subunit*. Proceedings of the National Academy of Sciences of the United States of America, 1996. **93**(24): p. 14193-8.
115. Kunkel, M.T. and E.G. Peralta, *Identification of domains conferring G protein regulation on inward rectifier potassium channels*. Cell, 1995. **83**(3): p. 443-9.
116. Conklin, B.R. and H.R. Bourne, *Structural elements of G alpha subunits that interact with G beta gamma, receptors, and effectors*. Cell, 1993. **73**(4): p. 631-41.
117. Doupnik, C.A., et al., *Time resolved kinetics of direct G beta 1 gamma 2 interactions with the carboxyl terminus of Kir3.4 inward rectifier K+ channel subunits*. Neuropharmacology, 1996. **35**(7): p. 923-31.
118. Benians, A., J.L. Leaney, and A. Tinker, *Agonist unbinding from receptor dictates the nature of deactivation kinetics of G protein-gated K+ channels*. Proceedings of the National Academy of Sciences of the United States of America, 2003. **100**(10): p. 6239-44.
119. Blumer, J.B., et al., *AGS proteins: receptor-independent activators of G-protein signaling*. Trends in pharmacological sciences, 2005. **26**(9): p. 470-6.
120. Cismowski, M.J., et al., *Activation of heterotrimeric G-protein signaling by a ras-related protein. Implications for signal integration*. The Journal of biological chemistry, 2000. **275**(31): p. 23421-4.
121. Peterson, Y.K., et al., *Stabilization of the GDP-bound conformation of Gialpha by a peptide derived from the G-protein regulatory motif of AGS3*. The Journal of biological chemistry, 2000. **275**(43): p. 33193-6.
122. Ghosh, M., et al., *Receptor- and nucleotide exchange-independent mechanisms for promoting G protein subunit dissociation*. The Journal of biological chemistry, 2003. **278**(37): p. 34747-50.



123. Siderovski, D.P., S.P. Heximer, and D.R. Forsdyke, *A human gene encoding a putative basic helix-loop-helix phosphoprotein whose mRNA increases rapidly in cycloheximide-treated blood mononuclear cells*. DNA and cell biology, 1994. **13**(2): p. 125-47.
124. Berman, D.M., T.M. Wilkie, and A.G. Gilman, *GAIP and RGS4 are GTPase-activating proteins for the Gi subfamily of G protein alpha subunits*. Cell, 1996. **86**(3): p. 445-52.
125. Ross, E.M. and T.M. Wilkie, *GTPase-activating proteins for heterotrimeric G proteins: regulators of G protein signaling (RGS) and RGS-like proteins*. Annual review of biochemistry, 2000. **69**: p. 795-827.
126. Popov, S., et al., *The regulators of G protein signaling (RGS) domains of RGS4, RGS10, and GAIP retain GTPase activating protein activity in vitro*. Proceedings of the National Academy of Sciences of the United States of America, 1997. **94**(14): p. 7216-20.
127. Zeng, W., et al., *The N-terminal domain of RGS4 confers receptor-selective inhibition of G protein signaling*. The Journal of biological chemistry, 1998. **273**(52): p. 34687-90.
128. Sjogren, B., L.L. Blazer, and R.R. Neubig, *Regulators of G protein signaling proteins as targets for drug discovery*. Progress in molecular biology and translational science, 2010. **91**: p. 81-119.
129. Hepler, J.R., *Emerging roles for RGS proteins in cell signalling*. Trends in pharmacological sciences, 1999. **20**(9): p. 376-82.
130. Bernstein, L.S., et al., *RGS4 binds to membranes through an amphipathic alpha-helix*. The Journal of biological chemistry, 2000. **275**(24): p. 18520-6.
131. Watson, N., et al., *RGS family members: GTPase-activating proteins for heterotrimeric G-protein alpha-subunits*. Nature, 1996. **383**(6596): p. 172-5.
132. Anderson, G.R., E. Posokhova, and K.A. Martemyanov, *The R7 RGS protein family: multi-subunit regulators of neuronal G protein signaling*. Cell biochemistry and biophysics, 2009. **54**(1-3): p. 33-46.
133. Cabrera, J.L., et al., *Identification of the Gbeta5-RGS7 protein complex in the retina*. Biochemical and biophysical research communications, 1998. **249**(3): p. 898-902.
134. Makino, E.R., et al., *The GTPase activating factor for transducin in rod photoreceptors is the complex between RGS9 and type 5 G protein beta subunit*. Proceedings of the National Academy of Sciences of the United States of America, 1999. **96**(5): p. 1947-52.
135. Snow, B.E., et al., *Fidelity of G protein beta-subunit association by the G protein gamma-subunit-like domains of RGS6, RGS7, and RGS11*. Proceedings of the National Academy of Sciences of the United States of America, 1999. **96**(11): p. 6489-94.
136. Witherow, D.S., et al., *Complexes of the G protein subunit gbeta 5 with the regulators of G protein signaling RGS7 and RGS9. Characterization in native tissues and in transfected cells*. The Journal of biological chemistry, 2000. **275**(32): p. 24872-80.

137. Anderson, G.R., et al., *Expression and localization of RGS9-2/G 5/R7BP complex in vivo is set by dynamic control of its constitutive degradation by cellular cysteine proteases*. The Journal of neuroscience : the official journal of the Society for Neuroscience, 2007. **27**(51): p. 14117-27.
138. Drenan, R.M., et al., *R7BP augments the function of RGS7\*Gbeta5 complexes by a plasma membrane-targeting mechanism*. The Journal of biological chemistry, 2006. **281**(38): p. 28222-31.
139. Stanfield, P.R., S. Nakajima, and Y. Nakajima, *Constitutively active and G-protein coupled inward rectifier K<sup>+</sup> channels: Kir2.0 and Kir3.0*. Reviews of physiology, biochemistry and pharmacology, 2002. **145**: p. 47-179.
140. Doupnik, C.A., et al., *RGS proteins reconstitute the rapid gating kinetics of gbetagamma-activated inwardly rectifying K<sup>+</sup> channels*. Proceedings of the National Academy of Sciences of the United States of America, 1997. **94**(19): p. 10461-6.
141. Saitoh, O., et al., *RGS8 accelerates G-protein-mediated modulation of K<sup>+</sup> currents*. Nature, 1997. **390**(6659): p. 525-9.
142. Herlitze, S., J.P. Ruppersberg, and M.D. Mark, *New roles for RGS2, 5 and 8 on the ratio-dependent modulation of recombinant GIRK channels expressed in Xenopus oocytes*. The Journal of physiology, 1999. **517** ( Pt 2): p. 341-52.
143. Chuang, H.H., et al., *Evidence that the nucleotide exchange and hydrolysis cycle of G proteins causes acute desensitization of G-protein gated inward rectifier K<sup>+</sup> channels*. Proceedings of the National Academy of Sciences of the United States of America, 1998. **95**(20): p. 11727-32.
144. Ulens, C., P. Daenens, and J. Tytgat, *Changes in GIRK1/GIRK2 deactivation kinetics and basal activity in the presence and absence of RGS4*. Life sciences, 2000. **67**(19): p. 2305-17.
145. Fujita, S., et al., *A regulator of G protein signalling (RGS) protein confers agonist-dependent relaxation gating to a G protein-gated K<sup>+</sup> channel*. The Journal of physiology, 2000. **526** Pt 2: p. 341-7.
146. Xie, K., et al., *Gbeta5 recruits R7 RGS proteins to GIRK channels to regulate the timing of neuronal inhibitory signaling*. Nature neuroscience, 2010. **13**(6): p. 661-3.
147. Ransom, C.B. and H. Sontheimer, *Biophysical and pharmacological characterization of inwardly rectifying K<sup>+</sup> currents in rat spinal cord astrocytes*. Journal of neurophysiology, 1995. **73**(1): p. 333-46.
148. Kurachi, Y., T. Nakajima, and T. Sugimoto, *Quinidine inhibition of the muscarine receptor-activated K<sup>+</sup> channel current in atrial cells of guinea pig*. Naunyn-Schmiedeberg's archives of pharmacology, 1987. **335**(2): p. 216-8.
149. Nakajima, T., et al., *Anti-cholinergic effects of quinidine, disopyramide, and procainamide in isolated atrial myocytes: mediation by different molecular mechanisms*. Circulation research, 1989. **64**(2): p. 297-303.
150. Katayama, J., T. Yakushiji, and N. Akaike, *Characterization of the K<sup>+</sup> current mediated by 5-HT1A receptor in the acutely dissociated rat dorsal raphe neurons*. Brain research, 1997. **745**(1-2): p. 283-92.

151. Krishna, S. and N.J. White, *Pharmacokinetics of quinine, chloroquine and amodiaquine. Clinical implications*. Clinical pharmacokinetics, 1996. **30**(4): p. 263-99.
152. Patel, U. and B.B. Pavri, *Short QT syndrome: a review*. Cardiology in review, 2009. **17**(6): p. 300-3.
153. Jin, W. and Z. Lu, *A novel high-affinity inhibitor for inward-rectifier K<sup>+</sup> channels*. Biochemistry, 1998. **37**(38): p. 13291-9.
154. Jin, W., et al., *Mechanisms of inward-rectifier K<sup>+</sup> channel inhibition by tertiapin-Q*. Biochemistry, 1999. **38**(43): p. 14294-301.
155. Kanjhan, R., et al., *Tertiapin-Q blocks recombinant and native large conductance K<sup>+</sup> channels in a use-dependent manner*. The Journal of pharmacology and experimental therapeutics, 2005. **314**(3): p. 1353-61.
156. Jin, W. and Z. Lu, *Synthesis of a stable form of tertiapin: a high-affinity inhibitor for inward-rectifier K<sup>+</sup> channels*. Biochemistry, 1999. **38**(43): p. 14286-93.
157. Tabata, T., et al., *GABAergic activation of an inwardly rectifying K<sup>+</sup> current in mouse cerebellar Purkinje cells*. The Journal of physiology, 2005. **563**(Pt 2): p. 443-57.
158. Chen, X. and D. Johnston, *Constitutively active G-protein-gated inwardly rectifying K<sup>+</sup> channels in dendrites of hippocampal CA1 pyramidal neurons*. The Journal of neuroscience : the official journal of the Society for Neuroscience, 2005. **25**(15): p. 3787-92.
159. Matsuda, T., et al., *Blockade by NIP-142, an antiarrhythmic agent, of carbachol-induced atrial action potential shortening and GIRK1/4 channel*. Journal of pharmacological sciences, 2006. **101**(4): p. 303-10.
160. Hashimoto, N., T. Yamashita, and N. Tsuruzoe, *Characterization of in vivo and in vitro electrophysiological and antiarrhythmic effects of a novel IKACH blocker, NIP-151: a comparison with an IKr-blocker dofetilide*. Journal of cardiovascular pharmacology, 2008. **51**(2): p. 162-9.
161. Machida, T., et al., *Effects of a highly selective acetylcholine-activated K<sup>+</sup> channel blocker on experimental atrial fibrillation*. Circulation. Arrhythmia and electrophysiology, 2011. **4**(1): p. 94-102.
162. Kobayashi, T., et al., *Ethanol opens G-protein-activated inwardly rectifying K<sup>+</sup> channels*. Nature neuroscience, 1999. **2**(12): p. 1091-7.
163. Lewohl, J.M., et al., *G-protein-coupled inwardly rectifying potassium channels are targets of alcohol action*. Nature neuroscience, 1999. **2**(12): p. 1084-90.
164. Yow, T.T., et al., *Naringin directly activates inwardly rectifying potassium channels at an overlapping binding site to tertiapin-Q*. British journal of pharmacology, 2011. **163**(5): p. 1017-33.
165. Weigl, L.G. and W. Schreiber, *G protein-gated inwardly rectifying potassium channels are targets for volatile anesthetics*. Molecular pharmacology, 2001. **60**(2): p. 282-9.
166. Bodhinathan, K. and P.A. Slesinger, *Molecular mechanism underlying ethanol activation of G-protein-gated inwardly rectifying potassium channels*.

- Proceedings of the National Academy of Sciences of the United States of America, 2013. **110**(45): p. 18309-14.
167. Aryal, P., et al., *A discrete alcohol pocket involved in GIRK channel activation*. Nature neuroscience, 2009. **12**(8): p. 988-95.
  168. Ramos-Hunter, S.J., et al., *Discovery and SAR of a novel series of GIRK1/2 and GIRK1/4 activators*. Bioorganic & medicinal chemistry letters, 2013. **23**(18): p. 5195-8.
  169. Kaufmann, K., et al., *ML297 (VU0456810), the first potent and selective activator of the GIRK potassium channel, displays antiepileptic properties in mice*. ACS chemical neuroscience, 2013. **4**(9): p. 1278-86.
  170. Lujan, R., et al., *New insights into the therapeutic potential of Girk channels*. Trends in neurosciences, 2014. **37**(1): p. 20-9.
  171. Nishizawa, D., et al., *Association between KCNJ6 (GIRK2) gene polymorphisms and postoperative analgesic requirements after major abdominal surgery*. PloS one, 2009. **4**(9): p. e7060.
  172. Lotsch, J., et al., *A KCNJ6 (Kir3.2, GIRK2) gene polymorphism modulates opioid effects on analgesia and addiction but not on pupil size*. Pharmacogenetics and genomics, 2010. **20**(5): p. 291-7.
  173. Clarke, T.K., et al., *KCNJ6 is associated with adult alcohol dependence and involved in gene x early life stress interactions in adolescent alcohol drinking*. Neuropsychopharmacology : official publication of the American College of Neuropsychopharmacology, 2011. **36**(6): p. 1142-8.
  174. Reeves, R.H., et al., *A mouse model for Down syndrome exhibits learning and behaviour deficits*. Nature genetics, 1995. **11**(2): p. 177-84.
  175. Sago, H., et al., *Ts1Cje, a partial trisomy 16 mouse model for Down syndrome, exhibits learning and behavioral abnormalities*. Proceedings of the National Academy of Sciences of the United States of America, 1998. **95**(11): p. 6256-61.
  176. Cooper, A., et al., *Trisomy of the G protein-coupled K<sup>+</sup> channel gene, Kcnj6, affects reward mechanisms, cognitive functions, and synaptic plasticity in mice*. Proceedings of the National Academy of Sciences of the United States of America, 2012. **109**(7): p. 2642-7.
  177. Yamada, K., et al., *Association study of the KCNJ3 gene as a susceptibility candidate for schizophrenia in the Chinese population*. Human genetics, 2012. **131**(3): p. 443-51.
  178. Yang, Y., et al., *Identification of a Kir3.4 mutation in congenital long QT syndrome*. American journal of human genetics, 2010. **86**(6): p. 872-80.
  179. Jabbari, J., et al., *Common polymorphisms in KCNJ5 [corrected] are associated with early-onset lone atrial fibrillation in Caucasians*. Cardiology, 2011. **118**(2): p. 116-20.
  180. Wang, F., et al., *The phenotype characteristics of type 13 long QT syndrome with mutation in KCNJ5 (Kir3.4-G387R)*. Heart rhythm : the official journal of the Heart Rhythm Society, 2013. **10**(10): p. 1500-6.

181. Scholl, U.I. and R.P. Lifton, *New insights into aldosterone-producing adenomas and hereditary aldosteronism: mutations in the K<sup>+</sup> channel KCNJ5*. *Current opinion in nephrology and hypertension*, 2013. **22**(2): p. 141-7.
182. Mulatero, P., et al., *Role of KCNJ5 in familial and sporadic primary aldosteronism*. *Nature reviews. Endocrinology*, 2013. **9**(2): p. 104-12.
183. Burt, D.R. and G.L. Kamatchi, *GABAA receptor subtypes: from pharmacology to molecular biology*. *FASEB journal : official publication of the Federation of American Societies for Experimental Biology*, 1991. **5**(14): p. 2916-23.
184. Bormann, J., *Electrophysiology of GABAA and GABAB receptor subtypes*. *Trends in neurosciences*, 1988. **11**(3): p. 112-6.
185. Jones, K.A., et al., *GABA(B) receptors function as a heteromeric assembly of the subunits GABA(B)R1 and GABA(B)R2*. *Nature*, 1998. **396**(6712): p. 674-9.
186. Kaupmann, K., et al., *GABA(B)-receptor subtypes assemble into functional heteromeric complexes*. *Nature*, 1998. **396**(6712): p. 683-7.
187. Kuner, R., et al., *Role of heteromer formation in GABAB receptor function*. *Science*, 1999. **283**(5398): p. 74-7.
188. White, J.H., et al., *Heterodimerization is required for the formation of a functional GABA(B) receptor*. *Nature*, 1998. **396**(6712): p. 679-82.
189. Malitschek, B., et al., *The N-terminal domain of gamma-aminobutyric Acid(B) receptors is sufficient to specify agonist and antagonist binding*. *Molecular pharmacology*, 1999. **56**(2): p. 448-54.
190. Margeta-Mitrovic, M., Y.N. Jan, and L.Y. Jan, *A trafficking checkpoint controls GABA(B) receptor heterodimerization*. *Neuron*, 2000. **27**(1): p. 97-106.
191. Galvez, T., et al., *Allosteric interactions between GB1 and GB2 subunits are required for optimal GABA(B) receptor function*. *The EMBO journal*, 2001. **20**(9): p. 2152-9.
192. Kammerer, R.A., et al., *Heterodimerization of a functional GABAB receptor is mediated by parallel coiled-coil alpha-helices*. *Biochemistry*, 1999. **38**(40): p. 13263-9.
193. Calver, A.R., et al., *The C-terminal domains of the GABA(b) receptor subunits mediate intracellular trafficking but are not required for receptor signaling*. *The Journal of neuroscience : the official journal of the Society for Neuroscience*, 2001. **21**(4): p. 1203-10.
194. Premkumar, L.S. and P.W. Gage, *Potassium channels activated by GABAB agonists and serotonin in cultured hippocampal neurons*. *Journal of neurophysiology*, 1994. **71**(6): p. 2570-5.
195. Kulik, A., et al., *Compartment-dependent colocalization of Kir3.2-containing K<sup>+</sup> channels and GABAB receptors in hippocampal pyramidal cells*. *The Journal of neuroscience : the official journal of the Society for Neuroscience*, 2006. **26**(16): p. 4289-97.
196. Wallenstein, G.V., *Simulation of GABAB-receptor-mediated K<sup>+</sup> current in thalamocortical relay neurons: tonic firing, bursting, and oscillations*. *Biological cybernetics*, 1994. **71**(3): p. 271-80.

197. Lacey, M.G., N.B. Mercuri, and R.A. North, *On the potassium conductance increase activated by GABAB and dopamine D2 receptors in rat substantia nigra neurones*. The Journal of physiology, 1988. **401**: p. 437-53.
198. Osmanovic, S.S. and S.A. Shefner, *Baclofen increases the potassium conductance of rat locus coeruleus neurons recorded in brain slices*. Brain research, 1988. **438**(1-2): p. 124-36.
199. Fowler, C.E., et al., *Evidence for association of GABA(B) receptors with Kir3 channels and regulators of G protein signalling (RGS4) proteins*. The Journal of physiology, 2007. **580**(Pt 1): p. 51-65.
200. Ciruela, F., et al., *Evidence for oligomerization between GABAB receptors and GIRK channels containing the GIRK1 and GIRK3 subunits*. The European journal of neuroscience, 2010. **32**(8): p. 1265-77.
201. Fajardo-Serrano, A., et al., *Association of Rgs7/Gbeta5 complexes with Girk channels and GABAB receptors in hippocampal CA1 pyramidal neurons*. Hippocampus, 2013. **23**(12): p. 1231-45.
202. Bonner, T.I., *The molecular basis of muscarinic receptor diversity*. Trends in neurosciences, 1989. **12**(4): p. 148-51.
203. Ikegaya, T., et al., *Interaction of atrial muscarinic receptors with three kinds of GTP-binding proteins*. Journal of molecular and cellular cardiology, 1990. **22**(3): p. 343-51.
204. Li, D., H. Sun, and P. Levesque, *Antiarrhythmic drug therapy for atrial fibrillation: focus on atrial selectivity and safety*. Cardiovascular & hematological agents in medicinal chemistry, 2009. **7**(1): p. 64-75.
205. Wickman, K., et al., *Abnormal heart rate regulation in GIRK4 knockout mice*. Neuron, 1998. **20**(1): p. 103-14.
206. Sakmann, B., A. Noma, and W. Trautwein, *Acetylcholine activation of single muscarinic K<sup>+</sup> channels in isolated pacemaker cells of the mammalian heart*. Nature, 1983. **303**(5914): p. 250-3.
207. Neubig, R.R., *And the winner is ... RGS4!* Circulation research, 2008. **103**(5): p. 444-6.
208. Signorini, S., et al., *Normal cerebellar development but susceptibility to seizures in mice lacking G protein-coupled, inwardly rectifying K<sup>+</sup> channel GIRK2*. Proceedings of the National Academy of Sciences of the United States of America, 1997. **94**(3): p. 923-7.
209. Duprat, F., et al., *Heterologous multimeric assembly is essential for K<sup>+</sup> channel activity of neuronal and cardiac G-protein-activated inward rectifiers*. Biochemical and biophysical research communications, 1995. **212**(2): p. 657-63.
210. Bettahi, I., et al., *Contribution of the Kir3.1 subunit to the muscarinic-gated atrial potassium channel IKACH*. The Journal of biological chemistry, 2002. **277**(50): p. 48282-8.
211. Arora, D., et al., *Acute cocaine exposure weakens GABA(B) receptor-dependent G-protein-gated inwardly rectifying K<sup>+</sup> signaling in dopamine neurons of the ventral tegmental area*. The Journal of neuroscience : the official journal of the Society for Neuroscience, 2011. **31**(34): p. 12251-7.

212. Mirkovic, K. and K. Wickman, *Identification and characterization of alternative splice variants of the mouse *Trek2/Kcnk10* gene*. *Neuroscience*, 2011. **194**: p. 11-8.
213. Wisner, O., et al., *Modulation of basal and receptor-induced GIRK potassium channel activity and neuronal excitability by the mammalian PINS homolog LGN*. *Neuron*, 2006. **50**(4): p. 561-73.
214. Huang, C.L., Y.N. Jan, and L.Y. Jan, *Binding of the G protein betagamma subunit to multiple regions of G protein-gated inward-rectifying K<sup>+</sup> channels*. *FEBS letters*, 1997. **405**(3): p. 291-8.
215. Rogalski, S.L., et al., *TrkB activation by brain-derived neurotrophic factor inhibits the G protein-gated inward rectifier Kir3 by tyrosine phosphorylation of the channel*. *The Journal of biological chemistry*, 2000. **275**(33): p. 25082-8.
216. Rubinstein, M., et al., *Galphai3 primes the G protein-activated K<sup>+</sup> channels for activation by coexpressed Gbetagamma in intact *Xenopus* oocytes*. *The Journal of physiology*, 2007. **581**(Pt 1): p. 17-32.
217. Hibino, H., et al., *Inwardly rectifying potassium channels: their structure, function, and physiological roles*. *Physiological reviews*, 2010. **90**(1): p. 291-366.
218. Yamakura, T., J.M. Lewohl, and R.A. Harris, *Differential effects of general anesthetics on G protein-coupled inwardly rectifying and other potassium channels*. *Anesthesiology*, 2001. **95**(1): p. 144-53.
219. Kobayashi, T. and K. Ikeda, *G protein-activated inwardly rectifying potassium channels as potential therapeutic targets*. *Current pharmaceutical design*, 2006. **12**(34): p. 4513-23.
220. Wydeven, N., et al., *Structural elements in the *Girk1* subunit that potentiate G protein-gated potassium channel activity*. *Proceedings of the National Academy of Sciences of the United States of America*, 2012. **109**(52): p. 21492-7.
221. Okamura, Y., Y. Murata, and H. Iwasaki, *Voltage-sensing phosphatase: actions and potentials*. *The Journal of physiology*, 2009. **587**(Pt 3): p. 513-20.
222. Van der Heyden, J.A., T.J. Zethof, and B. Olivier, *Stress-induced hyperthermia in singly housed mice*. *Physiology & behavior*, 1997. **62**(3): p. 463-70.
223. Blednov, Y.A., et al., *GIRK2 deficient mice. Evidence for hyperactivity and reduced anxiety*. *Physiology & behavior*, 2001. **74**(1-2): p. 109-17.
224. Pravetoni, M. and K. Wickman, *Behavioral characterization of mice lacking GIRK/Kir3 channel subunits*. *Genes, brain, and behavior*, 2008. **7**(5): p. 523-31.
225. Kofuji, P., et al., *A unique P-region residue is required for slow voltage-dependent gating of a G protein-activated inward rectifier K<sup>+</sup> channel expressed in *Xenopus* oocytes*. *The Journal of physiology*, 1996. **490** ( Pt 3): p. 633-45.
226. Wen, W., et al., *Discovery of 'molecular switches' within a GIRK activator scaffold that afford selective GIRK inhibitors*. *Bioorganic & medicinal chemistry letters*, 2013. **23**(16): p. 4562-6.
227. Arora, D., et al., *Altered neurotransmission in the mesolimbic reward system of *Girk* mice*. *Journal of neurochemistry*, 2010. **114**(5): p. 1487-97.
228. Hearing, M., et al., *Repeated cocaine weakens GABA(B)-Girk signaling in layer 5/6 pyramidal neurons in the prelimbic cortex*. *Neuron*, 2013. **80**(1): p. 159-70.

229. Hill, K.G., et al., *Reduced ethanol-induced conditioned taste aversion and conditioned place preference in GIRK2 null mutant mice*. *Psychopharmacology*, 2003. **169**(1): p. 108-14.
230. Mirshahi, T., T. Jin, and D.E. Logothetis, *G beta gamma and KACH: old story, new insights*. *Science's STKE : signal transduction knowledge environment*, 2003. **2003**(194): p. PE32.
231. Hollinger, S. and J.R. Hepler, *Cellular regulation of RGS proteins: modulators and integrators of G protein signaling*. *Pharmacological reviews*, 2002. **54**(3): p. 527-59.
232. Fu, Y., et al., *Endogenous RGS proteins modulate SA and AV nodal functions in isolated heart: implications for sick sinus syndrome and AV block*. *American journal of physiology. Heart and circulatory physiology*, 2007. **292**(5): p. H2532-9.
233. Fu, Y., et al., *Endogenous RGS proteins and Galpha subtypes differentially control muscarinic and adenosine-mediated chronotropic effects*. *Circulation research*, 2006. **98**(5): p. 659-66.
234. Martemyanov, K.A. and V.Y. Arshavsky, *Noncatalytic domains of RGS9-1.Gbeta 5L play a decisive role in establishing its substrate specificity*. *The Journal of biological chemistry*, 2002. **277**(36): p. 32843-8.
235. Martemyanov, K.A., et al., *R7BP, a novel neuronal protein interacting with RGS proteins of the R7 family*. *The Journal of biological chemistry*, 2005. **280**(7): p. 5133-6.
236. Martemyanov, K.A., J.A. Hopp, and V.Y. Arshavsky, *Specificity of G protein-RGS protein recognition is regulated by affinity adapters*. *Neuron*, 2003. **38**(6): p. 857-62.
237. Kennedy, M.E., J. Nemece, and D.E. Clapham, *Localization and interaction of epitope-tagged GIRK1 and CIR inward rectifier K+ channel subunits*. *Neuropharmacology*, 1996. **35**(7): p. 831-9.
238. Chen, C.K., et al., *Instability of GGL domain-containing RGS proteins in mice lacking the G protein beta-subunit Gbeta5*. *Proceedings of the National Academy of Sciences of the United States of America*, 2003. **100**(11): p. 6604-9.
239. Koyrakh, L., et al., *The heart rate decrease caused by acute FTY720 administration is mediated by the G protein-gated potassium channel I*. *American journal of transplantation : official journal of the American Society of Transplantation and the American Society of Transplant Surgeons*, 2005. **5**(3): p. 529-36.
240. McGrath, M.F. and A.J. de Bold, *Transcriptional analysis of the mammalian heart with special reference to its endocrine function*. *BMC genomics*, 2009. **10**: p. 254.
241. Doupnik, C.A., T. Xu, and J.M. Shinaman, *Profile of RGS expression in single rat atrial myocytes*. *Biochimica et biophysica acta*, 2001. **1522**(2): p. 97-107.
242. Hooks, S.B., et al., *RGS6, RGS7, RGS9, and RGS11 stimulate GTPase activity of Gi family G-proteins with differential selectivity and maximal activity*. *The Journal of biological chemistry*, 2003. **278**(12): p. 10087-93.



243. Mangoni, M.E. and J. Nargeot, *Genesis and regulation of the heart automaticity*. Physiological reviews, 2008. **88**(3): p. 919-82.
244. DiFrancesco, D., *The role of the funny current in pacemaker activity*. Circulation research, 2010. **106**(3): p. 434-46.
245. Dobrzynski, H., M.R. Boyett, and R.H. Anderson, *New insights into pacemaker activity: promoting understanding of sick sinus syndrome*. Circulation, 2007. **115**(14): p. 1921-32.
246. Vaseghi, M. and K. Shivkumar, *The role of the autonomic nervous system in sudden cardiac death*. Progress in cardiovascular diseases, 2008. **50**(6): p. 404-19.
247. Kovoov, P., et al., *Evaluation of the role of I(KACh) in atrial fibrillation using a mouse knockout model*. Journal of the American College of Cardiology, 2001. **37**(8): p. 2136-43.
248. Mesirca, P., et al., *The G-protein-gated K<sup>+</sup> channel, IKACH, is required for regulation of pacemaker activity and recovery of resting heart rate after sympathetic stimulation*. The Journal of general physiology, 2013. **142**(2): p. 113-26.
249. Mighiu, A.S. and S.P. Heximer, *Controlling Parasympathetic Regulation of Heart Rate: A Gatekeeper Role for RGS Proteins in the Sinoatrial Node*. Frontiers in physiology, 2012. **3**: p. 204.
250. Stewart, A., J. Huang, and R.A. Fisher, *RGS Proteins in Heart: Brakes on the Vagus*. Frontiers in physiology, 2012. **3**: p. 95.
251. Yang, J., et al., *RGS6, a modulator of parasympathetic activation in heart*. Circulation research, 2010. **107**(11): p. 1345-9.
252. Posokhova, E., et al., *RGS6/Gbeta5 complex accelerates IKACH gating kinetics in atrial myocytes and modulates parasympathetic regulation of heart rate*. Circulation research, 2010. **107**(11): p. 1350-4.
253. Posokhova, E., et al., *Essential role of the m2R-RGS6-IKACH pathway in controlling intrinsic heart rate variability*. PloS one, 2013. **8**(10): p. e76973.
254. Vasan, R.S., et al., *Genome-wide association of echocardiographic dimensions, brachial artery endothelial function and treadmill exercise responses in the Framingham Heart Study*. BMC medical genetics, 2007. **8 Suppl 1**: p. S2.
255. Davydov, I.V. and A. Varshavsky, *RGS4 is arginylated and degraded by the N-end rule pathway in vitro*. The Journal of biological chemistry, 2000. **275**(30): p. 22931-41.
256. Lee, M.J., et al., *RGS4 and RGS5 are in vivo substrates of the N-end rule pathway*. Proceedings of the National Academy of Sciences of the United States of America, 2005. **102**(42): p. 15030-5.
257. Blazer, L.L., et al., *Reversible, allosteric small-molecule inhibitors of regulator of G protein signaling proteins*. Molecular pharmacology, 2010. **78**(3): p. 524-33.
258. Vashisth, H., et al., *Conformational dynamics of a regulator of G-protein signaling protein reveals a mechanism of allosteric inhibition by a small molecule*. ACS chemical biology, 2013. **8**(12): p. 2778-84.

259. Huang, C., et al., *Attenuation of Gi- and Gq-mediated signaling by expression of RGS4 or GAIP in mammalian cells*. Proceedings of the National Academy of Sciences of the United States of America, 1997. **94**(12): p. 6159-63.
260. Yan, Y., P.P. Chi, and H.R. Bourne, *RGS4 inhibits Gq-mediated activation of mitogen-activated protein kinase and phosphoinositide synthesis*. The Journal of biological chemistry, 1997. **272**(18): p. 11924-7.
261. Hepler, J.R., et al., *RGS4 and GAIP are GTPase-activating proteins for Gq alpha and block activation of phospholipase C beta by gamma-thio-GTP-Gq alpha*. Proceedings of the National Academy of Sciences of the United States of America, 1997. **94**(2): p. 428-32.
262. Mittmann, C., et al., *Expression of ten RGS proteins in human myocardium: functional characterization of an upregulation of RGS4 in heart failure*. Cardiovascular research, 2002. **55**(4): p. 778-86.
263. Lan, K.L., et al., *A point mutation in Galphao and Galphai1 blocks interaction with regulator of G protein signaling proteins*. The Journal of biological chemistry, 1998. **273**(21): p. 12794-7.
264. Heximer, S.P., et al., *RGS2/G0S8 is a selective inhibitor of Gqalpha function*. Proceedings of the National Academy of Sciences of the United States of America, 1997. **94**(26): p. 14389-93.
265. Zhang, Q., M.A. Pacheco, and C.A. Doupnik, *Gating properties of GIRK channels activated by Galpha(o)- and Galpha(i)-coupled muscarinic m2 receptors in Xenopus oocytes: the role of receptor precoupling in RGS modulation*. The Journal of physiology, 2002. **545**(Pt 2): p. 355-73.
266. Jaen, C. and C.A. Doupnik, *RGS3 and RGS4 differentially associate with G protein-coupled receptor-Kir3 channel signaling complexes revealing two modes of RGS modulation. Precoupling and collision coupling*. The Journal of biological chemistry, 2006. **281**(45): p. 34549-60.
267. Kardestuncer, T., et al., *Cardiac myocytes express mRNA for ten RGS proteins: changes in RGS mRNA expression in ventricular myocytes and cultured atria*. FEBS letters, 1998. **438**(3): p. 285-8.
268. Huang, C.L., et al., *Evidence that direct binding of G beta gamma to the GIRK1 G protein-gated inwardly rectifying K+ channel is important for channel activation*. Neuron, 1995. **15**(5): p. 1133-43.
269. Sarac, R., et al., *Mutation of critical GIRK subunit residues disrupts N- and C-termini association and channel function*. The Journal of neuroscience : the official journal of the Society for Neuroscience, 2005. **25**(7): p. 1836-46.
270. Luchian, T. and W. Schreibmayer, *Ion permeation through a G-protein activated (GIRK1/GIRK5) inwardly rectifying potassium channel*. Biochimica et biophysica acta, 1998. **1368**(2): p. 167-70.
271. Velimirovic, B.M., et al., *Opposing mechanisms of regulation of a G-protein-coupled inward rectifier K+ channel in rat brain neurons*. Proceedings of the National Academy of Sciences of the United States of America, 1995. **92**(5): p. 1590-4.

272. Bajic, D., et al., *Two different inward rectifier K<sup>+</sup> channels are effectors for transmitter-induced slow excitation in brain neurons*. Proceedings of the National Academy of Sciences of the United States of America, 2002. **99**(22): p. 14494-9.
273. Koike-Tani, M., et al., *Signal transduction pathway for the substance P-induced inhibition of rat Kir3 (GIRK) channel*. The Journal of physiology, 2005. **564**(Pt 2): p. 489-500.
274. Stansfeld, P.J., et al., *PIP(2)-binding site in Kir channels: definition by multiscale biomolecular simulations*. Biochemistry, 2009. **48**(46): p. 10926-33.
275. Rubinstein, M., et al., *Divergent regulation of GIRK1 and GIRK2 subunits of the neuronal G protein gated K<sup>+</sup> channel by GalphaiGDP and Gbetagamma*. The Journal of physiology, 2009. **587**(Pt 14): p. 3473-91.
276. Vivaudou, M., et al., *Probing the G-protein regulation of GIRK1 and GIRK4, the two subunits of the KACH channel, using functional homomeric mutants*. The Journal of biological chemistry, 1997. **272**(50): p. 31553-60.
277. Doyle, D.A., et al., *The structure of the potassium channel: molecular basis of K<sup>+</sup> conduction and selectivity*. Science, 1998. **280**(5360): p. 69-77.
278. Jiang, Y., et al., *The open pore conformation of potassium channels*. Nature, 2002. **417**(6888): p. 523-6.
279. Abrams, C.J., et al., *The role of a single aspartate residue in ionic selectivity and block of a murine inward rectifier K<sup>+</sup> channel Kir2.1*. The Journal of physiology, 1996. **493** ( Pt 3): p. 643-9.
280. Lu, Z. and R. MacKinnon, *Electrostatic tuning of Mg<sup>2+</sup> affinity in an inward-rectifier K<sup>+</sup> channel*. Nature, 1994. **371**(6494): p. 243-6.
281. Ficker, E., et al., *Spermine and spermidine as gating molecules for inward rectifier K<sup>+</sup> channels*. Science, 1994. **266**(5187): p. 1068-72.
282. Stanfield, P.R., et al., *A single aspartate residue is involved in both intrinsic gating and blockage by Mg<sup>2+</sup> of the inward rectifier, IRK1*. The Journal of physiology, 1994. **478** ( Pt 1): p. 1-6.
283. Yang, J., Y.N. Jan, and L.Y. Jan, *Control of rectification and permeation by residues in two distinct domains in an inward rectifier K<sup>+</sup> channel*. Neuron, 1995. **14**(5): p. 1047-54.
284. Silverman, S.K., H.A. Lester, and D.A. Dougherty, *Asymmetrical contributions of subunit pore regions to ion selectivity in an inward rectifier K<sup>+</sup> channel*. Biophysical journal, 1998. **75**(3): p. 1330-9.
285. Silverman, S.K., H.A. Lester, and D.A. Dougherty, *Subunit stoichiometry of a heteromultimeric G protein-coupled inward-rectifier K<sup>+</sup> channel*. The Journal of biological chemistry, 1996. **271**(48): p. 30524-8.
286. Riven, I., et al., *Conformational rearrangements associated with the gating of the G protein-coupled potassium channel revealed by FRET microscopy*. Neuron, 2003. **38**(2): p. 225-35.
287. Inanobe, A., et al., *Interaction between the RGS domain of RGS4 with G protein alpha subunits mediates the voltage-dependent relaxation of the G protein-gated potassium channel*. The Journal of physiology, 2001. **535**(Pt 1): p. 133-43.

288. Lomax, A.E., R.A. Rose, and W.R. Giles, *Electrophysiological evidence for a gradient of G protein-gated K<sup>+</sup> current in adult mouse atria*. British journal of pharmacology, 2003. **140**(3): p. 576-84.
289. Ivanina, T., et al., *Mapping the Gbetagamma-binding sites in GIRK1 and GIRK2 subunits of the G protein-activated K<sup>+</sup> channel*. The Journal of biological chemistry, 2003. **278**(31): p. 29174-83.
290. Ivanina, T., et al., *Galphai1 and Galphai3 differentially interact with, and regulate, the G protein-activated K<sup>+</sup> channel*. The Journal of biological chemistry, 2004. **279**(17): p. 17260-8.
291. Wickman, K., W.T. Pu, and D.E. Clapham, *Structural characterization of the mouse Girk genes*. Gene, 2002. **284**(1-2): p. 241-50.